

Alma Mater Studiorum – Università di Bologna

DOTTORATO DI RICERCA IN  
BIOLOGIA CELLULARE E MOLECOLARE

Ciclo XXXI

**Settore Concorsuale: 05/I1**

**Settore Scientifico Disciplinare: BIO/18**

**Neuroblastoma targeted therapy:  
employment of CRISPR gene-editing to explore  
relevant markers and potential targets in aggressive tumours**

**Presentata da: Paolo Pigni**

**Coordinatore Dottorato**

**Prof. Giovanni Capranico**

**Supervisore**

**Prof. Giovanni Perini**

**Esame finale anno 2019**



## Abstract

Neuroblastoma is a tumour originating from the sympathetic nervous system, and represents the most common extracranial solid cancer in childhood. Despite the malignancy is extremely heterogeneous, about 25% of all cases is characterized by *MYCN*-gene amplification, aggressive tumour and poor survival. The network of genes that are deregulated in this group of patients represents a focal point for targeted-therapy discovery. Along this research line, the first objective of the present project was to investigate the prognostic significance of a single nucleotide polymorphism (SNP) located in the promoter of *ODCI*, a neuroblastoma prognostic marker involved in polyamine biosynthesis. The SNP genotype was first associated with survival of a large cohort of patients with aggressive neuroblastoma. Then, CRISPR-editing revealed that the SNP genotype affects *ODCI* expression and proliferation of neuroblastoma cells. At last, the SNP was found to influence cell sensibility to DFMO, an *ODCI* inhibitor that is currently under trial for treatment of aggressive neuroblastoma. The second objective was to investigate the role in neuroblastoma development and progression of *RUNX1T1*, a poorly studied transcription repressor involved in distinct development events and cancers. Survival analysis of a cohort of neuroblastoma patients revealed that *RUNX1T1* is a potential oncosuppressor. In apparent contrast, *RUNX1T1* knockout by CRISPR-editing demonstrated that the gene promotes aggressiveness of neuroblastoma cells. Transcriptome analysis of the mutant cells then evidenced deregulation of a significant number of genes and pathways that are prognostic markers in neuroblastoma, therefore depicting a multifunctional regulation network that could be exploited for new therapies. The third and last objective was to test a novel therapeutic approach based on *MYCN*-amplification targeting via CRISPR-cleavage. *In vitro* experiments demonstrated that the system efficiently and specifically impairs the survival of aggressive neuroblastoma cells, thus providing a proof of principle for the development of an innovative therapy.

# Table of contents

<b>Introduction</b> .....	1
<b>1-Neuroblastoma: a challenging cancer in childhood</b> .....	2
1.1-Neuroblastoma classification and treatment .....	3
1.2-Embryonal origin of neuroblastoma .....	7
1.3-The genetic landscape of neuroblastoma tumours .....	10
<b>2-Oncogenic drivers and targeted therapy: an extended view on <i>MYCN</i>, <i>ODCI</i> and <i>RUNXIT1</i></b> .....	12
2.1- <i>MYCN</i> : leading oncodriver and possible therapeutic target .....	12
2.2- <i>ODCI</i> and the prognostic significance of a single nucleotide polymorphism .....	18
2.3-The multiple faces of <i>RUNXIT1</i> in cancer and development .....	24
<b>3-The CRISPR technology: from genome editing to <i>genetic surgery</i></b> .....	30
<b>Objectives and project design</b> .....	38
<b>Results and discussion</b> .....	43
<b>1-<i>ODCI</i> +316 A/G SNP has prognostic significance in neuroblastoma</b> .....	44
1.1-The A allele predicts favourable outcome in neuroblastoma patients .....	44
1.2-The A SNP impairs <i>ODCI</i> expression in neuroblastoma cells .....	47
1.3- The A allele correlates with decreased cell proliferation and increased sensibility to DFMO....	57
<b>2-<i>RUNXIT1</i> represents a novel player in neuroblastoma development and progression</b> .....	61
2.1- <i>RUNXIT1</i> is a potential oncosuppressor in neuroblastoma patients .....	61
2.2-Mutation of <i>RUNXIT1</i> gene impairs proliferation and migration, and promotes differentiation in neuroblastoma cells .....	63
2.3-Mutation of <i>RUNXIT1</i> affects signalling pathways involved in neuroblastoma progression and neural crest development .....	76
<b>3-CRISPR-targeting of <i>MYCN</i> amplification is a potential therapeutic strategy in neuroblastoma</b> .....	88

<b>Conclusions and future perspectives</b> .....	92
<b>Materials and methods</b> .....	101
<b>Bibliography</b> .....	113
<b>Acknowledgments</b> .....	133

# *Introduction*

# 1-Neuroblastoma: a challenging cancer in childhood

Neuroblastoma is a childhood solid tumour mainly originating in the sympathetic nervous system. First described in 1864, neuroblastoma represents the most common extracranial solid tumour of childhood, with an incidence of 10.7 cases per million patients aged under 15 years (data relative to the United States in 2010) [1-3]. It is the primary cause of death from pediatric cancer for children aged between 1 and 5 years, and it accounts for 7-10% of pediatric cancers and 13-15% of all pediatric cancer mortality [1, 3]. It is usually diagnosed under 21 years, while almost 50% of all cases is diagnosed within the first year of life [1-5]. Neuroblastoma is an extreme heterogeneous tumour, both clinically and genetically. The most frequent onset sites are the adrenal gland and the paraspinal ganglia of the abdomen, but it can potentially arise in any site of the sympathetic system, such as the ganglia of the chest (20%), neck (5%) and pelvis (5%) (Figure 1) [3]. The onset spectrum reflects the cellular origin of neuroblastoma, which is supposed to derive from the migrating cells of the neural crest during embryogenesis. Also the clinical behaviour, depending on different factors, can be extremely variable, ranging from spontaneous regression in some cases, to aggressive metastases affecting lymph nodes, liver, lungs, bone, bone marrow and even the central nervous system. The least aggressive cases are successfully treated with either surgery, chemotherapy, irradiation or a combination of them. Unfortunately, more than 50% of all patients are diagnosed with metastatic disease and the prognosis is mostly unfavourable [1-3]. In addition to a wide clinical spectrum, the genetic landscape of neuroblastoma tumours is quite complicated and not yet completely defined. Despite the effort of scientific research, no genetic lesion accounting for all conditions is currently known. However, much attention is focused on DNA amplification of the oncogene *MYCN*, which is found in about 20% of all cases and is significantly associated to poor prognosis [1-3]. This gene, a member of the well-known *MYC* family, encodes for a transcription factor involved in the control of several cell functions, including cell cycle control, differentiation, apoptosis and metabolism, and its deregulation is a strong oncogenic driver and prognosis indicator. Other genetic alterations are commonly associated to neuroblastoma, though their molecular roles in tumour formation and progression remain mostly undiscovered [1-3]. Considering the severity of the disease and the extreme heterogeneity of the tumour, it's not surprising that the development of new therapies for neuroblastoma still remains a challenging objective.

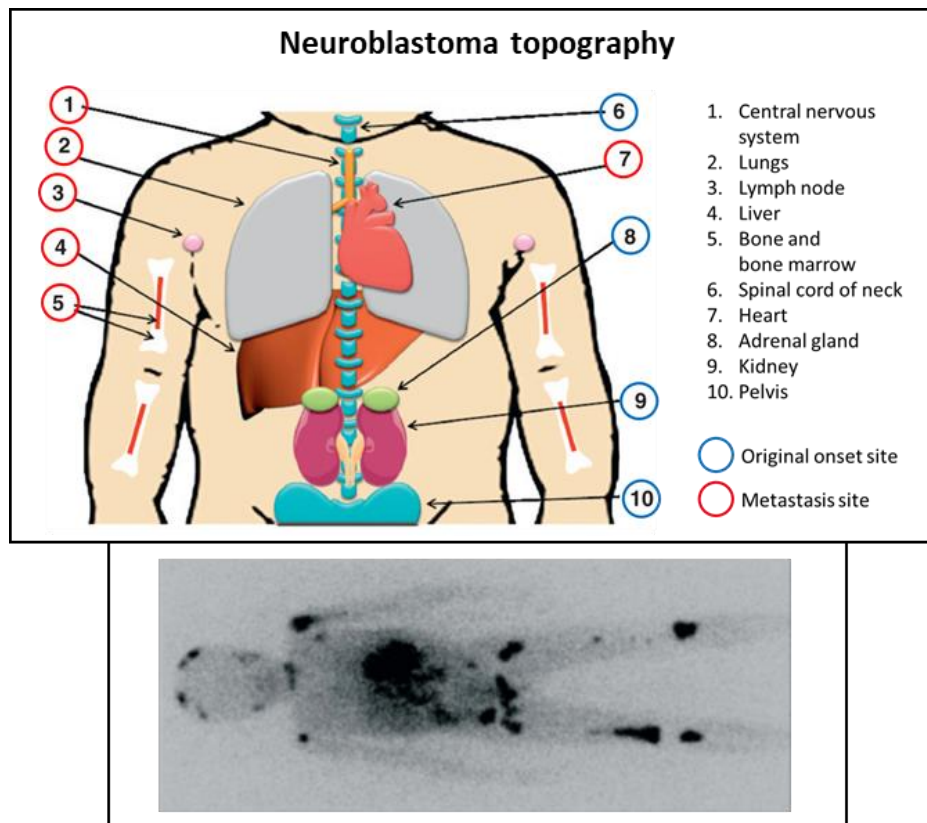


**Figure 1.** Top panel: typical onset and metastasis invasion sites of neuroblastoma [3]. Bottom panel: scintigraphy of a young patient with metastatic neuroblastoma.

## 1.1-Neuroblastoma classification and treatment

The wide spectrum of neuroblastoma clinical behaviour represents a challenging limit for diagnosis, prognosis and selection of the most efficacious treatment strategy. Moreover, it prevents comparison of clinical trials among different studies. In 1988 an international congress was held to elaborate a system aimed at facilitating the comparison of clinical trials performed throughout the world. The result was the International Neuroblastoma Staging System (INSS), according to which neuroblastoma can be classified into 5 different stages (Figure 2) [4]. Stage 1 and stage 2 neuroblastoma are considered low risk tumours (> 90% survival rate). They are relatively small, specifically localized, not metastatic and can be completely removed by surgery; however, stage 2 neuroblastoma could be persistent after surgery, requiring a further treatment with chemotherapy and/or irradiation. Stage 3 neuroblastoma is an intermediate/high

risk tumour (30-50% survival rate), with metastases infiltrated in lymph nodes nearby the original onset site, but not disseminated to distal parts of the body; it requires chemotherapy and irradiation, even though the tumour could become resistant to the treatment. Stage 4 neuroblastoma is a high-risk tumour (< 30% survival rate) with metastases spread through different parts of the body, including lymph nodes, liver, skin and, particularly, bone marrow. In this case, several cycles of chemotherapy and irradiation are required, although the prognosis remains extremely poor. The fifth stage, 4S, is significantly different from the previous ones; it can initially show features typical of aggressive tumours, but then it undergoes spontaneous regression with minimum treatment or even without medical intervention (average survival rate 50-80%). Neuroblastoma is usually diagnosed via standard histology analysis and detection of unusual urinary catecholamines, while the 5 stages are distinguished according to a series of features that include age of diagnosis, *MYCN* amplification status, histology and localization of eventual metastases [4]. More than 50% of all patients are diagnosed with either stage 3 or stage 4 neuroblastoma [3].

INSS stage	Age	MYCN status	Histology	Risk group	3-year survival rate
1	0–21 years	Any	Any	Low	>90%
2	0–21 years	Non-Amp	Any	Low	70–90% in this stage
	1–21 years	Amp	Favorable	Low	
	1–21 years	Amp	Unfavorable	High	
3	<1 year	Non-Amp	Any	Intermediate	30–50% in this stage
	1–21 years	Non-Amp	Favorable	Intermediate	
	0–21 years	Amp	Any	High	
	0–21 years	Non-Amp	Unfavorable	High	
4	<1 year	Non-Amp	Any	Intermediate	<30% in this stage
	0–21 years	Amp	Any	High	
4S	<1 year	Non-Amp	Favorable	Low	50–80% in this stage
	<1 year	Non-Amp	Unfavorable	Intermediate	
	<1 year	Amp	Any	High	

**Figure 2.** INSS, International Neuroblastoma Staging System: Amp, amplified; Non-Amp, not amplified [3].

Despite 20 years of application, INSS showed a considerable variability, especially due to the location of the primary tumour. In 2009 an improved system for risk stratification (International Neuroblastoma Risk Group Staging System, INRGSS) was introduced to compensate such variability (Figure 3) [5]. INGRSS was elaborated based on the analysis of 8,800 children diagnosed with neuroblastoma between 1990 and 2002, from North America, Australia, Europe and Japan. The system takes into account a large range of clinical features, imaging data and genetic lesions. These, among others, include age of diagnosis, histology categorization, metastasis location, grade of tumour differentiation, *MYCN* amplification and chromosomal aberrations. Overall, INGRSS includes 5 stages, which can be subclassified in a total of 16 specific risk groups. Stages L1, L2 and L1/L2 generally include groups with low-risk localized tumours, stage M mostly include groups with high risk metastatic tumours, while MS only include groups with precisely localized metastases [5].

INRG Stage	Age (months)	Histologic Category	Grade of Tumor Differentiation	<i>MYCN</i>	11q Aberration	Ploidy	Pretreatment Risk Group
L1/L2		GN maturing; GNB intermixed					A Very low
L1		Any, except GN maturing or GNB intermixed		NA			B Very low
				Amp			K High
L2	< 18	Any, except GN maturing or GNB intermixed		NA	No		D Low
					Yes		G Intermediate
	≥ 18	GNB nodular; neuroblastoma	Differentiating	NA	No		E Low
			Poorly differentiated or undifferentiated	NA	Yes		H Intermediate
				Amp		N High	
M	< 18			NA		Hyperdiploid	F Low
	< 12			NA		Diploid	I Intermediate
	12 to < 18			NA		Diploid	J Intermediate
	< 18			Amp			O High
	≥ 18						P High
MS					No		C Very low
	< 18			NA	Yes		Q High
					Amp		

**Figure 3.** International Neuroblastoma Risk Groups:

L, locoregional tumour; M, metastatic tumour; GN, ganglioneuroma; GNB, ganglioneuroblastoma; Amp, amplified; NA, not amplified; very low risk, 5-year event free survival > 85%; low risk, 5-year event free survival > 75% to < 85%; intermediate risk, 5-year event free survival > 50% to < 75%; high risk, 5-year event free survival < 50% [5].

Clinical treatment of neuroblastoma ranges from classical surgery, chemotherapy and irradiation, to molecular targeted therapy and biotherapy. The choice of the most efficient strategy is highly dependent on patient's risk stratification, but the outcome is still considerably variable. According to INRGSS, low-, very low- and some intermediate-risk tumours can be completely resected via surgery and following moderate-dose chemotherapy. The survival rate of these patients is usually greater than 90%. Irradiation and high-dose chemotherapy might also be necessary for tumours that do not completely respond to the initial treatment. These patients, often characterized by *MYCN* amplification, usually show a much worse survival rate (>50%) [1, 3, 5]. In all patients, chemotherapy is commonly applied through multiagent strategies and the FDA-approved drugs for neuroblastoma treatment include Clafen, Cyclophosphamide, Cytosan, Dinutuximab, Doxorubicin, Hydrochloride, Neosar, Unituxin, Vincasar PFS, Vincristine, Sulfate, BuMel and CEM [list provided by NIH, last update in 2014]. Like low-risk groups, patients diagnosed with 4S neuroblastoma and that do not present with *MYCN* amplification show a relatively high survival rate, since the tumour might regress without the necessity of any treatment [1, 3, 5].

Patients diagnosed with high-risk neuroblastoma usually require a much more aggressive and specific therapy. Also some intermediate-risk and 4S tumours might require this treatment. These tumours are typically characterized by *MYCN* amplification and/or metastases, with a survival rate strictly below 30%. The standard clinical strategy is comprised of 4 steps: initial induction chemotherapy, local control, consolidation and biological therapy. Initial induction chemotherapy is based on a multi-agent strategy, and it is followed by local control consisting of aggressive surgery resection and beam radiation. The consolidation step is then provided by high-dose chemotherapy and, occasionally, by focal radiotherapy toward the primary site. The last step, biological therapy, is aimed at eradicating any residual disease and to avoid any possible relapse, a likely occurrence in high-risk neuroblastoma. It involves the application of neuroblastoma-specific biological agents, reason for which it is also referred to as targeted therapy. The most common agent is *cis*-retinoic acid, a noncytotoxic differentiation inducer whose mechanism of action is based on the undifferentiated/proliferative status of neuroblastoma cells [1, 3]. A further strategy was recently identified in immunotherapy, which in neuroblastoma employs a chimeric monoclonal antibody targeting the GD2 ganglioside. Until the last few years, immunotherapy for neuroblastoma treatment was considered extremely difficult, since neuroblastoma cells are poorly immunogenic due to a narrow epitope landscape. In addition, neuroblastoma cells evade the immune system by releasing molecules that either inhibit or kill T cells and NK cells. However, GD2 belongs to a unique family of T cell-

independent carbohydrate antigens, and it is specifically expressed as during development as in neuroblastoma cells. This provided an opportunity to develop an immunotherapy that, nowadays, is a standard of care showing very promising results [1-3].

Despite the goals reached by scientific research so far and the aggressive treatment strategy, high-risk neuroblastoma remains extremely challenging to cure, with a survival rate lower than 30%. Much effort from scientific research is currently focused on understanding the complex molecular and genetic landscape of neuroblastoma, with the objective to discover specific biomarkers to be exploited in a highly specific therapy.

## **1.2-Embryonal origin of neuroblastoma**

It is widely accepted that neuroblastoma originates from deregulation of the neural crest development during embryogenesis. The most direct evidences supporting this hypothesis are the low age of patients and the spectrum of the onset sites, which reflects the lineages of cells deriving from the neural crest. The majority of neuroblastoma indeed arises from the adrenal medulla and the paraspinal sympathetic ganglia, two structures that, as part of the sympathetic nervous system, typically originate from the neural crest during neural development [1-3].

The neural crest consists of a transient, migratory population of multipotent cells that emerges from the dorsal side of the neural tube during the early vertebrate development. It migrates along the entire body to give rise to a wide range of cell types, including sensory, autonomic, and enteric ganglia of the peripheral nervous system, the adrenal medulla, melanocytes and a range of skeletal, connective, adipose, and endocrine cells (Figure 4). Formation and migration of the neural crest cells take place in the context of primary and secondary neurulation. During primary neurulation (E7-7.5 in mouse, embryo stage 8 in humans), the ectoderm region corresponding to the neural plate folds in order to generate the neural tube. Neural crest cells develop during this stage from the dorsal side of the neural tube, beneath the overlying epidermis. They are located in the head, in the trunk region and in the sacral region. As the embryo proceeds through secondary neurulation, neural crest cells migrate from the dorsal side of the neural tube to distant sites of the body. These cells separate from the neighbouring neuroepithelial cells by delamination, which involves a process called epithelial-

to-mesenchymal transition (EMT). During EMT, cells turn from epithelial to mesenchymal phenotype through a series of molecular events such as changes in cytoskeleton organization and loss of cell adhesion, with a consequent enhancement of migratory abilities. Neural crest cell migration is then orchestrated by multiple environmental signals that direct them to the final settlement sites for differentiation. The dorsal aorta, the first blood vessel to form in embryo, has an essential role in releasing the signals that guide the migrating cells. Most of the neural crest cells derive from the trunk region, and they can either migrate to a ventrolateral position, in order to differentiate into the dorsal root ganglia of the sensory system, or further ventrally to differentiate into the sympathetic ganglia of the autonomic system and chromaffin cells of the adrenal glands. Additionally, neural crest can also give rise to enteric nervous system cells and Schwann cells, with the last type representing the most widely distributed cells in the body deriving from this embryonal structure [3, 6, 7].

The signalling pathways leading to formation, migration and differentiation of neural crest cells are multiple and not yet completely elucidated (Figure 4). Induction of the neural crest occurs in the neural plate border and it is thought to be mediated by the WNT, BMP and FGF pathways [7]. These signals specifically activate a series of neural plate border specifiers, which include *ZIC1*, *MSX1*, *MSX2*, *DLX3*, *DLX5*, *PAX3*, *PAX7*, *SNAIL1*, *TPAP2A*, *NOTCH*, *PRDM1A* and *AP-2* [1, 7]. Among these, *PAX3* and *ZIC1* induce the expression of neural crest specifiers, such as *SNAIL2* and *FOXD3*. Following induction, neural crest cells undergo delamination through EMT, which is mediated by both BMP and canonical WNT pathways, involving factors such as *BMP2*, *BMP4*, *BMP7*, *WNT1*, *TGF $\beta$* , *MSX1* and *c-MYB*. The result is the expression of *SNAIL2*, *FOXD3*, *SOX9* and *SOX10*, which directly mediate the transition to the mesenchymal status by modulating the expression of integrins, cadherins and *ROHB*. After separating from the surrounding tissue, the neural crest cells start to migrate throughout the embryo following a series of both internal and environmental signals. *SOX9* and *SOX10*, already expressed during EMT, have an early and major role in migration [7]. The dorsal aorta directs the migrating cells via the BMP signalling pathway [3, 6]. At last, *MYCN* transiently promotes cell migration and proliferation in the ventrolateral migrating cells committed to become sympathetic ganglia. This gene, indeed, represents a fundamental regulator of neural crest migration as well as the driving oncogene in a significant number of neuroblastoma cases, in which *MYCN* overexpression dictates tumour aggressiveness and metastasization [8]. Following migration, *SOX10* regulates a series of downstream effectors involved in the final differentiation process. These include: *MASH1*, which promotes the differentiation of the sympathetic lineage via activation of *PHOX2B*; neurotrophin receptors such as *NTRK1* (*TrkA*) and *NTRK2* (*TrkB*),

which both mediate the differentiation of the sympathoadrenal lineage; *NEUROG1*, essential for sensory neuron specification; *PAX3* and *c-RET*, which regulate the development of the enteric nervous system via activation of the RET pathway; Schwann cell-specific genes, including protein zero (*P0*), myelin basic protein (*MBP*), *proteolipid protein*, *connexin-32* and *connexin-47*; *MITF*, which controls the differentiation of melanocytes [3, 7]. The process that leads to chromaffin cells differentiation is still poorly understood, but factors such as *IGFII*, *FGF* and *EGF* are known to be involved [3]. It is not surprising that important differentiation regulators such as *PHOX2B*, *NTRK1* *NTRK2* are typically mutated in neuroblastoma, especially in those tumours showing low level of differentiation [1-3].

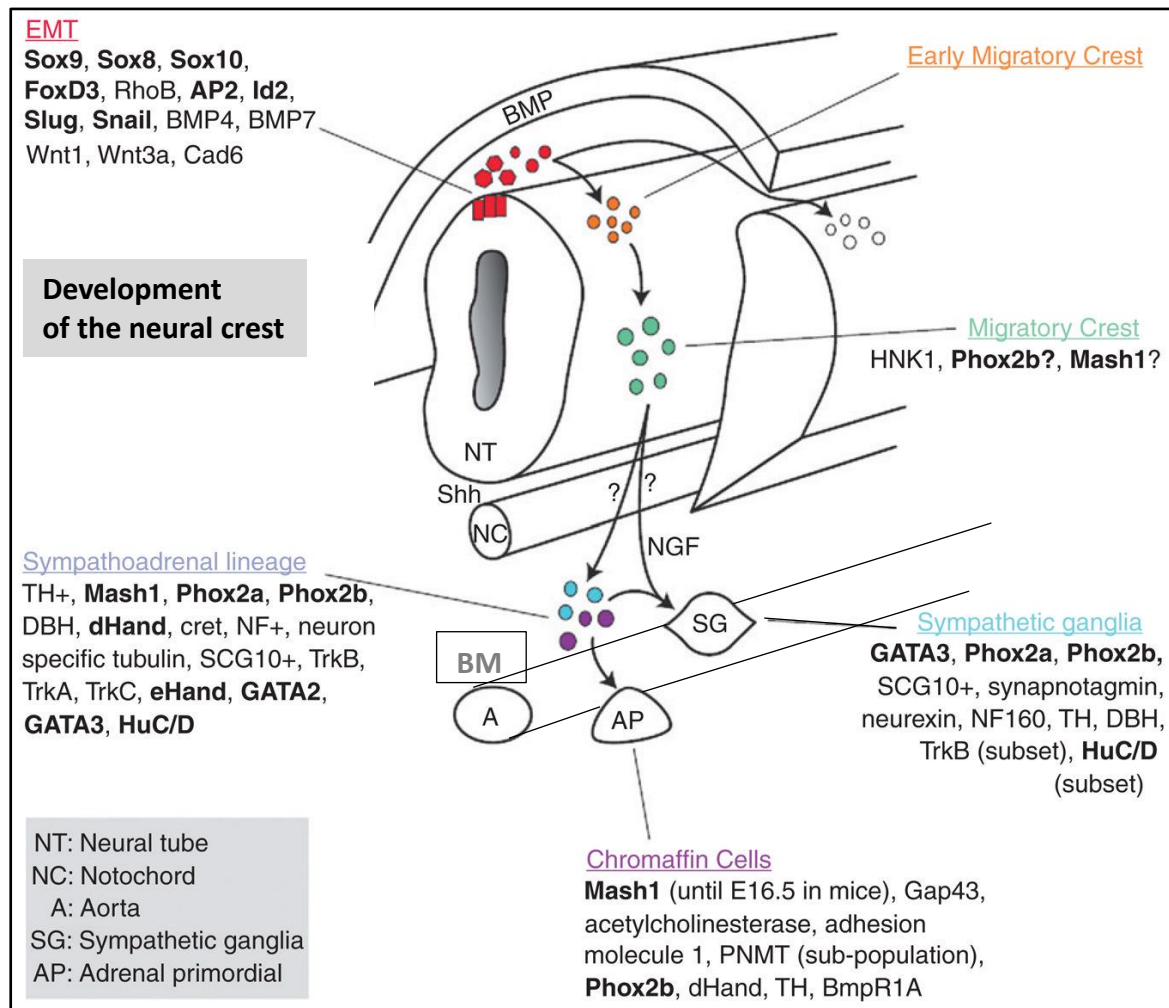


**Figure 4.** Genes involved in development and differentiation of neural crest cells deriving from the trunk region [3].

### 1.3-The genetic landscape of neuroblastoma tumours

Neuroblastoma is an extremely heterogeneous disease and no single genetic lesion is known to account for all cases, supporting the concept that neuroblastoma is a spectrum of diseases rather than a single pathological condition. However, some genetic lesions and oncogenic drivers are demonstrated to have diagnostic and prognostic significance in specific stratification groups [1-3]. In contrast, known tumour suppressor genes such as *p16INK4a*, *pRb*, *p53* and *p14ARF* are rarely deleted or mutated in neuroblastoma (except for caspase 8) [3]. Based on origin of the genetic lesion, neuroblastoma can be classified as either sporadic or familial, depending on whether the mutation occurred in the patient or was inherited. Most of neuroblastoma cases are sporadic, while the familial forms are fewer than 2% [1-3].

Amplification of the oncogene *MYCN* is the most important genetic lesion in sporadic neuroblastoma. It is found in more than 20% of all cases and it is strongly correlated to poor prognosis. *MYCN* belongs to the *MYC* family and, similarly to *c-MYC*, encodes for a transcription factor that regulates the expression of many genes involved in cell proliferation, survival, apoptosis and differentiation. Consequently, *MYCN* amplification and overexpression is associated to increased cell proliferation and decreased differentiation, two typical conditions of aggressive neuroblastoma [1-3]. The gene is considered amplified when either there are more than 10 copies in a diploid genome or the signal from chromosome 2 is 4-fold increased [2, 3]. In some cases, *MYCN* amplification consists of more than 500 copies, but the average is comprised between 50 and 100 copies. The amplified sequence typically contains a region of chromosome 2 ranging from 100 Kb to 1Mb, including *MYCN* gene and a variable amount of the surrounding DNA. The amplified sequence is usually found in chromosomes different from chromosome 2, or, more frequently, as double minutes [3, 9].

Another gene typically mutated in a subset of sporadic neuroblastoma is *ATRX*, encoding for an epigenetic regulator of the SWI/SNF family. Mutations are found in 44% of stage 4 neuroblastoma with age greater than 12 years, but only 9% of those with age less than 12 years. No mutations are found in patients aged less than 1 year [1, 2]. Interestingly, *ATRX* mutation alone is not enough for tumorigenesis, and no mutation occurring in this gene can be found in *MYCN*-amplified tumours [2].

Extensive evidence suggests that also the neurotrophin receptors *TRKA*, *TRKB*, *TRKC* and *p75NGR* might have a role in neuroblastoma development. These receptors, which bind neurotrophins (NGF, BDNF and NT-3) with different affinities, are involved in the

sympathoadrenal lineage differentiation. High expression of *TRKA*, as instance, is typically associated to regressing neuroblastoma, a correlation likely due to promotion of differentiation at the expense of cell proliferation [3].

*MYCN* amplification is not the only chromosome rearrangement typically found in neuroblastoma. For example, gain of 17q is a frequent abnormality, since it is found in about half of all neuroblastoma tumours. It is estimated that more than 200 genes are contained in the translocated region, including some possible oncogenes. Another lesion is the loss of heterozygosity of the small arm of chromosome 1 (1p36). It is found in 25-30% of neuroblastomas and typically correlates with *MYCN* amplification. The genetic traits included in this region that might be relevant for neuroblastoma development and progression are not identified, even though loss of genes such as *p73*, *CHD5*, *mir-34a* and *KIF1B $\beta$*  has been implied in tumour progression. Also loss of 11q and 14q are typically found in neuroblastoma, with an incidence of about 44% and 16-27% respectively. Loss of 11q is even used as a risk stratification parameter. Notably, these two rearrangements inversely correlate with *MYCN* amplification [3].

In recent years, much attention was focused on deregulation of non-coding RNAs in pathologies, including neuroblastoma. For example, the microRNA regulator *LIN28* is proved to be involved in neuroblastoma development by inhibiting the tumour suppression function of *Let7a* microRNA [1, 2]. In addition, also deregulation of *miR-9*, *miR-17-92a* and the *miR-25-106b* cluster are directly implicated in tumorigenesis, metastasis and regulation of differentiation in neuroblastoma [1].

For what concerns familial neuroblastoma, activating mutations of *ALK* gene (anaplastic lymphoma kinase) have been found in almost all cases, but it was also found in 6-10% of spontaneous tumours. This gene encodes for a receptor tyrosine kinase activating multiple pathways, such as MAPK/ERK, Shc and RAP1, and it is demonstrated to be involved in survival of migratory neural crest cells and sympathetic neuron development [1-3]. *ALK* is also known to be a transcriptional target of *MYCN* [1].

At last, *PHOX2B* is another gene typically mutated in a subset of familial neuroblastoma, as well as in 4% of sporadic cases. It is a fundamental driver of sympathetic lineage specification, and its loss-of-function mutations are associated with reduced cell differentiation [1-3]. *PHOX2B* inactivation could also activate *ALK* expression, thus contributing to severity of the tumour [1, 2].

## **2-Oncogenic drivers and targeted therapy: an extended view on *MYCN*, *ODC1* and *RUNX1T1***

Targeted therapy is defined as a therapy that uses drugs and biotechnology tools to interfere with cancer-specific molecular pathways involved in development, progression and spread of the tumour (definition by the *National Institute of Health*). Targeted therapy mainly differs from conventional chemotherapy by the specificity of the treatment, since cytotoxicity of chemotherapy is relatively independent from cell type and it has stronger side-effects. Targeted therapies typically rely on drugs blocking cancer-specific pathways, but some strategies also adopt hormones triggering anti-tumour mechanisms. In addition, immunotherapy has emerged as a promising therapy in the past few years, while new technologies of RNA-interference and genome editing are now evaluated as future opportunities for cancer gene therapy. In neuroblastoma only two targeted FDA-approved drugs are employed in clinical practice: *13-cis retinoic acid*, which induces differentiation of neuroblastoma cells thereby blocking proliferation, and *dinutuximab*, a monoclonal antibody used in immunotherapy to target GD2 ganglioside. However, neuroblastoma remains a much challenging disease, and opportunities to develop new drugs may be found by studying the typical genetic signatures of the tumour. For example, *MYCN*, the most relevant driver of high-risk neuroblastoma, is an important focus of cancer research. Also, *ODC1*, which encodes for an enzyme of polyamine biosynthesis, is known to be an oncodriver in different types of cancer, and it was recently identified as an independent prognostic marker and potential therapy target in neuroblastoma. Then, a multitude of genes that are already demonstrated to be involved in development and progression of some types of cancer are now evaluated as possible players in neuroblastoma. *RUNX1T1*, which is studied in this project, is for instance one of these.

### **2.1-*MYCN*: leading oncodriver and possible therapeutic target**

***MYCN* and the Myc/Max/Mad network.** Amplification of the oncogene *MYCN* is considered the most determinant genetic lesion for neuroblastoma prognosis. Gene amplification and high expression strongly correlate with metastatic tumour and poor survival.

*MYCN* encodes for a transcription factor typically expressed in poorly differentiated cells and regulating a wide set of genes involved in pluripotency, self-renewal, proliferation, cell-cycle control, apoptosis, angiogenesis, metastasis and immune surveillance [10]. As a result of that, cells with high *MYCN* expression are usually undifferentiated, highly proliferating and metastatic. Similarly, neural crest cells with ectopic overexpression of *MYCN* are transformed into neuroblastoma cells [10, 11], as well as transgenic mice with neural crest-localized overexpression of *MYCN* develop neuroblastoma with high penetrance [117].

*MYCN* belongs to the MYC family of transcription factors. As such, the protein structure has a C-term basic region/helix-loop-helix/leucine zipper (bHLHZip) domain and an N-term transactivation domain (TAD). The first, responsible of both DNA binding and protein-protein interaction, is common to all members of the MYC family and to most of the associated proteins. Interaction with other proteins is essential for *MYCN* function, since DNA binding is possible only as dimer. The most important dimerization partner of *MYCN* is *MAX*, which also contains a bHLHZip but not any effector domain. The consensus sequence recognized and bound by the *MYCN/MAX* dimer is CACGTG, also known as Enhancer box (E-box). *MYCN* transactivation domain is essential for exerting chromatin remodelling and transcription activation functions. Indeed, it interacts with a large histone acetyl transferase (HAT) complex, which includes proteins such as TRRAP, GCN5, PCAF, Tip60 and NuA4 [14, 15]. The C-term portion of *MYCN* is also supposed to interact with a member of the SWI/SNF complex, INI1/hSNF5 [14]. However, although transcription activation is the best characterized function, *MYCN* can also repress transcription of a wide set of genes. The mechanism is supposed to be mediated by the basal transcription factor 1 (*SP1*) and the initiator factor *MIZ-1* [16]. In the context of *MYCN* functions, it is also worth mentioning that the steady state intracellular levels of *MYCN* also depend on intrinsic stability of the protein and on those factors that can affect it. For instance, *MYCN* is first stabilized through phosphorylation of Serine-62 by kinases of the RAS signalling pathway, such as CDK1 or MAPK. When also Threonine-58 gets phosphorylated by GSK-3 $\beta$ , a PI3K-driven kinase, S62 is dephosphorylated by PP2A. Then FBW7 binds *MYCN* and brings it to degradation through ubiquitination. Furthermore, other proteins are supposed to be involved in *MYCN* stability. One of these is the aurora kinase A (*AURKA*), which stabilizes the transcription factor by affecting the phosphorylation status [10, 14].

*MYCN* and *MAX* are two members of a larger network known as Myc/Max/Mad network (Figure 5). In this system, a series of dimerization partners interact in order to regulate the expression of different groups of genes in a modular pattern. All the members of the MYC

family, which include MYCN, cMYC and MYCL in humans, can interact with MAX and subsequently bind DNA in order to regulate gene expression. At the same time, MAX can interact with a series of transcription repressors such as MAD1, MAD3, MAD4, MXI1, MNT and MGA. Most of these factors contain both a bHLHZip domain and a mSin3-interaction domain (SID). This last domain is responsible of interaction with HDAC partners, like mSin3. In a parallel subset of the network, the protein MLX can interact with the same transcription repressor partners of MAX, or, in alternative, with a different series of transcription activation factors, which includes MondoA and WBSCR14. MAX and MLX therefore represent two focal members of the interaction system. Overall, the Myc/Max/Mad network is complicated and still poorly understood, but its functions are known to be at the base of some physiological processes and pathological conditions [14].

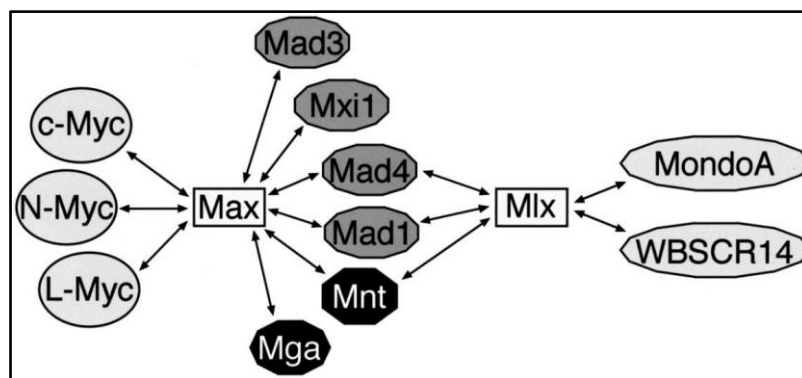


**Figure 5.** Myc/Max/Mad interaction network [14].

**MYCN regulation of cell functions.** MYCN expression is tissue/time-specific, with the highest expression characterizing the early developmental stages of the forebrain, hindbrain and kidney in new born mice. In the adult, it's almost completely absent, except for a weak expression in the thymus and the spleen. The gene is essential for neural system development, in which it regulates several aspects of the cell lineages undergoing differentiation [10]. Such wide effect comes through the transcription regulation of a large range of genes (Figure 6). Integration of both ChIPseq data, transcriptome-wide data and dataset-crossed analysis revealed a series of 874 direct MYCN targets, including 339 activated and 535 repressed genes [13].

The best characterized activity of MCYN is the promotion of cell proliferation and cell cycle progression through the regulation of several genes. As instance, MYCN activates CDK4 and

*SKP2*, and represses *TP53INP1*, therefore allowing *CDK2* to escape *p21* inhibition and to regulate the G1-S transition. It also activates the expression of *CHK1*, an important regulator of S-phase and G2/M checkpoints. *ID2*, a transcription factor which inactivates retinoblastoma (*Rb*), is another *MYCN*-upregulated gene leading to cell cycle progression and proliferation, as well as *MCM7* and *NLRRI*, which are involved in DNA replication and S-phase entry [10, 12]. On the other hand, *MYCN* represses the expression of anti-proliferative proteins, including *DKK1*, an inhibitor of the Wnt pathway, and *CDKL5*, which arrests the cells between G0 and G1 phases. Self-renewal and pluripotency are also massively studied aspects which *MYCN* is involved in. *KLF2*, *KLF4*, *LIN28B*, *SSEA-1* and *BMII* are some pluripotency genes up-regulated by *MYCN*. *MYCN*-mediated upregulation of Notch pathway regulators, such as *DLL3* and *Notch1*, is described as a mechanism maintaining neural stem cell pluripotency [10]. *PAX3*, another upregulated gene, is involved in neural crest cell differentiation [12]. In addition, *MYCN* downregulates a wide set of differentiation markers, including *BMP4* and *GATA6* in endoderm and mesoderm, *STAT1*, *EGR1* and *ELK3* in lymphocytes, *TRKA* in neural cells [10]. The oncogene is also supposed to affect the retinoic acid-mediated differentiation through upregulation of *CRABP II* [12]. Consistent with activation of cell-cycle progression and proliferation, *MYCN* cooperates with suppressors of *p53* signalling and apoptosis, including *miRNA-350-5p*, *CUL7*, *BMII*, *H-Twist*, *NDRG1* and *MDM2* [10, 12]. However, the mechanism through which *MYCN* affects apoptosis is double-faced. Indeed, it potentially activates both *p53* and *MDM2*, the last being an E3-ubiquitin ligase that promotes *p53* degradation. As a result, *MYCN* can either promote or repress apoptosis depending on an extremely sensitive equilibrium between *p53* and *MDM2* expression [10]. In addition to cell cycle progression and differentiation, metabolism is largely influenced by *MYCN*. The transcription factor is known to drive glutaminolysis and to directly regulate metabolic enzymes such as *LDHA* and *HK2*, in addition to regulate signalling pathways that are involved in metabolism, such as hypoxia or Akt/PI3K pathway. Also, the metabolism of polyamines, compounds involved in several cell functions, is strongly influenced by *MYCN*, which directly regulates the expression of the rate limiting enzyme of polyamine biosynthesis, *ODCI*. Notably, polyamine metabolism is sensitive to glutamine, whose concentration in the cell is influenced by *MYCN* itself [10, 12, 13, 160]. *MYCN* is also an important regulator of cell motility, especially during neural crest cell migration and metastasis invasion in neuroblastoma [8, 10]. Integrins  $\alpha 1$  and  $\beta 1$  are directly downregulated by *MYCN*, promoting cell detachment from the extracellular matrix. Similarly, *MYCN* can promote epithelial-to-mesenchymal transition by indirectly downregulating E-cadherin expression. Also, *MYCN* promotes cell migration by activating the expression of

important regulators of both integrin pathway and matrix metalloproteinases (*MMPs*) activity, such as focal adhesion kinase (*FAK*) and *BCL2* respectively [10]. At last, *MYCN* finds a role even in angiogenesis and immune surveillance. For example, it can either activate angiogenesis promoters (e.g. *angiogenin* and *VEGF*) via the PI3K/mTOR pathway or repress angiogenesis inhibitors (e.g. *LIF*, *Activin A* and *IL-6*), while the antigen *MCP-1/CCL2*, which is required for natural killer T cells chemoattraction, is typically downregulated by the oncogene [10, 12].

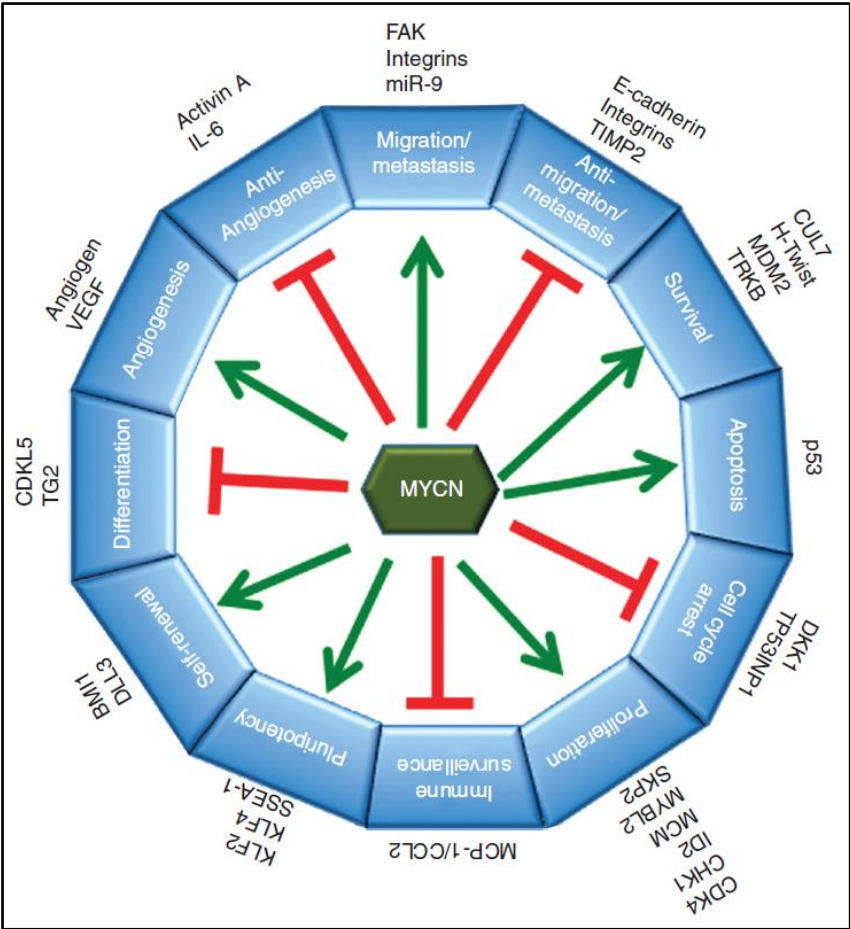


**Figure 6.** MYCN regulation network [10].

**MYCN and neuroblastoma treatment.** The association of *MYCN* amplification with the most aggressive stage of neuroblastoma can be clearly explained through the deep role of *MYCN* in maintaining the cells in an undifferentiated state and in promoting cell proliferation and motility. The importance of *MYCN* as neuroblastoma oncodriver led to the study of therapies targeting either *MYCN* itself or its transcriptional targets (Figure 7). Strategies directly

targeting MYCN protein expression, for example antisense-mediated gene knockdown, are proven to be a potential therapeutic option. However, the development of inhibitors of MYCN protein is challenging, since the protein structure has no obvious surfaces for small molecule binding. An alternative strategy might be the usage of chromatin-reader inhibitors which prevent MYCN to bind the target DNA. JQ1, as instance, is an inhibitor of BRD2-4, a bromodomain protein required for MYCN binding, and it is demonstrated to be a therapeutic option for neuroblastoma treatment [10]. Similarly, HDAC inhibitors, such as Cambinol or BL1521, can prevent MYCN to exert its repressor function. The mechanism regulating the stability of MYCN protein has also been exploited to define new therapeutic strategies. Indeed, MYCN stability is promoted by PI3K/mTOR-mediated phosphorylation, and inhibitors of the pathway, such as BEZ235, are demonstrated to be a feasible strategy to target *MYCN*-amplified tumours. Also, some inhibitors of Aurora kinase are now undergoing clinical trial. Targeting downstream mechanisms, rather than *MYCN* itself, represents an alternative option. For example, *MYCN*-amplified cells are sensitive to Nutlin-3 and MI63, antagonist drugs of MDM2 that can activate apoptosis [10, 12]. Cell cycle-related kinases, which include *CDK2*, *4*, *6* and *7*, are typically deregulated in *MYCN*-driven tumours and represent druggable targets for therapy [10, 161, 162]. Also, strategies targeting cell cycle regulators of Wnt pathway, such as *SKP2*, are currently tested [12].

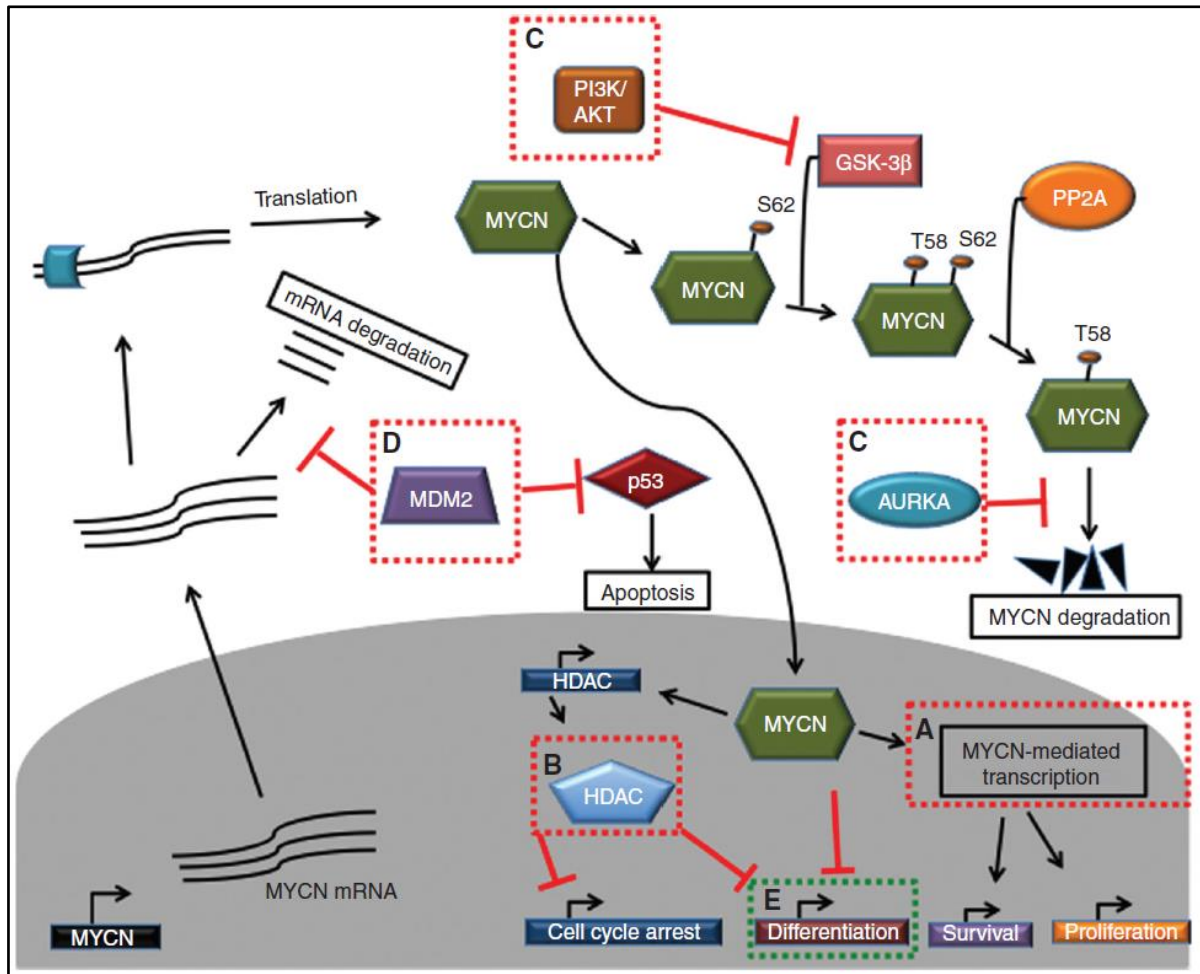


**Figure 7.** Therapeutic strategies targeting *MYCN* and its regulation network: (A) blocking *MYCN*-dependent transcription with BET-bromodomain inhibitors; (B) inhibiting HDACs; (C) targeting proteins involved in *MYCN* protein stability; (D) suppressing MDM2; (E) inducing differentiation [10].

## 2.2-*ODC1* and the prognostic significance of a single nucleotide polymorphism

***ODC1* and polyamine biosynthesis.** Ornithine decarboxylase 1 (*ODC1*) is the rate limiting enzyme of polyamine biosynthetic pathway. *ODC1* dimers catalyse the conversion of ornithine, the precursors of all polyamines, into putrescine, which is then converted into spermidine and spermine by spermidine synthase and spermine synthase respectively (Figure 8) [17].

Polyamines are ubiquitous small basic molecules found in almost all organisms, including bacteria, plants and animals, but putrescine, spermidine and spermine are the only polyamines produced by Mammals. Polyamines are demonstrated to be essential for physiological functions and viability in multiple organism, and to have a critical role in Mammalian development. As instance, *ODC* knockout in mice results to be lethal at early embryonal stage, while spermidine synthase knockout is lethal in yeast. However, because of the extensive interactive nature of polyamines, information about their molecular functions inside cells is far from being conclusive. Indeed, the strong positive charge at physiological pH makes polyamines capable of interacting with several macromolecules, including proteins, nucleic acids and phospholipid membranes. As a consequence of that, the free-polyamine content is a very small part of the total. Many studies demonstrated that changes of polyamine concentration have effects on expression of several genes, including *c-MYC* and *c-JUN*, while other studies evidenced also a role in translation modulation of specific mRNAs. It is inevitable to infer that polyamines can potentially affect a wide range of signalling pathways and cell functions, such as proliferation and differentiation. Indeed, high polyamine level strongly correlates with high cell proliferation and poor differentiation. At the same time, polyamines can also interact with ion channels, thus extending their involvement also to metabolism [18].

Given the importance of polyamines for a variety of cellular functions, their concentration inside the cell requires fine control. *ODC1* is obviously the first and most important regulation point. *ODC1* promoter contains three E-boxes, one -488 bp upstream of the TSS and the other two included in the first intron, respectively +287 and +321 bp downstream of the TSS (USCS assembly GRCh37/hg19, NM\_2539). The MYC/MAX complex is the main transcription activator of this gene, a mechanism that is typically observed in highly proliferative cells [18, 19]. On the contrary, the E-boxes are bound by the MNT/MAX complex and the gene is consequently repressed in quiescent cells [18]. *ODC1* is also regulated at protein stability level by two proteins, namely antizyme (AZ) and antizyme inhibitor (AZIn). The first protein, the expression of which is increased in response to high polyamine level, binds *ODC1* protein and mediates its inactivation and degradation via the 26S proteasome. The second protein binds AZ and prevents it from destabilizing *ODC1* [17, 18]. In addition to *ODC1*, the other enzymes of the polyamine biosynthetic pathway are also finely regulated, as much as the enzymes involved in the catabolic way. Furthermore, polyamine levels are controlled by uptake and efflux mechanisms, which involve non-specific membrane transporters. However, all the transporters involved in this process are not completely described [18].

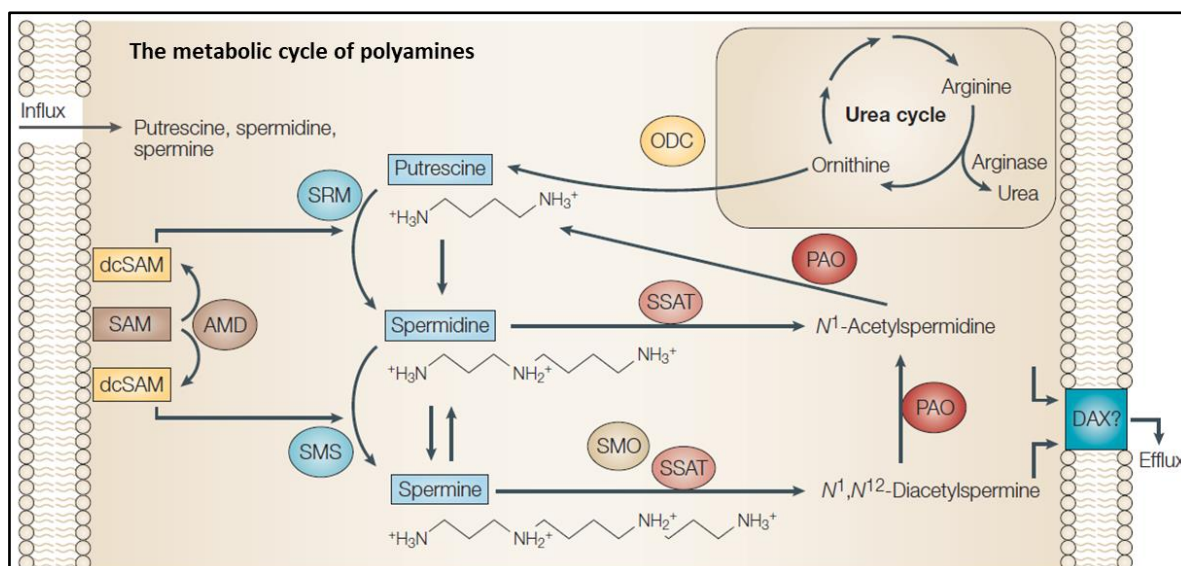


**Figure 8.** Polyamine metabolism in Mammals [21]. Ornithine decarboxylase (ODC), S-adenosylmethionine (SAM), S-adenosylmethionine decarboxylase (AMD), decarboxylated SAM (dcSAM), spermidine synthase (SRM), spermine synthase (SMS), spermidine/spermine N1-acetyltransferase (SSAT), diamine exporter (DAX), flavin-dependent polyamine oxidase (PAO), spermine oxidase (SMO).

***ODCI* involvement in cancer.** Much attention has been focused on polyamines since the '70, when they were associated with cancer for the first time [20, 21]. During the years, several types of cancer were associated with polyamine metabolism, including colorectal, skin, cervical, bladder, oesophageal, breast and prostate cancer (Figure 9). As for the physiological polyamine functions, high polyamine synthesis and levels strongly correlates with sustained cell growth and proliferation, as much as with aggressive cancer. Many factors can be responsible for increased polyamine synthesis and consequent poor prognosis, the most import among all being high *ODCI* expression and stability [18, 21, 22]. Indeed, *ODCI* is demonstrated to be an independent prognostic marker in many tumours, including colorectal cancer, lung cancer, breast cancer, prostate cancer, lymphoma and epidermal tumours [21, 22, 23, 24, 25, 26, 27, 28]. Only recent works demonstrated that high *ODCI* expression and polyamine levels are indicative of poor prognosis in neuroblastoma too. A study in 2008 first demonstrated that high *ODCI* expression is strongly associated with high proliferation rate in neuroblastoma cell lines and poor survival in neuroblastoma patients (Figure 9) [29]. High *ODCI* expression also correlates with high *MYCN* expression, which characterizes aggressive neuroblastoma. This is not surprising, since *MYCN* directly regulates the E-boxes located in *ODCI* promoter. Nonetheless, high *ODCI* expression is prognostic of poor survival also in

*MYCN*-non amplified tumours, thus confirming this gene as an independent prognostic marker [29, 30].

The importance of polyamine synthesis and *ODC1* expression in different types of cancer brought the scientific community to develop new targeted therapies. A first evidence that the polyamine synthesis pathway can be a therapy target came in the early '70, when methylglyoxal (bis) guanyldiazide (MGBG), a drug used for leukemia treatment, was found to inhibit S-adenosylmethionine decarboxylase (AMD), an enzyme involved in polyamine biosynthesis (Figure 8). Following this first discovery, different drugs targeting polyamine-related enzymes were developed, including inhibitors of AMD and flavin-dependent polyamine oxidase (PAO) (Figure 8). However, difluoromethylornithine (DFMO), an irreversible inhibitor of ODC1, is so far the most widely studied drug for cancer treatment (Figure 9). DFMO immediately showed a strong capability to inhibit polyamine synthesis and cell proliferation *in vitro*, in addition to low toxicity and favourable pharmacokinetic properties in animal models. Unfortunately, clinical trials demonstrated a general ineffectiveness of DFMO in tumour suppression, which is not surprising since the drug blocks cell proliferation but it is not cytotoxic [17, 21, 22]. This brought the DFMO to be applied as a chemopreventive agent in those patients that are found to be at risk, and, nowadays, DFMO is in clinical trial for treatment of different types of cancer [21-28]. More precisely, DFMO is currently in phase 3 clinical trial for treatment of colon, bladder and skin cancer, while it is in phase 2 trial for prostate, cervical, gastric and oesophageal cancer [*ClinicalTrials.gov*]. Only in 2008, when *ODC1* expression was first correlated with neuroblastoma prognosis, DFMO was evaluated for neuroblastoma treatment. As for other cancer types, DFMO demonstrated to inhibit proliferation of neuroblastoma cell lines *in vitro*, but did not appear to have substantial effects in mouse model. However, DFMO was found to enhance chemotherapy efficiency and to increase relapse-free survival of the treated mice [29]. Recently, a phase 2 trial was successfully completed, demonstrating that DFMO increases survival in high-risk neuroblastoma if applied as single agent during the maintenance therapy [163]. These findings hastened research to more deeply explore the involvement of polyamines and *ODC1* in neuroblastoma. Along this line, recent studies demonstrated that multiple enzymes of polyamine metabolism are predictive of outcome, and further confirmed the leading role of *ODC1* in neuroblastoma aggressiveness and its importance as a therapeutic target [31, 32].

### Examples of cancer treatment via DFMO administration

Cancer	Preclinical evidence for activity	Supportive evidence from pilot/Phase I/Phase II trials <sup>‡</sup>	Target	Definitive or pivotal randomized trials
Colorectal	Strong	Strong	Polyps	DFMO and sulindac <sup>  </sup> ; accrual 75% complete
Colorectal	Strong	Strong	Polyps	DFMO and celecoxib <sup>  </sup> ; accrual ongoing
Skin	Strong	Strong	Actinic keratosis	DFMO; accrual complete
Cervical	Moderate	Moderate	Cervical intraepithelial neoplasia	DFMO; accrual ongoing
Bladder	Moderate	Moderate	New squamous-cell carcinoma	DFMO; accrual complete
Oesophageal	Moderate	None	Barrett's oesophagus	–
Breast	Weak	None	Surrogate markers of breast cancer	–

### ODC1 involvement in neuroblastoma outcome

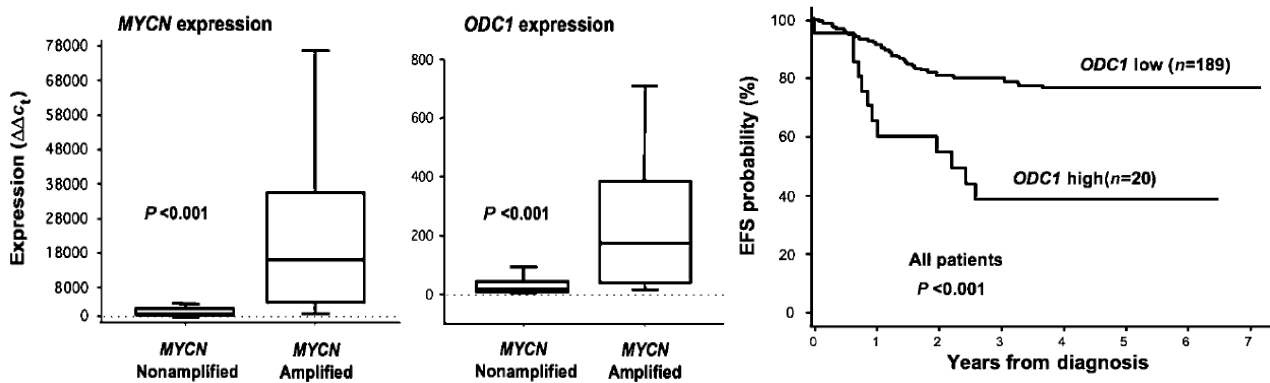


**Figure 9.** Top panel: examples of cancers treated by DFMO and relative efficiency in preclinical and clinical trial [21]. Bottom panel: experimental results demonstrating correlation between *MYCN* and *ODC1* expression (left) and prognostic significance of *ODC1* expression in a cohort of neuroblastoma patients [29].

***ODC1* promoter and +316 A/G SNP.** Given the deep involvement in polyamine metabolism and disease outcome, regulation of *ODC1* gene expression is a focal aspect of cancer development. In 1989 two different *ODC1* alleles were discovered, distinguished by a single nucleotide polymorphism (SNP) A/G located +316 bp in *ODC1* locus (+316 A/G SNP, GRCh37/hg19, NM\_2539) (Figure 10) [33]. The SNP, which is found in the population with an incidence of ~56% GG, ~37% AG and ~7% AA, was later demonstrated to influence *ODC1* transcription, with the A allele associated to reduced expression in a reporter assay experiment performed in mouse NIH 3T3 cell. The same study also demonstrated that when the reporter

assay is performed in a rat cell line with inducible *c-MYC* expression (YY8ME4), the A allele is significantly more activated by *c-MYC* induction than the G allele [34]. This result was not surprising, because +316 A/G SNP is located in the first intron of *ODCI* gene, exactly 5 bp upstream of the third E-box and 24 bp downstream of the second E-box (Figure 10), and binding of the c-MYC/MAX complex to E-boxes is notoriously affected by the flanking sequences. This condition is also observed for the MAX/MAX complex and can be potentially valid for any of the E-box interactors [35, 36]. Indeed, a second study in 2003 demonstrated that induction of *MAD1* expression in human colon cancer cells (HT29) reduces the expression of an A-allele reporter gene much more greatly than a reporter with the G allele [37]. The same study and a further one also found that the AA genotype is associated with decreased recurrence of colon adenoma in patients that take aspirin for chemoprevention [37, 38]. In apparent contrast to this last evidence, another study correlated poor survival of colorectal cancer patients with the presence of at least one A allele (meaning either AG or AA genotype). However, the same study demonstrated that both c-MYC and MAD1 preferentially bind the A allele in colon cancer cells (HT29 and HCT116), which is consistent with the previous results [39]. Colorectal adenoma recurrence was also positively associated with the A allele after DFMO treatment [40]. At last, a study in 2015 demonstrated that the GG genotype is prognostic of survival in breast cancer patients. It also demonstrated that c-MYC and MAD1 preferentially bind the A allele in human breast cancer cells (MCF-7, MDA-435) [41]. Overall, these studies show not an obvious role of +316 A/G SNP in cancer prognosis, with even contradictory results. Indeed, while the A SNP is associated with worse prognosis and/or recurrence in colorectal and breast cancer, it is also associated with decreased recurrence in colorectal cancer patients that take aspirin as chemoprevention, and, interestingly, a recent study demonstrated that aspirin impairs *c-MYC* expression in colon cancer cells [115]. This finding confirms the strong dependence of the SNP function on the expression pattern of transcription factors. Besides, almost all the studies consistently demonstrate a major binding capacity and transcription regulation activity of c-MYC and MAD1 towards the A allele. Given the opposite functions of these two factors, the first being an activator and the second a repressor, the effect of the allele genotype on *ODCI* expression, and consequent disease outcome, likely depends on the genetic background.



some homology to human TBP-associated factor 130, but its specific function is still not clear [42, 43]. NHR2 is a small domain containing a hydrophobic heptad repeat, which is found to be essential for homodimerization or heterodimerization with the co-repressor mSin3A or other ETO members [42, 43, 46-48]. NHR3, characterized by an alpha-helix structure, does not have any remarkable function, except for a partial role in protein-protein interaction [42, 43, 47]. The C-terminal domain, NHR4, contains two zinc-finger motifs, and, even though there is no experimental evidence of DNA-binding properties, it is fundamental for *RUNX1T1* repression activity. Actually, NHR4 mediates the interaction with transcription-repression factors such as N-CoR, SMRT and histone deacetylases (HDAC1, 3, 4, 5, 7) [42, 43, 46-48]. Consistently with a nuclear-specific role, *RUNX1T1* protein preferentially localizes in nuclear speckles known as *ETO nuclear bodies* (ENB) (Figure 11), where it is also found to co-localize with Atrophin-1 [42, 45, 53]. According to the most recent model, NHR2 and NHR4 together define the *core repressor domain* of *RUNX1T1*, which assembles with mSin3A, N-CoR, SMRT and HDACs to mediate the formation of a high-molecular-weight corepressor complex (300-600 KDa). The protein complex is supposed to direct chromatin remodelling and transcription repression (Figure 11) [42, 43, 46-48]. Although *in vitro* studies demonstrated the formation of such complex and its transcription-repression activity, neither the physiological existence of the complex nor the specific functions have been completely elucidated [42, 43, 47, 48]. In addition, according to the corepressor model, *RUNX1T1* needs to interact with DNA-binding proteins in order to exert the repression function. Despite DNA-binding factors such as PLZF, Gfi1 and Bcl6 are demonstrated to recruit *RUNX1T1* and its repression function to specific target genes, the complete targetome of this factor is not already defined. Indeed, *omic* knowledge based on RNAseq and ChIPseq data is still missing, and chromatin immunoprecipitation directed toward this protein is made hard-to-achieve by the lack of direct DNA binding [42, 43, 47-51].

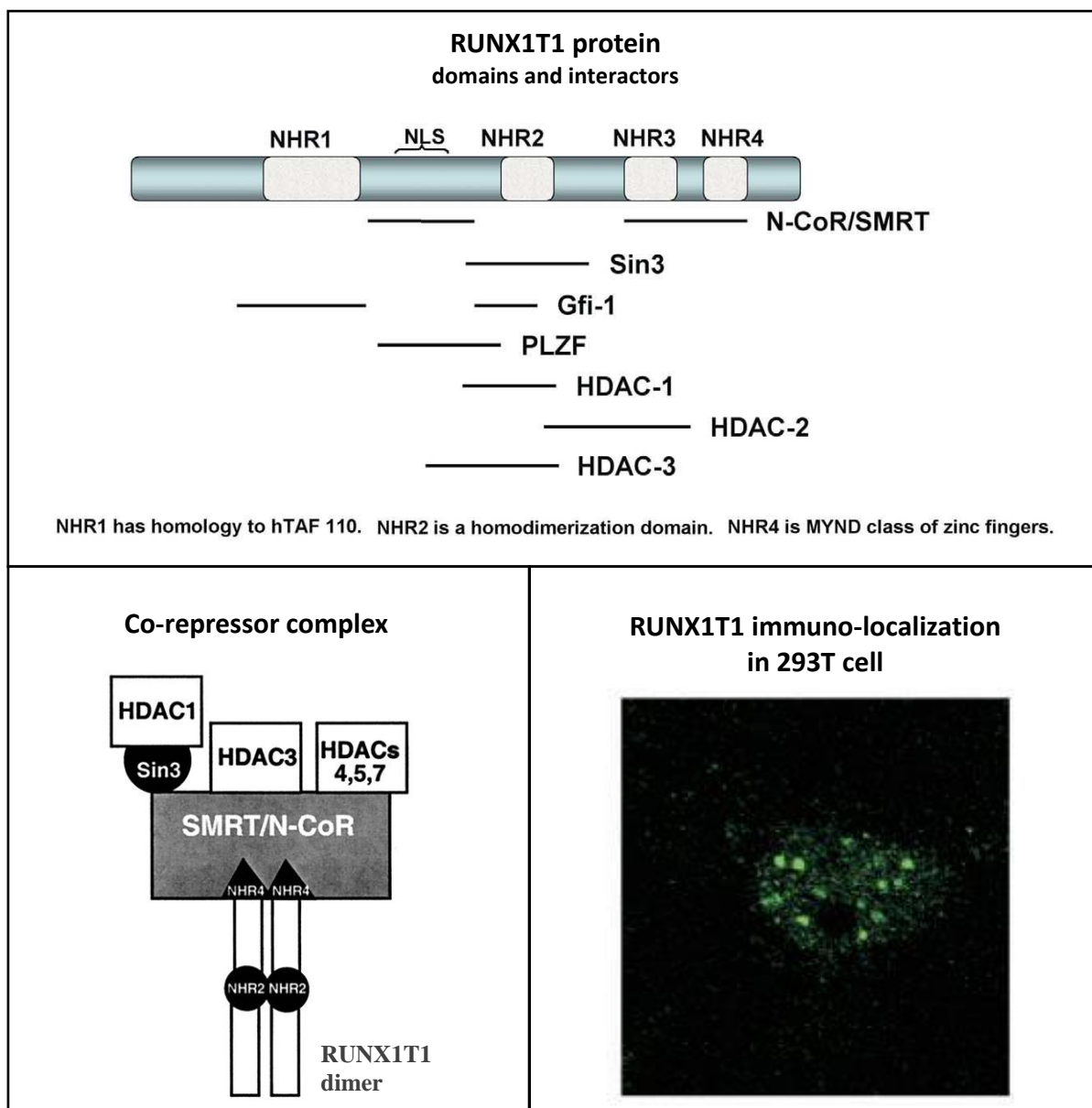


**Figure 11.** Top: graphical representation of RUNX1T1 protein domains and interactors [42]. Bottom-left: a model of the co-repressor complex [46]. Bottom-right: RUNX1T1 immuno-localization in 293T cells [51]; *ETO nuclear bodies* are visible in immunostaining.

***RUNX1T1* involvement in development and cancer.** Little is known about *RUNX1T1* role in cell functions or physiological processes. The gene caught the attention of researchers for the first time when it was found to be directly involved in the development of acute myeloid leukemia. Approximately 12-15% of all acute myeloid leukemia cases are characterized by the translocation t(8;21), which involves the formation of a fusion gene between *RUNX1T1* and *AML-1*, also known as *ALM1-ETO*. The resulting fusion protein, termed as AML-1/ETO,

contains the DNA binding domain of AML-1 and the C-term portion of RUNX1T1, which is supposed to function as a transcription corepressor. As a consequence, AML-1/RUNX1T1 deregulates a series of genes that, in co-occurrence with additional mutations, induce the development of acute myeloid leukemia [42, 52]. Specifically, AML-1/ETO is demonstrated to interfere with Notch signalling, a mechanism that is suggested to be fundamental for acute myeloid leukemia insurgence [54]. In the following few years, the expression status of *RUNX1T1* was associated to different pathological conditions (Figure 12). For instance, copy gains of *RUNX1T1* gene are correlated with insurgence of malignant mesothelioma [55]. An analysis of bladder cancer samples demonstrated that upregulation of *RUNX1T1* might be associated with tumour progression [56]. In contrast to the idea of *RUNX1T1* as tumour promoter, the gene is demonstrated to be a potential ovarian cancer suppressor in separate studies [57, 58]. Also, an increase in *RUNX1T1* expression is correlated with decrease of glioblastoma aggressiveness [59], and, consistently, low *RUNX1T1* expression is found to be predictive of pancreatic metastases [60].

Parallel studies demonstrated that *RUNX1T1* also has a direct role in development (Figure 12). Adipogenesis is probably the most studied developmental process in which *RUNX1T1* is involved. Several studies evidenced that *RUNX1T1*, usually upregulated in undifferentiated adipocytes, is able to repress pro-adipogenesis genes [61-64]. The mechanism that is suggested to explain such role in adipogenesis involves the direct inhibition of *C/EBP $\beta$*  activity and a consequent downregulation of *C/EBP $\alpha$* , a fundamental adipogenesis promoter [61]. *RUNX1T1* is also associated to development of different nervous tissues, as well as to development disorders of the nervous system. Specifically, overexpression of *RUNX1T1* is detected in differentiating radial glial cells of the hippocampus and in activated microglia during development, in addition to tissues of patients affected by autism spectrum disorders [65-68]. However, adipose and nervous tissues are not the only ones where *RUNX1T1* has a functional role, since different studies demonstrated that the gene promotes development of the gut and the pancreas, as well as angiogenesis [69-71]. Furthermore, *RUNX1T1* is among a series of 8 genes that, when co-transfected, induce dedifferentiation of prolymphocytes into multipotent haematopoietic stem cells [72].

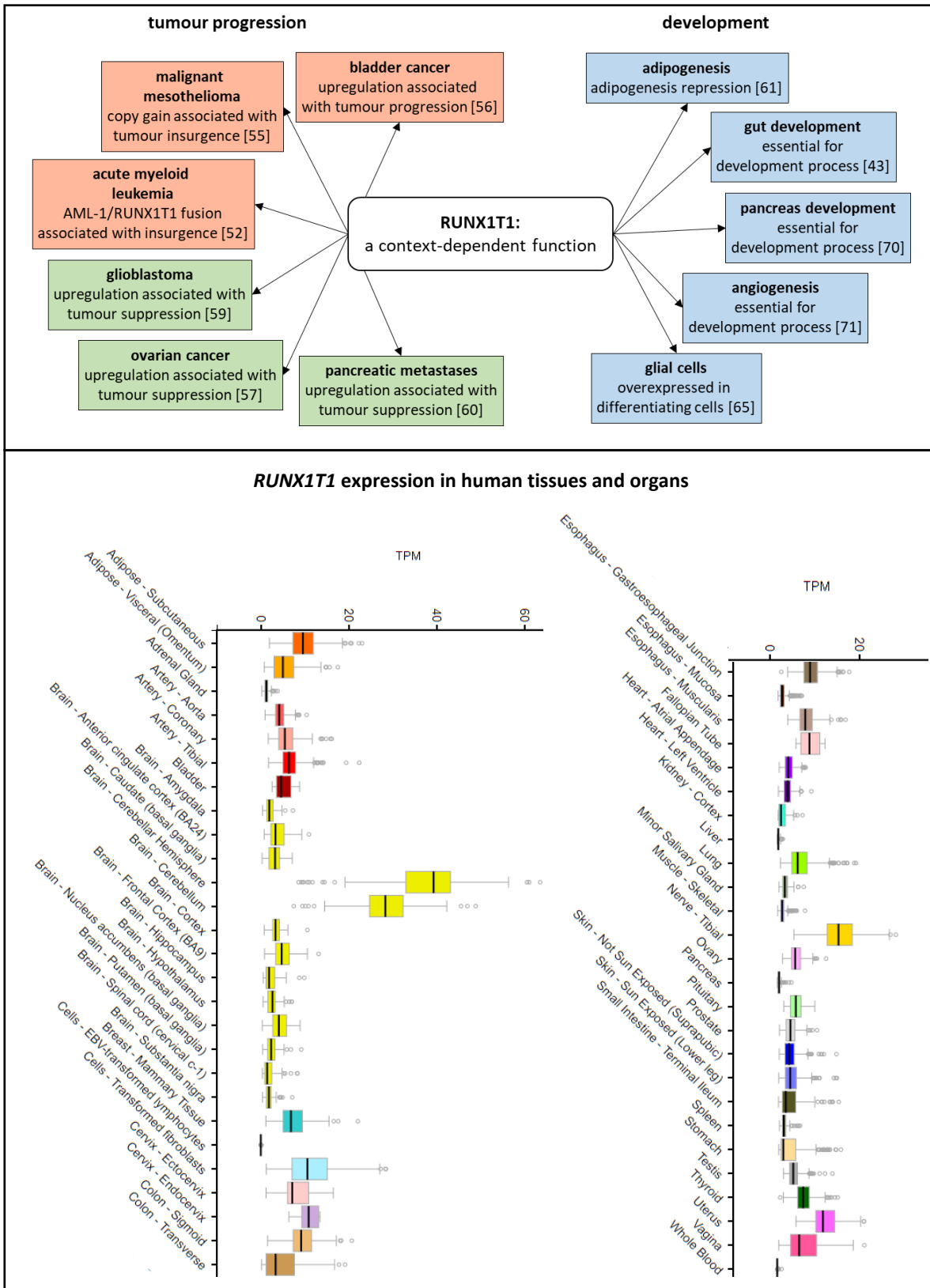


**Figure 12.** Top panel: schematic representation of RUNX1T1 involvement in different case studies of tumour progression and tissue development. Bottom panel: *RUNX1T1* expression in human tissues and organs by *GTEX*; note the significant expression in cerebellum (yellow).

To summarize the previous paragraphs, *RUNX1T1* is a leading player in physiological tissue development, and an important contributor to specific human diseases, including cancer. For example, *RUNX1T1* translocation promotes acute myeloid leukemia, and gene upregulation is predictive of malignant mesothelioma and bladder cancer. On the other hand, the same gene acts as tumour suppressor in ovarian cancer, glioblastoma and pancreatic metastases. In the development context, *RUNX1T1* is upregulated in undifferentiated adipocytes, but it also promotes differentiation of glial cells and other lineages. Overall, the role of *RUNX1T1* in insurgence of specific diseases and development processes seems to be context-dependent. Further complexity derives from the fact that the mechanism behind *RUNX1T1*-mediated transcription regulation is not perfectly clear, while *RUNX1T1* regulon is almost completely unknown. So far, no study has ever been associated with *RUNX1T1* in neuroblastoma or to neural crest development. However, given the robust and wide involvement of this gene in a large variety of disease and development conditions, it is reasonable to hypothesize a role in an embryo-originated tumour such as neuroblastoma. In addition, *RUNX1T1* expression is already associated with development of neural lineages, and, notably, both *RUNX1T1* and *MYCN* are among the 8 genes that, when co-transfected, can dedifferentiate prolymphocytes into multipotent haematopoietic stem cells. This last evidence suggests a possible interaction between the regulation networks of the two factors.

### **3-The CRISPR technology: from genome editing to *genetic surgery***

Only a few discoveries shocked the scientific world in the last decades as much as CRISPR did. Originally discovered in 1987 in Prokaryotes, the CRISPR system is now routinely used as genome editing tool in a wide range of biological systems. The main contribution of this editing technology is relative to reverse Genetics, making the study of genetic traits much more accessible and reliable than before. Nonetheless, CRISPR technology is also employed for a variety of other functions due to extreme flexibility and efficiency [80-82].

**Origin and mechanism of CRISPR technology.** The CRISPR system originates from Prokaryotes, in which it functions as an immune-like system (Figure 13). It basically consists of genomic repeats (Clustered Regularly Interspaced Short Palindromic Repeats, or CRISPR) interspaced by short sequences that derive from exogenous DNA (or RNA). This, which originally could be either viral or plasmidic, is recognized by a complex nuclease apparatus and converted into small fragments (about 20 bp long) during a first contact. The fragments are then inserted into specific genomic arrays, spanning between already existing repeats. During a second encounter, the single fragments are transcribed along with the adjacent repeat in order to generate a so-called guide RNA (gRNA). At last, designated nucleases, known as Cas, interact with the repeat-sequence scaffold, incorporate the gRNA, and eventually cleave the exogenous nucleic acid after annealing via the gRNA itself. Interestingly, this system has developed a strategy to avoid self-targeting of the exogenous sequences included into the CRISPR arrays. It is based on short sequences called PAM (protospacer adjacent motif) that are necessary for the Cas protein to recognize the target, but that are not included in the fragments inserted into the CRISPR arrays. Overall, 2 classes, 6 types and 19 sub-types of CRISPR systems are known across Bacteria and Archaea. The 2 classes mainly differ in the Cas nucleases and their targets: class I systems (including type I, III and IV) employ multiple Cas proteins to target both double-stranded DNA (dsDNA), single-stranded DNA (ssDNA) and RNA; class 2 systems (including type II, V and VI) employ a single Cas protein and mainly target dsDNA [80-82, 126].

About 25 years after the discovery, the CRISPR system was adapted for precise editing of genomic DNA in living organisms, mainly Eukaryotes. The editing strategy is based on two different phases and respective mechanisms. First, the nuclease activity of a Cas protein is

directed, via a properly designed gRNA, toward a target DNA sequence in order to generate a DNA break. Second, the endogenous DNA-repair system of the organism is exploited, and occasionally re-directed, to repair and edit the target sequence [80-82]. The first system to be adapted in this way, and the most currently used, is CRISPR-Cas9 from *Streptococcus pyogenes* (SpCas9), belonging to type II (Figure 13). SpCas9 is a 1367 aa protein composed of two large domains with nuclease activity, RuvC and HNH. The enzyme interacts with a gRNA long about 40 nt, with the 19-21 nucleotides at the 5'-end being complementary to the target sequence, and the others generating a secondary structure functioning as scaffold for the interaction with Cas9 [80-82, 126]. The assembled ribonucleoprotein was observed to investigate the genome via continuous collisions (61 collisions/second) in search of the target sequence [127, 128]. Once Cas9 finds a PAM, it pauses, allowing the gRNA to interrogate the surrounding region. If the target sequence is recognized, Cas9 generates an R-loop structure, where the gRNA is annealed to the strand known as *target* (the complementary being the *non-target*). The PAM 5'-NGG-3', located downstream of the *non-target* sequence, is fundamental for Cas9 interaction with the target DNA. Importantly, the 8 PAM-closest nucleotides, which constitute the *seed region*, are demonstrated to be essential for recognizing the target sequence, since eventual mismatches would prevent the annealing to be completed. Once the R-loop is formed, Cas9 induces a double-strand break (DBS) exactly 3 bp upstream of the PAM, with the RuvC and the HNH domain cleaving the *non-target* and the *target* strand respectively [80-82, 126]. After cleavage, the PAM-distal end is immediately released, while Cas9 remains bound to the PAM-proximal end for up to 5.5 hours [124, 128]. Complete release of the cleaved site is then followed by activation of the endogenous DNA-repair systems. CRISPR-Cas9 is not the only system to be used for genome editing. As instance, a type V Cas nuclease, Cpf1, was also adapted from *Lachnospiraceae bacterium* (LbCpf1) and *Acidaminococcus species* (AsCpf1) for this purpose (Figure 13). Cpf1 has some differences compared to Cas9. It assembles with a scaffold sequence 19 nt long and located at the 5'-end of the gRNA, while the sequence complementary to the target is 23-25 nt long and located at the 3'-end; in this case, the *seed region* includes the 19 nucleotides located at the 5'-end of the target sequence. The PAM sequence is 5'-(T)TTN-3' and it is located upstream of the *non-target* strand. The cut induced by Cpf1 is a 5 nt-staggered DNA break, with the nicks on the *non-target* and on the *target* strand located 18 and 23 nt downstream of the PAM respectively (5'-overhanging ends). Generally, Cpf1 is found to be slightly less efficient than Cas9 [129].

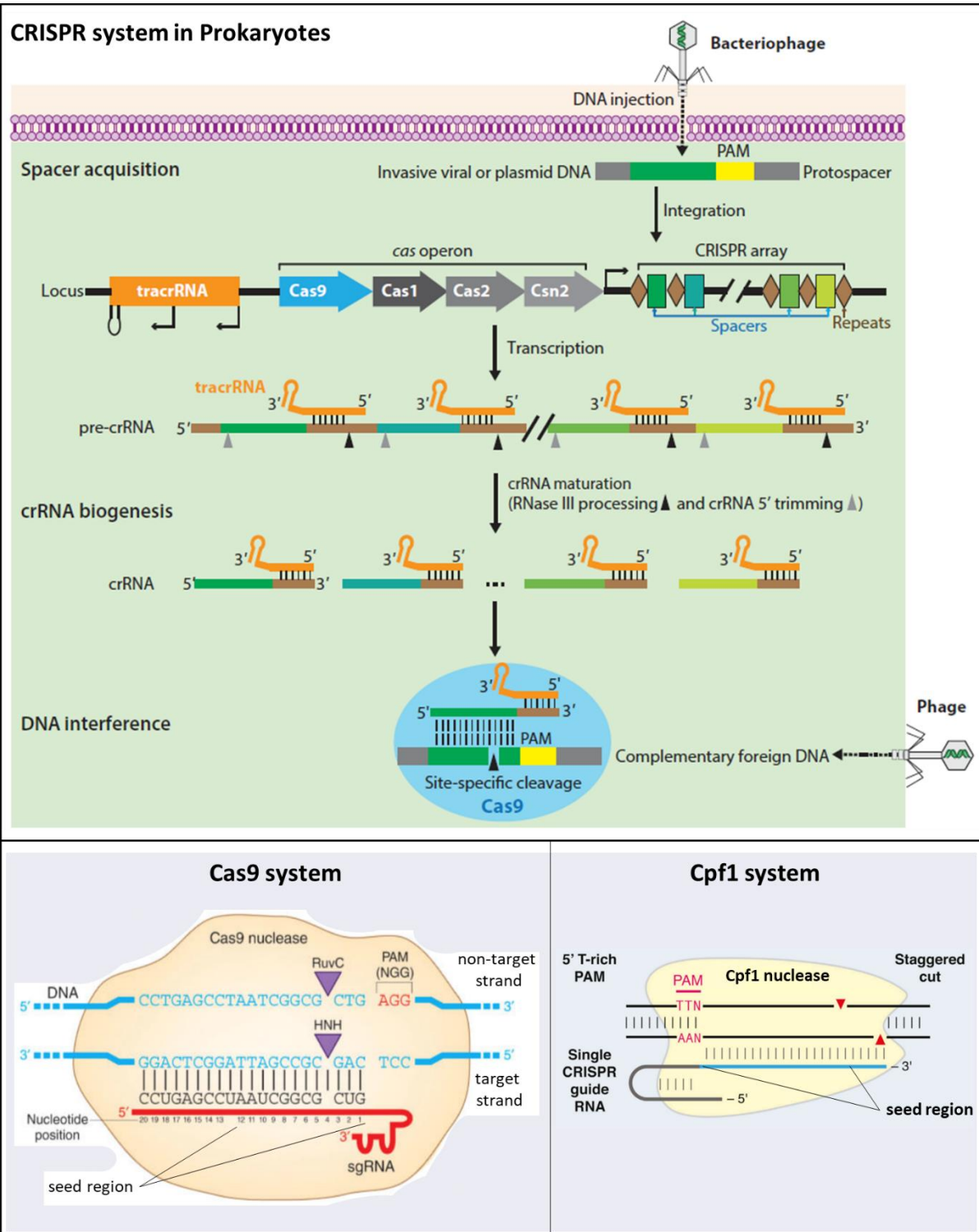


**Figure 13.** Top panel: example of the original CRISPR system working for immune-like defence in Prokaryotes [127]. Bottom panels: representation of the genome editing systems based on Cas9 (left) [82] and Cpf1 (right) [129].

The second phase of genome editing, following induction of a targeted DNA break via a Cas nuclease, involves the intervention of the endogenous DNA-repair systems. In Eukaryotes, the two main systems are non-homologous end joining (NHEJ) and homology-directed repair (HDR). Their respective mechanisms are significantly different, as much as the function they are exploited for (Figure 14) [80-82, 127, 129]. NHEJ machinery is activated following a DNA break with the purpose of re-joining the broken ends. The DSB is first recognized and bound by a factor (*Ku*) that subsequently recruits a nuclease (*Artemis*), a DNA-polymerase (*Pol $\lambda$* ) and a DNA-ligase (*DNA-ligase IV*) in a non-determined order. Then, nuclease and/or polymerase activity produces random deletions, insertions or insertion/deletions (*indel*) of a few base pairs, until the ligase repairs the break [131]. The result is the possible introduction of random mutations into a Cas-gRNA target site. This possible variant of CRISPR editing is now the most efficient and precise method for production of knockout mutations in living organisms [80-82, 127, 129]. NHEJ-mediated editing can also be employed to delete large genomic regions. For this purpose, it is sufficient to target, via Cas cleavage, two distal sites flanking the region to be deleted. Consequently, the NHEJ machinery could join the two distal broken ends with an efficiency that mainly depends on the region size and the chromatin structure [134]. In alternative to NHEJ, genome editing via HDR is used to introduce customized mutations into a target sequence, although this editing strategy is far less efficient and utilized than the previous one. HDR is the cellular mechanism usually intervening to repair a DSB via recombination. In this system, the broken DNA ends are first bound by a protein complex (MRN in Mammals) that provokes resection of the 5'-ends (up to 50 Kb) via recruitment of nucleases (*CtIP*, *Exo1* and *BLM*). Then, proteins such as *Rad51* and *Rad52* drive the resulting 3'-overhanging ends in search of a homologous sequence. Once the homology is found, the sequence is used as template for reconstruction (via *Pol $\delta$* ) of the resected region starting from the 3'-ends (up to 2 Kb of newly synthesized DNA from each end). Eventually, the original DSB could be repaired with 3 different outcomes: the newly synthesized sequence replaces the resected ends in a process called synthesis-dependent strand annealing (SDSA); formation of a *Holliday junction* is resolved through crossover and consequent recombination between the homologous sequences in a process called double-stranded break repair (DSBR); in case the homologous sequences are located on the two sides of the DSB, they are joined with consequent deletion of the included region, in a process that is called microhomology end joining (MMEJ) for sequences up to 25 bp long, or single-strand annealing (SSA) for longer sequences [132, 133]. Occurring of SDSA and DSBR is fundamental for CRISPR editing via HDR. In this case, an exogenous donor-DNA (dDNA) is introduced in the system to function as homologous template

for re-directed reconstruction of the target sequence (knock-in). The dDNA must carry two arms homologous to the target sequence (about 500 bp long each) and flanking a custom mutation to be introduced into the target site (up to 2 Kb long insertion). Utilization of a single-stranded dDNA (ssODN) is usually more efficient, as long as it contains 50 nt-long homology arms and small mutations, as it is complementary to the *non-target* strand [80-82, 124, 125, 127, 129, 130]. Currently, NHEJ and HDR are the two main strategies adopted for application of the CRISPR technology in genome editing, and they proved to be reliable editing systems in a wide range of organisms (from cell cultures to plants and Mammals) [80-82, 127].

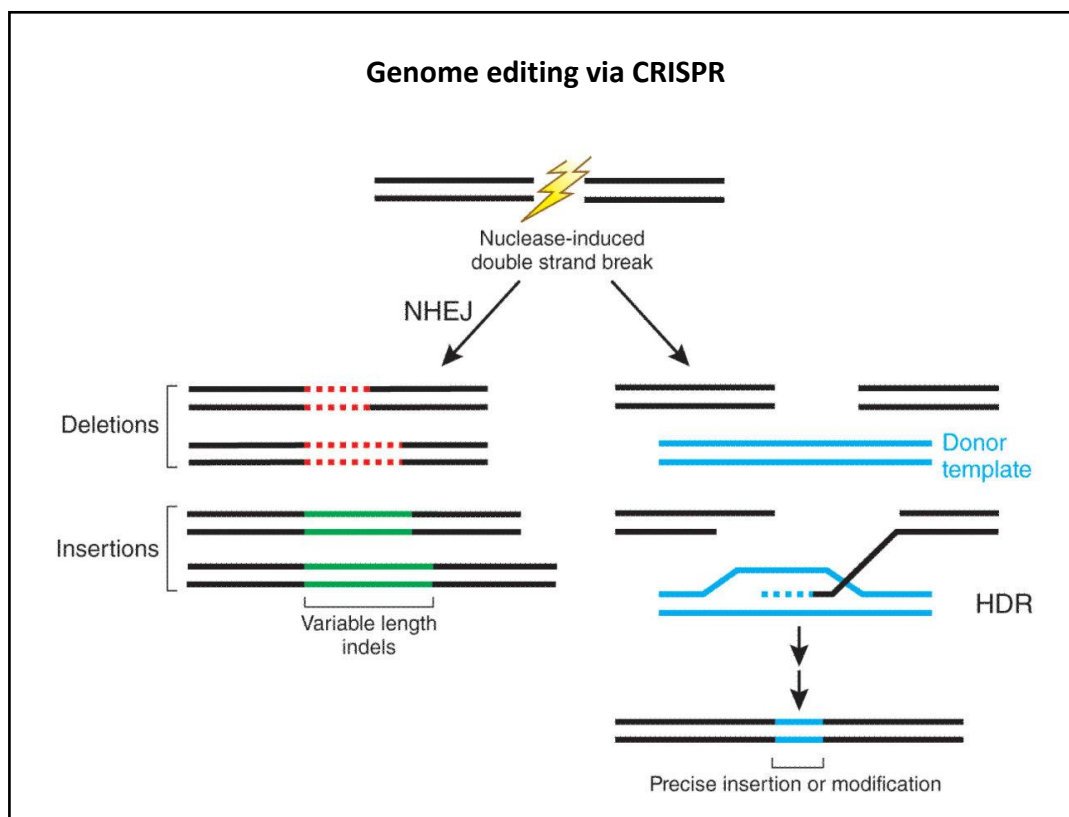


**Figure 14.** Application of CRISPR technology for genome editing via NHEJ (left branch) or HDR (right branch) [82].

**Limitations, improvements and applications of CRISPR technology.** Despite the undeniable success of CRISPR, the technology is relatively young, and it is affected by some limitations. First among all aspects, off-target activity is a great issue of this technology. It is due to the capacity of the gRNAs to anneal target sequences regardless the presence of

mismatches, therefore bringing the Cas nuclease to cleave off-target sites. This significantly undermines precision and reliability of the editing system. Obviously, the higher is the number of mismatches, especially if included in the *seed region*, the lower is the probability to cut the off-target. Prior to editing, a proper gRNA design is essential, preferentially selecting gRNAs with the lowest number of off-targets and, at the same time, the highest number of mismatches for the most probable off-targets. Also, shorter gRNAs (17-18 nt) are demonstrated to have lower off-target activity. A number of different software tools are now available for comprehensive gRNA design [80-82, 127, 135, 136]. An alternative strategy that is usually adopted to overcome the off-target problem involves the employment of already-assembled ribonucleoproteins (RNPs) instead of plasmids expressing Cas9-gRNA, since RNPs have a shorter half-life and, hence, lower probability of off-targeting [80, 124, 125, 130]. Also, a Cas9 variant called nick-Cas9 (nCas9), and resulting from point mutations inactivating either the RuvC (D10A variant) or the HNH domain (H840A variant), represents a valid strategy. nCas9 can only produce single-strand nicks instead of DSBs, and, consequently, it cannot induce any mutation at the off-target sites. The DSB in the target sequence is here induced by designing a couple of gRNAs targeting two sequences located 15-50 bp apart on the opposite strands, thus producing a staggered DSB. This strategy, known as *double nicking*, revealed to be extremely accurate, but it is relatively inconvenient due to complex design and low probability of a double nick. However, selection of gRNAs with external PAMs (*PAM-out* configuration) and producing 5'-overhanging ends is demonstrated to improve the efficiency [80, 124, 125, 130]. At last, a series of Cas9 variants were recently improved in order carry low off-target activity. The most efficient to be developed so far, named HypaCas9, carries mutations that make the nuclease domain activation possible only if the alignment between gRNA and *target* strand is perfect [137].

A second main limitation of CRISPR technology is the relative low efficiency of HDR-mediated editing. In an experimental context, from 40 to 90% of cells transfected with a CRISPR system results NHEJ-edited, while only 1 to 10% results edited via HDR. There are two main reasons at the base of this imbalance: higher complexity of HDR-editing; a competitive relation between the NHEJ and HDR factors in recognizing DSBs, competition that favours NHEJ in a ratio 9:1. Additionally, HDR-editing of more than one allele in the same genome is even more improbable (10% of total HDR-editing) [124, 125, 130-133]. As a basic approach, HDR efficiency can be improved by using properly designed dDNAs (better if asymmetric ssODNs), and by using Cas9 and gRNAs already-assembled into ribonucleoproteins (higher transfection efficiency) [80, 124, 125, 130]. Competition between

NHEJ and HDR can be bent in favour of recombination by using NHEJ-inhibitors [139] and/or HDR-enhancers [140]. Also, double-nick editing via nCas9 improves HDR, especially if 5'-overhanging ends are generated. These are easily processed by the HDR machinery in order to create 3'-overhanging ends suitable for recombination [80, 124, 125, 130]. Interestingly, HDR-editing is possible even with a single nick, which could be explained if the nick itself is converted into a DSB. Such a possibility, nonetheless, would question nCas9 incapability to cleave off-targets [124, 125, 130, 138]. Similarly to double-nick editing, production of staggered ends via Cpf1 is demonstrated to increase HDR efficiency [129]. At last, a new strategy was developed to precisely edit single bases. It relies on Cas9 variants fused to enzymes that directly modify the nucleotides. The most used variant is composed of an inactive Cas9, carrying both D10A and H840A mutation (also known as dead-Cas9, or dCas9), fused to a cytidine-deaminase that converts a C:G into a T:A [141]. Despite all improvements, the current state of the art is still far from a definitive strategy for efficient HDR-editing.

In the last few years, improvement and deeper knowledge of CRISPR technology brought to the development of new applications for a variety of purposes. The inactive dCas9 can be fused to any possible protein for integration of a large number of functions. For example, fluorescent proteins (i.e. GFP or RFP) can be fused to dCas9 in order to visualize specific genomic loci [142] or to track RNA molecules [143] in living cells. dCas9 can also be fused to transcription regulators and epigenome editors, such as VP64, p65 or p300 for transcription activation [144], or KREB, Dnmt3A or HDAC for repression (also known as CRISPR interference, or CRISPRi) [145]. Cas9 variants regulating gene expression are currently evaluated and tested for circuit building in Synthetic Biology [146]. Another relevant research application of CRISPR is represented by gRNA libraries that are employed to screen genes of interest in specific biological conditions [147]. In a more visionary prospect, several research groups are currently studying CRISPR technology as a tool for curing genetic diseases through what is generally called *genetic surgery*. In support, *in vivo* application of CRISPR editing via viral delivery has already succeeded in mouse and dog models (Figure 15). In some of these cases, the mutation occurring in *DMD* gene and leading to dystrophy was corrected with positive outcome [148-150]. However, no study involving CRISPR application to human patients has been completed so far. In addition, the scientific community is concerned about side effects such as off-targeting and immunity response. Recent studies indeed evidenced that the human immune system is reactive to Cas9 protein, as it would be expected for any protein with bacterial origin [164]. In alternative to direct delivery of Cas9 components to patients, a research group recently employed the CRISPR technology to improve primary T cells for

immunotherapy [165], and some ongoing clinical trials are now aimed to employ the same technology for treatment of non-small lung cell cancer, bladder cancer, prostate cancer and renal cell cancer [*ClinicalTrials.gov*]. In another attempt to find a clinical application of CRISPR, human embryos were genetically manipulated to overcome the inheritance of Mendelian diseases, but all the studies completed thus far were limited to early stage embryos [166]. At last, a further *in vivo* application of CRISPR is *gene drive* for population control. A representative case study was conducted in mosquito populations with the aim at reducing malaria diffusion. The technology relies on introduction into selected individuals of a Cas9-based system that makes the females sterile once the gene is spread through mating [151]. In conclusion, considering the outstanding efficiency of CRISPR editing and the wide range of possible applications, it cannot be excluded that this tool is going to play a leading role during the upcoming years of scientific and technological research.

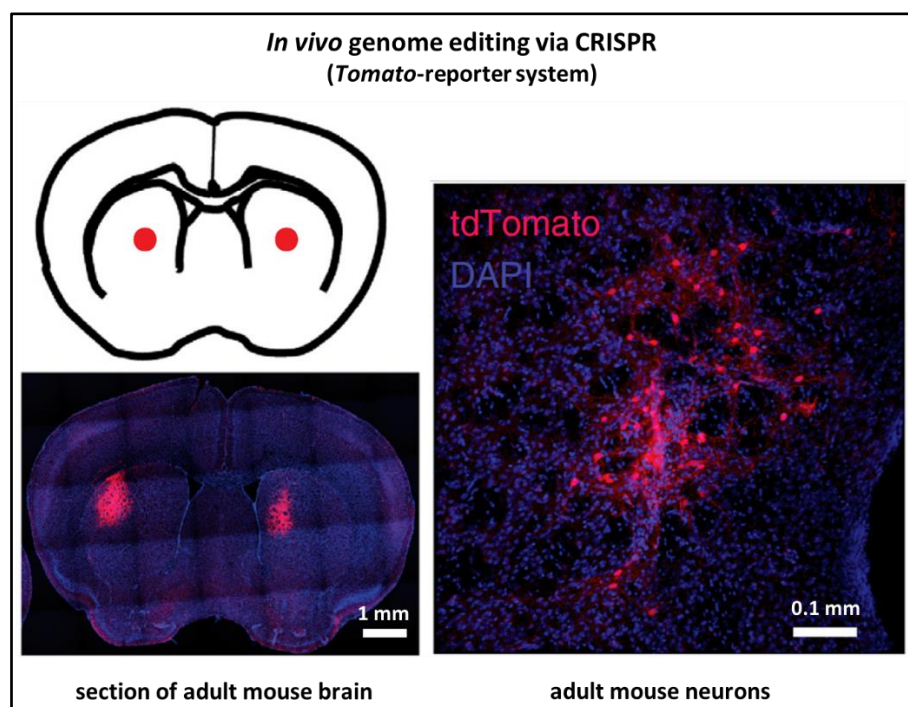


**Figure 15.** The microscopy images depict a brain section of an adult mouse injected with Cas9-gRNA ribonucleoproteins targeting a reporter system (*Tomato*). Successful editing and subsequent reporter activation are marked by red fluorescence [149].

## ***Objectives and project design***

The project described in this thesis was aimed at discovering and characterizing genetic markers of neuroblastoma with the perspective of laying the bases for novel targeted therapies. The importance of targeted therapy in neuroblastoma relies on the failing approach of conventional strategies (surgery, chemotherapy, radiotherapy) in the treatment of high-risk patients (stage 4). These are characterized by metastatic/aggressive tumour and very poor prognosis (< 30% survival rate). Some therapies are already adopted in clinical practice, including application of *cis*-retinoic acid and GD2-directed immunotherapy. However, relative inefficacy of the current systems and variable response to the treatment are pushing research to discover alternative ways. The pipeline of this project was directed to study cell line models of aggressive neuroblastoma under three aspects: therapy-relevant features of known neuroblastoma markers; uncharacterized players of neuroblastoma development and progression that can be exploited for therapy; application of new biotechnologies for targeting relevant neuroblastoma markers. The pipeline was then developed into the three main objectives of the current project, which respectively are:

1. study of the expression regulation of *ODCI*, a gene encoding for the rate-limiting enzyme of polyamine biosynthesis and representing a prognostic marker in neuroblastoma;
2. evaluation of the involvement in neuroblastoma development and progression of *RUNX1T1*, a gene encoding for a poorly characterized transcription repressor, and demonstrated to play a role in many distinct cancers and development processes;
3. application of CRISPR technology as a novel therapy tool for targeting the amplification of *MYCN*, the genetic lesion that characterizes most of aggressive neuroblastoma and that is prognostic of very poor outcome.

The three branches of this project shared a common strategy based on CRISPR technology, an extremely efficient and accurate tool widely employed for genome editing and reverse genetics. Here, CRISPR-editing was applied with a 360-degree approach. Multiple CRISPR-based techniques, made possible by an extreme versatility of the system, were employed in this project: gene knockout through NHEJ-mediated editing, which relies on random *indel* mutations introduced into the Cas9 target site via non-homologous end joining; deletion of large genomic regions through NHEJ-editing, a strategy based on joining distant DNA breaks via the NHEJ machinery; gene knock-in through HDR, which is based on redirected-recombination of the Cas9 target site with a customized donor DNA; localized assembly of multiple DNA sequences into a specific genomic locus of living cells through the Cas protein Cpf1.

**Objective 1: Evaluating the prognostic significance of a single nucleotide polymorphism located in *ODCI* promoter.** *ODCI* encodes for ornithine decarboxylase, the rate limiting enzyme of polyamine biosynthesis. Polyamines are ubiquitous compounds that are involved in a variety of cell functions, ranging from transcription regulation to modulation of ion channel activity. High polyamine levels typically correlate with sustained cell proliferation and are found in several types of aggressive tumours, making *ODCI* expression an independent marker of prognosis. Likewise, high *ODCI* expression is prognostic of poor outcome in neuroblastoma. Such condition is typically found in *MYCN*-amplified patients, where the transcription factor *MYCN* directly promotes the expression of *ODCI*. The genotype of a single nucleotide polymorphism located in *ODCI* promoter (+316 A/G SNP) is known to influence gene expression and, consequently, tumour progression. This is demonstrated for colorectal and breast cancer. The objective of this part of the project was therefore to evaluate the prognostic significance of +316 A/G SNP genotype in neuroblastoma. First, the prognostic significance of the SNP was evaluated in a cohort of neuroblastoma patients. Then, CRISPR technology was applied to switch the SNP genotype in a neuroblastoma cell line that represents the aggressive stage of the tumour. Molecular analyses were performed to assess whether the SNP modification affects *ODCI* expression in neuroblastoma, and to investigate the transcriptional mechanism involved. Cell proliferation was analysed in mutant cells as an indicator of tumour aggressiveness, and, at last, the mutated cells were tested for sensitivity to DFMO, an *ODCI*-specific inhibitor that was already identified as a potential therapeutic drug for neuroblastoma treatment. The results obtained in this study, were aimed at demonstrating and mechanistically explaining the role of *ODCI* SNP as a potential stratification factor for prognosis of neuroblastoma patients in remission.

**Objective 2: Evaluating the role of *RUNX1T1* in aggressiveness of neuroblastoma.** *RUNX1T1* is a ~140,000 bp-long gene coding for a transcription repressor whose functions are poorly understood. Many studies demonstrated that *RUNX1T1* protein regulates gene expression by recruiting a transcription-repressor complex with HDAC activity. However, *RUNX1T1* is unable to directly bind DNA, and the partners that mediate such interaction are not perfectly defined. This makes the regulation network of *RUNX1T1* almost completely unknown. Several other studies demonstrated that *RUNX1T1* is involved in a wide range of development processes and cancers, and that its role in these events is context-dependent. Since *RUNX1T1* has never been studied in the context of neuroblastoma, and given that this cancer originates from a condition of deregulated development, the second objective of this project

was to evaluate whether *RUNX1T1* is involved in progression of aggressive neuroblastoma. First, involvement of *RUNX1T1* in neuroblastoma outcome was evaluated in multiple cohorts of patients through bioinformatics tools. Second, CRISPR technology was employed to produce *RUNX1T1*-knockout cells from a neuroblastoma line deriving from an aggressive tumour. The phenotype of the knockout cells was characterized in relation with the main cell functions, which include proliferation, migration, differentiation and apoptosis. These characteristics are all relevant for neuroblastoma aggressiveness and progression. At last, the molecular pathways resulting impaired in *RUNX1T1*-KO cells were investigated by transcriptome analysis, with the aim at defining the regulation network of *RUNX1T1* and, eventually, identifying significant pathways involved in neuroblastoma cell behaviour. The results obtained in this second part of the project were intended to define *RUNX1T1* as a novel prognostic marker in neuroblastoma, and to find new molecular mechanisms and pathways that can potentially be targeted in therapy.

**Objective 3: Assessing the potentiality of a CRISPR-based therapy targeting *MYCN* amplification.** Amplification of *MYCN* gene is found in about 20% of all neuroblastoma patients, and in most of highly aggressive cases. Amplification typically consists of 50-100 copies per genome of a 100-1000 Kb region that includes *MYCN* locus. The consequent overexpression of *MYCN* represents a strong prognostic marker of poor survival. The direct correlation between this oncogene and neuroblastoma aggressiveness is largely demonstrated. The gene encodes for a transcription factor that regulates expression of a huge number of genes involved in cell growth, cell-cycle progression, differentiation and apoptosis. As a result, *MYCN* amplification induces increased proliferation, poor differentiation and apoptosis inhibition, three typical features of aggressive neuroblastoma cells. Strategies aimed at disrupting *MYCN* activity and its regulation network are currently under evaluation. However, despite the enduring effort of realizing *MYCN*-targeted therapies, most strategies developed to date are still far from being realistically effective. Based on such a background, the third objective of this project was targeting *MYCN*-gene amplification via Cas9-cleavage in order to decrease, or even abolish, the aggressiveness of neuroblastoma cells. The principle behind this innovative approach relied on induction of a *MYCN*-directed/large-scale DNA damage to simultaneously reduce *MYCN* expression and induce cell-cycle arrest and apoptosis. A previous attempt to impair *MYCN* expression in neuroblastoma cells was performed through RNA-interference, obtaining a reduction of cell proliferation and an increase of differentiation and apoptosis [152]. However, the total effect was not significant enough to proceed over the development of a concrete therapy. Differently, a CRISPR-based approach was expected to be

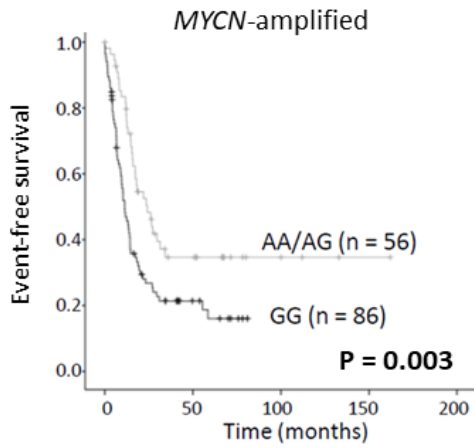
much more efficient, since the target gene is irreversibly knocked-out. In addition, induction of multiple DNA breaks, due to amplification of the target-gene, was expected to promote cell-cycle arrest and, in case the damage is not repaired, apoptosis, an event that is significantly more probable in the considered context. In support of this, a previous work demonstrated that Cas9 cleavage activates p53 pathway and induces apoptosis in immortalized cells [153]. With the objective to provide a proof of principle for a possible therapeutic application, multiple cell lines were transfected with a *MYCN*-targeting CRISPR-system and their survival was then analysed over time. In order to evaluate the specificity of the system, the analysed samples included *MYCN*-amplified neuroblastoma cells, *MYCN*-non amplified cells and cells with a non-neuroblastoma origin. Importantly, advances in CRISPR technology evidenced how this editing system can be efficiently adapted for treatment of genetic diseases *in vivo*, thus supporting the idea of a CRISPR-bases therapy in aggressive neuroblastoma.

## ***Results and discussion***

# **1-*ODCI* +316 A/G SNP has prognostic significance in neuroblastoma**

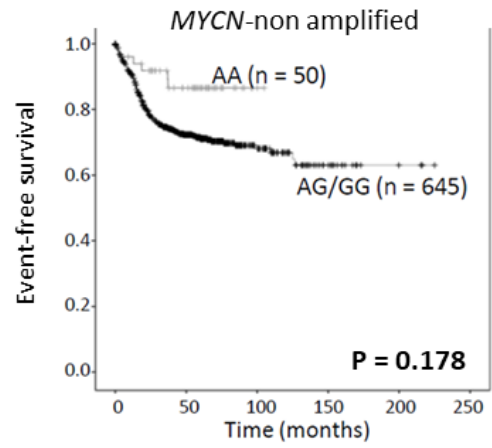
## **1.1- The A allele predicts favourable outcome in neuroblastoma patients**

As a proof of principle, the prognostic significance of the genotype of *ODCI* +316 A/G SNP was studied in a group of neuroblastoma patients. In collaboration with Children's Cancer Institute of Sydney, a large cohort of neuroblastoma samples was analysed with the aim to evaluate the correlation between SNP genotype and outcome. The cohort included primary neuroblastoma samples from 839 patients recruited in Europe, the USA and Australia. The SNP genotype distribution in the cohort, which included 506 patients with GG genotype, 272 with AG and 61 with AA, was comparable to the average distribution in human population (GG 50%, AG 41.6%, AA 8.4%). Since *ODCI* expression is mainly activated by the transcription factor MYCN in neuroblastoma, and given the importance of aggressive *MYCN*-amplified tumours, the patients were grouped according to *MYCN*-status. The cohort included 142 *MYCN*-amplified and 695 *MYCN*-non amplified neuroblastomas. Survival analysis of the 839 samples revealed an association between the A SNP and favourable outcome. In patients characterized by *MYCN* amplification, the AA and AG genotypes correlate with higher survival than the GG genotype (P = 0.003 in event-free survival, P = 0.006 in overall survival) (Figure 16A). In *MYCN*-non amplified tumours, only the AA genotype is prognostic of higher survival, but with lower significance than the *MYCN*-amplified patients (P = 0.178 in event-free survival, P = 0.558 in overall survival) (Figure 16A). As expected, also *MYCN* amplification was strongly prognostic of outcome itself, while no evident correlation was observed between SNP genotype and *MYCN* status, thus excluding any bias. Previous studies demonstrated that the SNP genotype directly affects *ODCI* expression and, consequently, tumour progression. In order to evaluate the same condition in neuroblastoma, *ODCI* RNA expression was measured in tumour samples of the European and the USA cohorts. Expectedly, high *ODCI* expression correlated with *MYCN*-amplification and poor outcome. Although the GG genotype group included the patients with the highest expression, the results did not evidence any specific expression pattern in relation with the SNP genotype, regardless of *MYCN* status (Figure 16B).

**A****Survival analysis in relation with the SNP genotype**

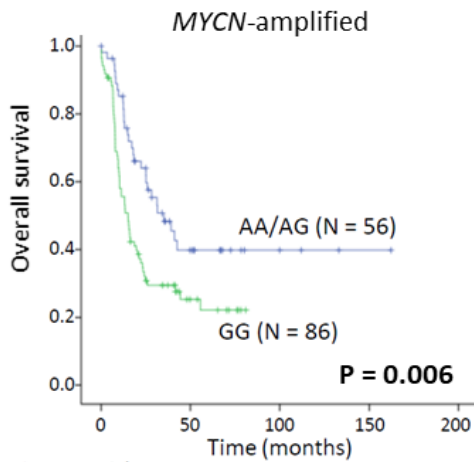
Patients at risk:

AA/AG	56	12	3	1	0
GG	86	9	0	0	0



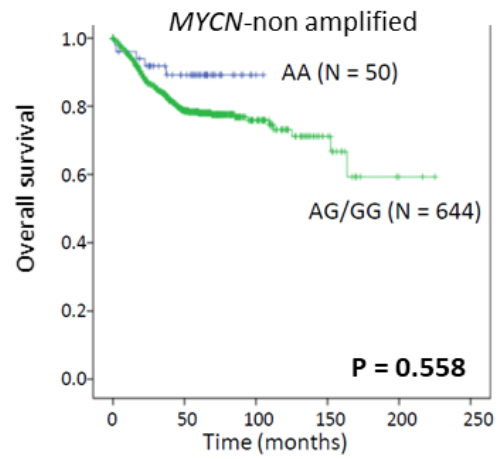
Patients at risk:

AA	50	29	1	0	0	0
AG/GG	645	289	67	15	3	0



Patients at risk:

AA	56	12	3	1	0
AG/GG	86	9	0	0	0



Patients at risk:

AA	50	30	1	0	0	0
AG/GG	644	316	73	17	2	0

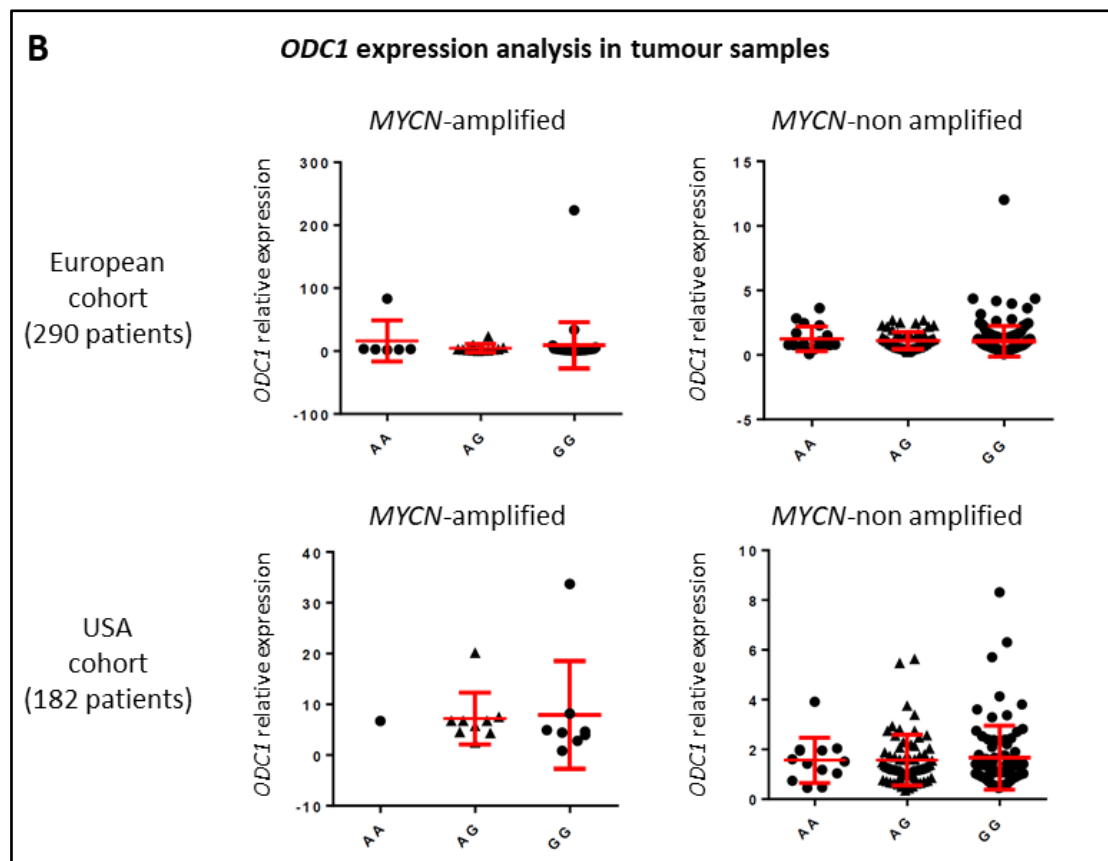


**Figure 16.** Prognostic significance of *ODC1* SNP in neuroblastoma patients.

**A.** Survival analysis of 839 neuroblastoma patients in relation with *ODC1* SNP genotype (GG, AG or AA) and *MYCN* status. In each analysis, the genotypes are grouped according to the highest value of statistical significance (GG/AG vs AA, or GG vs AG/AA). Statistical significance is indicated as P value and calculated by t-test. **B.** *ODC1* mRNA expression analysis in primary neuroblastoma tumours from the European and the USA cohorts. The samples are grouped according to SNP genotype and *MYCN* status. Data were normalised to a panel of control genes: HPRT1, GUSB, PPIA, HMBS, and SDHA.

The preliminary observation that the A allele of *ODC1* gene is prognostic of favourable outcome in neuroblastoma was new and expected at the same time. Indeed, some studies already demonstrated that +316 A/G SNP influences outcome in different cancers. However, the A allele was found to be prognostic of poor outcome in colorectal and breast cancer, which is in contrast with the observation in neuroblastoma. Some of these studies also evidenced that the SNP genotype directly influences the transcriptional regulation of *ODC1* expression, and that the A SNP is associated with increased binding of transcription regulators to the two E-boxes nearby. The effect of the SNP genotype on *ODC1* regulation would hence depend on what kind of regulator is influenced, whether an activator or a repressor. In neuroblastoma, *MYCN* is the

main transcription activator of *ODCI*, and the experimental data demonstrated that the SNP genotype is significantly prognostic of outcome mainly in *MYCN*-amplified patients. Therefore, the evidence that at least one A allele correlates with better prognosis suggests that the SNP counteracts *MYCN* activity and then involves decreased *ODCI* expression. This, according to the model proposed in previous studies, could be explained by increased activity of a transcription repressor. Unfortunately, no significant change in *ODCI* expression was measured in relation with the SNP genotype. Given the nature of neuroblastoma, it cannot be excluded that this result is due to heterogeneity of the tumour samples. In addition, sample preparation did not take into consideration tumour metastases in this study.

## 1.2- The A SNP impairs *ODCI* expression in neuroblastoma cells

**SNP genotype and *ODCI* expression in neuroblastoma cell lines.** In order to evaluate the influence of +316 A/G SNP on *ODCI* expression in neuroblastoma, *ODCI* transcription was analysed in a series of 12 human neuroblastoma cell lines with different genotype. *In vitro* cultures of neuroblastoma cells were used instead of primary tumour samples to study the molecular mechanism behind *ODCI* expression regulation in a more reliable system. The 12 lines included IMR-32 (GG), SH-SY-5Y (GG), BE(2)-C (GG), SHEP (GG), CHP-134 (GG), NB-69 (GG), SK-N-FI (AG), SK-N-AS (AG), SK-N-DZ (AG), LAN-1 (AG), KELLY (AG) and NBL-S (AA). The genotype distribution among the 12 cell lines (GG 50%, AG 41.6%, AA 8.4%) was consistent with the genotype distribution in the human population (GG 56%, AG 37%, AA 7%). Analysis by qRT-PCR evidenced a significant variability of *ODCI* expression among the cell lines, but no correlation with the SNP genotype (Figure 17). The highest *ODCI* expression was detected for the lines CHP-134 (GG), NB-69 (GG) and LAN-1 (AG), the lowest expression was detected in SK-N-AS (AG), while the other lines showed similar expression levels despite the SNP genotype. Since *ODCI* promoter contains three E-boxes that can be potentially regulated by a great number of different factors, such expression variability is likely due to the different genetic backgrounds of the lines taken for analysis. The same lines were then analysed for expression of *MYCN*, *c-MYC*, *MAX* and *MADI*, fundamental *ODCI* regulators and MYC/MAX/MAD network members. As a rule, high *ODCI* expression was

expected to correlate with high expression of *MYCN* or *c-MYC* (transcription activators), and *vice versa* low *ODCI* expression was expected to correlate with high expression of *MADI* (transcription repressor). Quantitative RT-PCR revealed great expression variability of these genes, but no functional correlation was found with *ODCI* expression, nor with the SNP genotype (Figure 17). Basically, there were no cell lines with similar conditions that can be compared to evaluate the influence of the SNP genotype on *ODCI* expression. This result highlighted the complex variability of the genetic background in neuroblastoma cell lines, which nevertheless resembles the extreme genetic heterogeneity of neuroblastoma tumours.

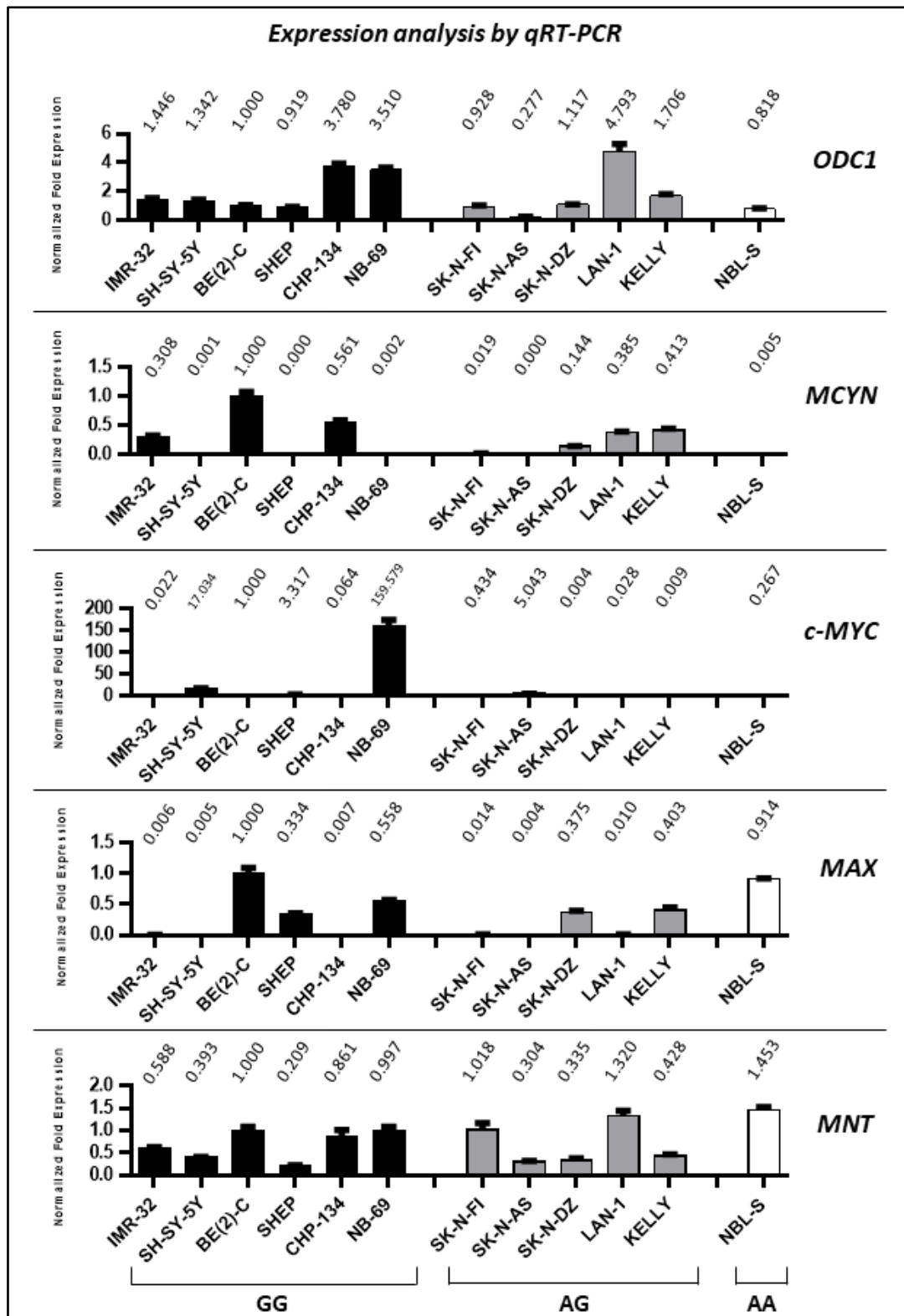
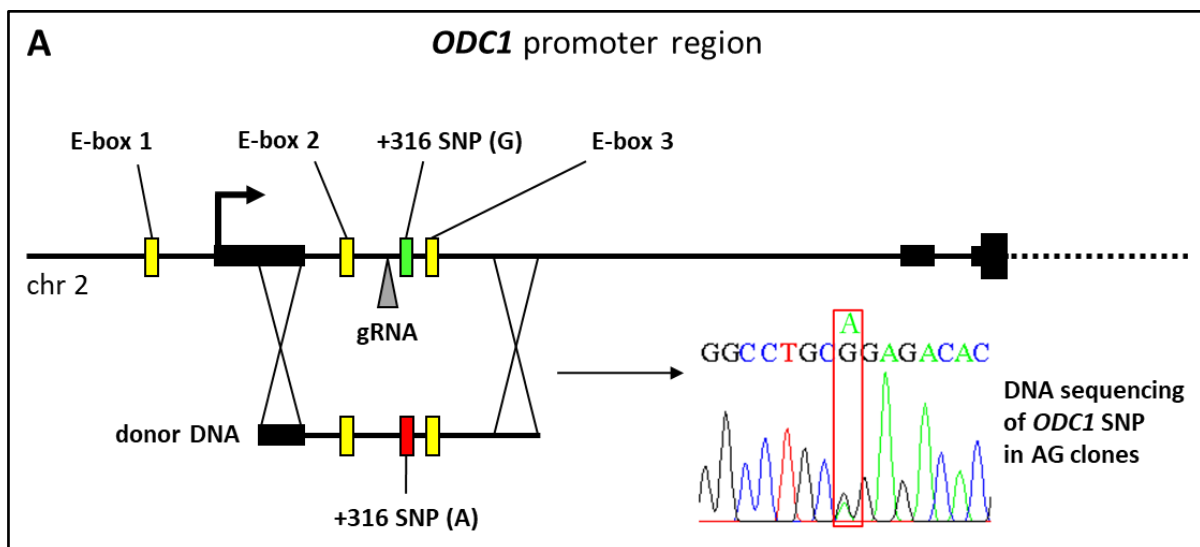


**Figure 17.** Expression of *ODC1*, *MYCN*, *c-MYC*, *MAX*, and *MNT* is analysed by qRT-PCR in 12 human neuroblastoma cell lines. Normalized fold expression ( $2^{-\Delta\Delta C_t}$ ) are indicated in black, grey and white for respectively the GG, AG and AA genotype. BE(2)-C cells were used as control sample, and *GUSB* as reference gene.

**SNP genotype editing by CRISPR-Cas9 in BE(2)-C cells.** The SNP genotype was edited by CRISPR-Cas9 technology in a singular cell line with the aim to evaluate the effect of the genotype change in an isogenic background and, thus, to overcome the significant heterogeneity of neuroblastoma lines. The line BE(2)-C, carrying a GG genotype, was chosen for this task. The choice was motivated by three reasons: first, BE(2)-C is an important model for neuroblastoma research, since it's a *MYCN*-driven and metastasis-derived line; second, the *MYCN*-amplification condition was supposed to be more sensitive to the SNP genotype; third, the moderate expression of *ODCI* in this cell line did not exclude either a possible increase or a decrease in gene expression following the genotype change, in contrast to cell lines with much higher or lower expression levels (Figure 17). BE(2)-C cells were then edited by CRISPR-mediated HDR. A single gRNA was used to target a site close to the G SNP, and to promote recombination with a double-stranded donor DNA carrying the A allele (Figure 18A). Single cell lines were isolated after transfection and screened for selection of AG and/or AA clonal lines. The screening was performed with an allele-specific PCR, which is based on primers designed for specifically recognizing either an A or a G through the 3'-end. Overall, 2 AG clonal lines (named as AG-1 and AG-2) were found, thus obtaining a successful-editing rate of 2.5%. Such editing efficiency is similar to the efficiency usually detected in average non-primary cell cultures, therefore delineating BE(2)-C as a model suitable for CRISPR-precise editing. DNA sequencing of the SNP region confirmed successful editing of the clonal lines (Figure 18A). In order to verify editing specificity and precision, all the off-target sites possibly targeted by the gRNA were ranked (via *CasOT* software) according to the cleaving probability, which is based on the number of mismatches and their position in relation with the *seed region*. The most probable off-target site was therefore sequenced in both clones as a control, and no mutation was detected (data not shown). No AA lines were found, while clones with *indel* mutations (insertion/deletion) were obtained with 16% efficiency. At last, one line resulted with the insertion of the donor DNA into the target site (data not shown). The absence of AA clones was not surprising, since bi-allelic editing is notoriously hard to achieve (supposed to be 10% of total HDR editing) [125].

In a second parallel experiment, editing of the SNP genotype via HDR was attempted to be improved through some expedients that are known to increase the efficiency: employment of a 120 nt-long single-stranded (ssODN) instead of a double-stranded donor DNA (dsDNA); induction of a staggered DNA break with 5'-overhanging hands (38 nt long) via double nickase-Cas9 (nCas9) in *PAM-out* configuration; application of an NHEJ-inhibitor (SCR7) and an HDR-enhancer drug (RS-1). The cell pools transfected with these systems were screened

through allele-specific/semi-quantitative PCR in order to find the condition with the highest HDR rate (Figure 18B). In absence of any drug, no significant difference was observed when ssODN was used instead of dsDNA, or when dual-nCas9 was used instead of canonical Cas9. However, a significant improvement was observed when the drugs SCR7 and RS-1 were applied individually. In both cases, ssODN revealed to be much more efficient than dsDNA, while canonical Cas9 was demonstrated to be slightly more efficient than double nCas9. In addition, application of the HDR-enhancer RS-1 appeared to be a better strategy than inhibition of NHEJ by SCR7. While the result relative to ssODN was relatively expected, it was not the same for the double-nickase strategy. Lower HDR-editing rate of dual-nCas9 could be explained by lower transfection efficiency, since more components than the canonical Cas9 are required for successful editing (2 plasmids and 1 dDNA construct instead of 1 plasmid and 1 dDNA). For what concerns employment of RS-1, higher efficiency than SCR7 could be explained by two reasons: enhancing HDR is a more direct strategy than inhibiting NHEJ; inhibition of NHEJ potentially brings to death a cell with a DNA damage induced by Cas9. This parallel experiment demonstrated that CRISPR-editing via HDR can be improved in neuroblastoma cells, indicating that mutations of the DNA-repair machinery, which commonly occur in tumours, do not affect this cell system. By the way, despite editing efficiency was successfully improved, screening of clonal lines with AG or AA genotype was not performed, and the AG clonal lines previously obtained were used for the following experiments.



**B** Screening of edited cells via allele-specific PCR

cell line	NBLS (AA)	BE(2)-C (GG)					
CRISPR	//	//		Cas9		double nCas9	
donor DNA	//	dsDNA	ssODN	dsDNA	ssODN	dsDNA	ssODN
no drug							
SCR7 1 $\mu$ M	//	//	//				
RS-1 7.5 $\mu$ M	//	//	//				

**Figure 18.** SNP genotype editing by CRISPR in BE(2)-C cells.

**A.** SNP localization in *ODC1* promoter and CRISPR-editing strategy. An example of DNA-sequencing of the SNP in one of the AG clones is represented on the left; the double A/G peak corresponding to the SNP is labelled by a red square. **B.** Results obtained by screening, via allele-specific/semi-quantitative PCR, the cell pools transfected with different CRISPR systems for HDR-editing of the SNP. The PCR was performed with A SNP-specific primers, and the PCR products were analysed on agarose gel. The table indicates the type of cell line that were transfected (either BE(2)-C or NBLS), the CRISPR strategy (either Cas9 or dual-nCas9) the type of dDNA (double or single-stranded) and the drug applied (either SCR7 or RS-1). NBLS cells, carrying an AA genotype, were used as positive control of the PCR.

**Analysis of ODC1 expression in SNP-mutated clonal lines.** The two AG lines were both kept for analysis, since data obtained from a single line could be affected by clonal variability. AG-1 and AG-2 were first tested for *ODC1* expression. Western blot and qRT-PCR revealed a significant decrease of respectively protein and mRNA level compared to the wild type GG line (Figure 19A). This result is consistent with the previous observation that the A allele is prognostic of favourable outcome in neuroblastoma. Furthermore, decreased activity of *ODC1* promoter was already associated with the A SNP in mouse fibroblasts and human colon cancer cells by reporter assay [34]. Interestingly, *ODC1* mRNA expression appeared to be halved in both clones, suggesting that gene expression is completely abrogated for the A allele, provided that the G allele is not affected in the mutant lines. *ODC1* protein level was also approximately halved in the AG lines. This confirmed that the SNP genotype directly affects *ODC1* protein expression and, potentially, the whole polyamine biosynthetic pathway.

Previous studies suggested that the SNP effect on *ODC1* expression occurs through a differential affinity of transcription factors toward the two different SNP forms. Factors such as c-MYC, MAX and MAD1 were demonstrated to preferentially bind *ODC1* E-boxes that are

close to the A SNP. In neuroblastoma, *ODCI* is notoriously regulated by MYCN, but a multitude of other transcription factors can potentially bind and regulate the region that is supposed to be affected by the SNP genotype. Actually, *ODCI* regulation is more likely mediated by a binding equilibrium between multiple factors. In order to identify a causative relation between the A SNP and decreased *ODCI* expression, the epigenetic status of *ODCI* promoter was evaluated via analysis of H3-histone pan-acetylation, which represents a strong marker of open chromatin and active transcription. Chromatin immunoprecipitation (ChIP) and quantitative-PCR analysis revealed that pan-acetylation of H3 histone is significantly decreased in proximity of the SNP (+316 bp from the TSS) in AG-1 and AG-2 (Figure 19B). This is perfectly consistent with the decreased gene expression observed in the mutant clones. Histone acetylation was also assessed for E-box 1 (-488 bp from the TSS), Exon 9 (starting at +6165 bp from the TSS) and  $\beta$ -*ACTIN* locus as control. As expected, E-box 1 is modestly acetylated in all the lines, while Exon 9 is not acetylated and histone acetylation at  $\beta$ -*ACTIN* locus is not affected by CRISPR-editing (Figure 19B). H3-acetylation resulted impaired also in proximity of E-box 1, but the decrease is not as much significant as for the SNP region. This indicates that the SNP influence range is very specific to the surrounding sequence, which includes E-box 2 and 3. On the other hand, the slight effect on E-box 1 could be due to chromatin super-folding and consequent interaction between transcription factors and sequences that are virtually distant. A more accurate examination of H3 acetylation in proximity of the SNP revealed that the acetylation level in AG-1 and AG-2 is approximately half of the level detected in the GG wild-type line. These findings allow to infer that the substitution of the G with the A SNP induces complete de-acetylation of the surrounding region, which would be consistent with the complete abrogation of *ODCI* expression that was previously deduced. Binding dynamics of the main transcription factors possibly involved in *ODCI* regulation were not further investigated.

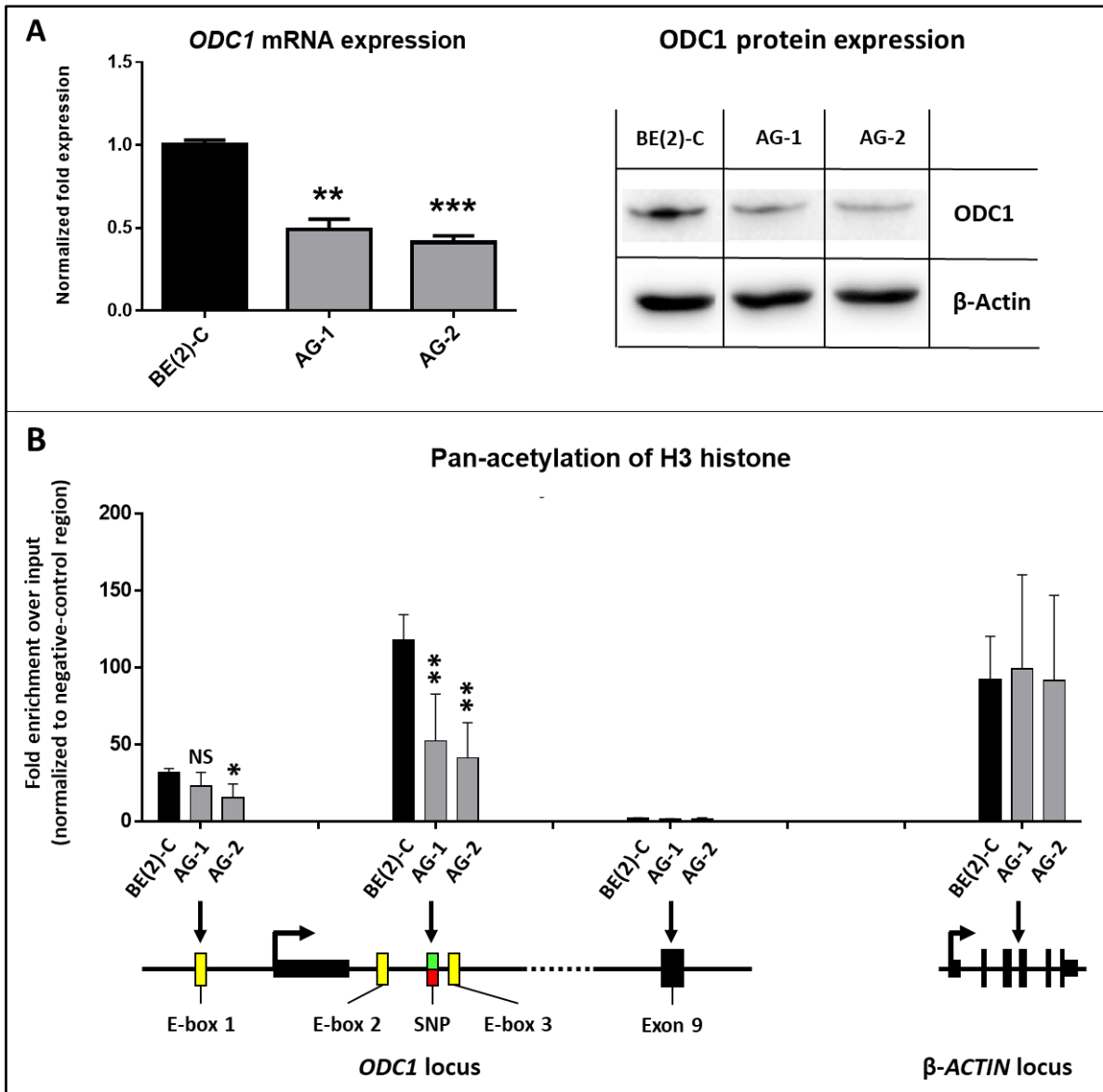


**Figure 19.** Analysis of *ODC1* expression regulation in CRISPR-edited cells. **A.** *ODC1* expression by qRT-PCR (left) and Western blot (right) in the mutant AG clones. Expression of *GUSB* was used for normalization in qRT-PCR, while  $\beta$ -ACTIN was used as housekeeping gene in Western blot. Statistical significance was measured by t-test (\* =  $P < 0.05$ , \*\* =  $P < 0.01$ , \*\*\* =  $P < 0.001$ ). **B.** Analysis of H3-histone acetylation of *ODC1* promoter by H3-PanAcetylated ChIP in the CRISPR-edited AG clones. Immunoprecipitated DNA was analysed by quantitative PCR. A poorly acetylated region located 15,000 bp upstream of *ODC1* TSS was used as negative-control region for normalization ( $\Delta Ct$ ). Data are presented as fold enrichment over the input sample ( $2^{-(\Delta\Delta Ct)}$ ). The analysed regions are illustrated at the bottom of the figure. Statistical significance was measured by t-test (\* =  $P < 0.05$ , \*\* =  $P < 0.01$ , \*\*\* =  $P < 0.001$ ).

In order to validate the role of the SNP genotype in *ODC1* regulation, a dual-reporter assay was performed with the promoter region containing the SNP and the two E-boxes nearby. The

sequence, 74 bp long and containing either the G or the A SNP, was cloned upstream of a reporter cassette coding for Luciferase. Reporter expression can be estimated by measuring bioluminescence produced in the reaction catalysed by Luciferase. The construct was then transfected into Tet21N cells, a neuroblastoma line carrying a Tet-Off system that controls exogenous overexpression of *MYCN*. Cells treated with tetracycline, in which *MYCN* is low expressed, showed no significant difference between the G and the A allele (Figure 20). Differently, the A allele led to lower reporter expression than the G allele in cells overexpressing *MYCN* (Figure 20). In a separate control experiment, cells in either conditions were transfected with the empty Luciferase vector and no significant difference was detected for the reporter expression (data not shown). In conclusion, this assay confirmed the relation between the SNP genotype and *ODC1* promoter, demonstrating that the A allele is associated with lower promoter activity. In addition, the difference between the two *MYCN* conditions supports the idea that the SNP directly counteracts the activity of *MYCN*, the main *ODC1* activator in neuroblastoma. This is consistent with the survival study, where the A allele was significantly prognostic of survival preferentially in *MYCN*-amplified patients.

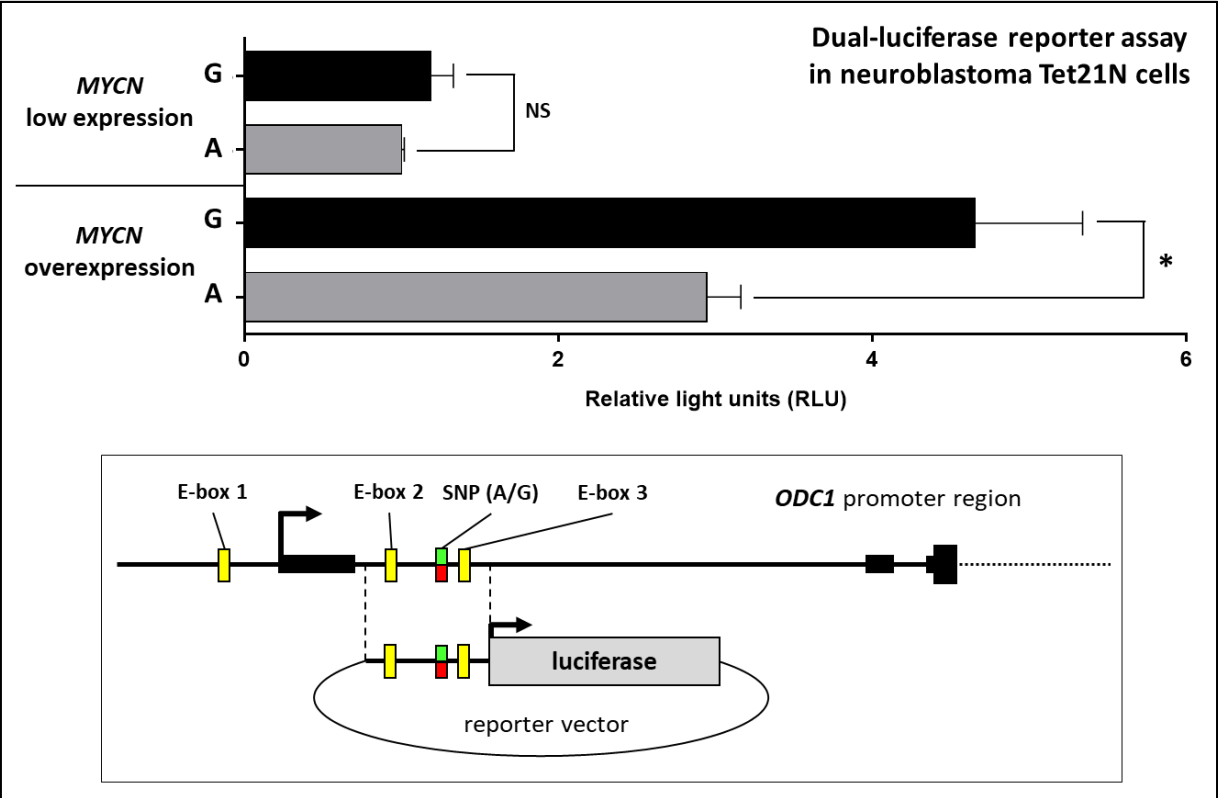


**Figure 20.** Dual-reporter assay with the two alleles of *ODCI* promoter.

The effect of the SNP genotype on expression of a reporter gene (Luciferase) was evaluated in a *MYCN* Tet-Off system (Tet21N cells). The region containing the SNP (G or A), E-box 2 and E-box 3 was cloned upstream of the Luciferase cassette (bottom of the figure). The assay was performed in a condition of either low (tetracycline treatment) or high *MYCN* expression.

Bioluminescence produced by Luciferase was measured and normalized to the bioluminescence produced by a control reporter (Renilla). Data are related to the A allele in a condition of low *MYCN* expression. Statistical significance was measured by t-test (\* =  $P < 0.05$ , \*\* =  $P < 0.01$ , \*\*\* =  $P < 0.001$ ).

Overall, genotype editing of the single nucleotide polymorphism suggested that the A allele is associated with inhibition of *ODCI* expression, resulting in halved expression in AG cells compared to GG. Similarly, the region of *ODCI* promoter that surrounds the A SNP is supposedly characterized by complete deacetylation of H3 histone, which results in halved acetylation in AG cells. These results confirmed the tumour-protective role of the A allele that was evidenced in survival analysis of neuroblastoma patients. It can be assumed that *ODCI* expression is also decreased in tumours with AG or AA genotype, a condition that was not possible to demonstrate in primary tumour samples. Notoriously, *in vitro* cell cultures are more reliable systems for studying transcription regulation dynamics. In addition, all the cells used for *in vitro* experiments (BE(2)-C and Tet21N) were derived from bone metastases, while the samples analysed in the survival study were prepared from solid primary tumours. All these circumstances represent substantial differences between the two systems, which could explain why reduced *ODCI* expression was observed in AG cell cultures but not in AG/AA patients' tumours. Notably, one A allele appeared to be enough for a significant reduction of *ODCI* expression in *MYCN*-amplified neuroblastoma cells, which is consistent with the evidence that the presence of at least one A allele is prognostic of favourable outcome in *MYCN*-amplified patients. At last, the reporter assay provided a further evidence of the mechanism behind the SNP influence on *ODCI* promoter, indicating that the A allele counteracts the *MYCN*-mediated activation of *ODCI* expression. This also supports the finding that the effect of the SNP genotype is more significant in *MYCN*-amplified patients, where the sustained expression of *ODCI* plays a fundamental role in tumour progression.

### 1.3- The A allele correlates with decreased cell proliferation and increased sensibility to DFMO in neuroblastoma

*ODC1* is an independent prognostic marker in neuroblastoma, and high expression is strongly correlated with sustained cell proliferation and poor prognosis. In order to demonstrate the prognostic significance of +316 A/G SNP in neuroblastoma, cell proliferation was assessed for the AG mutant clones by BrdU assay. The assay measures the inclusion of bromodeoxyuridine into DNA during replication as indicator of cell-cycle progression. In agreement with impaired *ODC1* expression, AG-1 and AG-2 were found to be significantly less proliferative than the wild type BE(2)-C (Figure 21). Since the cell line edited by CRISPR was derived from metastases, this result demonstrated the involvement of *ODC1* SNP in neuroblastoma progression and aggressiveness. It also validated the observation that the presence of at least one A allele is prognostic of good outcome in neuroblastoma patients with *MYCN* amplification.

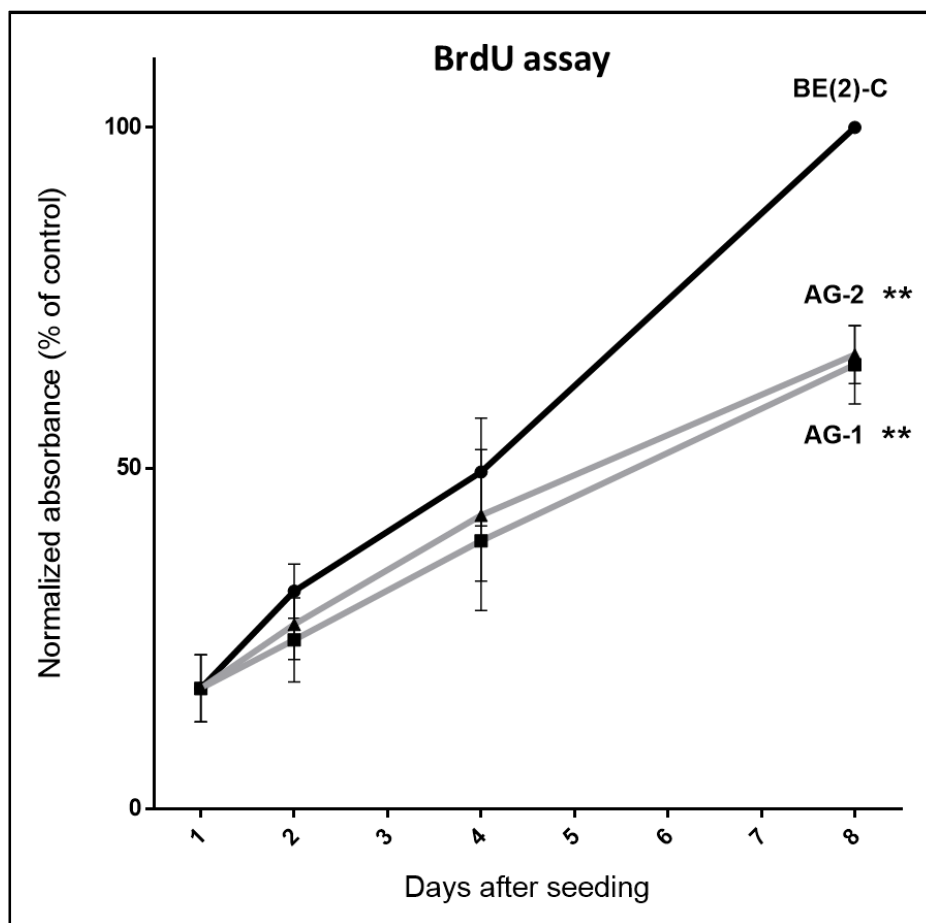


**Figure 21.** Proliferation analysis of the AG cells by BrdU assay.

BrdU incorporation into DNA during replication was directly measured in fixed cells by immunoassay. Colorimetric data are shown as fold change with respect to BE(2)-C cells at day 8. Statistical significance was measured by t-test

(\* =  $P < 0.05$ , \*\* =  $P < 0.01$ , \*\*\* =  $P < 0.001$ ).

The observations made in this study indicate *ODCI* SNP as a novel stratification factor for neuroblastoma. SNP genotyping can be potentially used to include neuroblastoma patients into specific risk subgroups, thus improving tumour prognosis and treatment. Importantly, the stratification system would be suitable for *MYCN*-amplified patients, which still represent a challenge for therapy. *ODCI* inhibitor DFMO is a new promising resource for treatment of aggressive neuroblastoma, characterized by *MYCN* amplification and high *ODCI* expression in most cases. DFMO dosage and efficiency are strictly dependent on *ODCI* expression in tumour cells. The response to DFMO treatment was therefore evaluated in relation to the SNP genotype. BE(2)-C, AG-1 and AG-2 cells were treated with increasing concentrations of DFMO (0.1, 0.2, and 0.4 mM) and, after 10 days of incubation, the three lines were tested for their capacity of colony formation, an indicator of aggressiveness in metastatic cells. DFMO concentration was suggested by collaborators of Children Cancer Institute (Sydney) on the base of previous works [29]. As expected, the assay revealed higher sensitivity of the AG lines to DFMO (Figure 22). Colony formation of the AG cell lines was almost completely abolished at all DFMO concentrations. Only few small colonies were formed with 0.1 mM DFMO. Differently, BE(2)-C cells retained colony formation capacity with 0.1 and 0.2 mM DFMO, detecting respectively 70 and 80% reduction of colony generation. With 0.4 mM DFMO, colony formation was significantly reduced also for BE(2)-C. Increased sensitivity of AG cells to DFMO is perfectly consistent with the reduced *ODCI* expression associated to the A allele. Indeed, a fixed concentration of DFMO is supposed to be more efficient against cells with lower *ODCI* expression, provided that the DFMO concentration is not saturated.

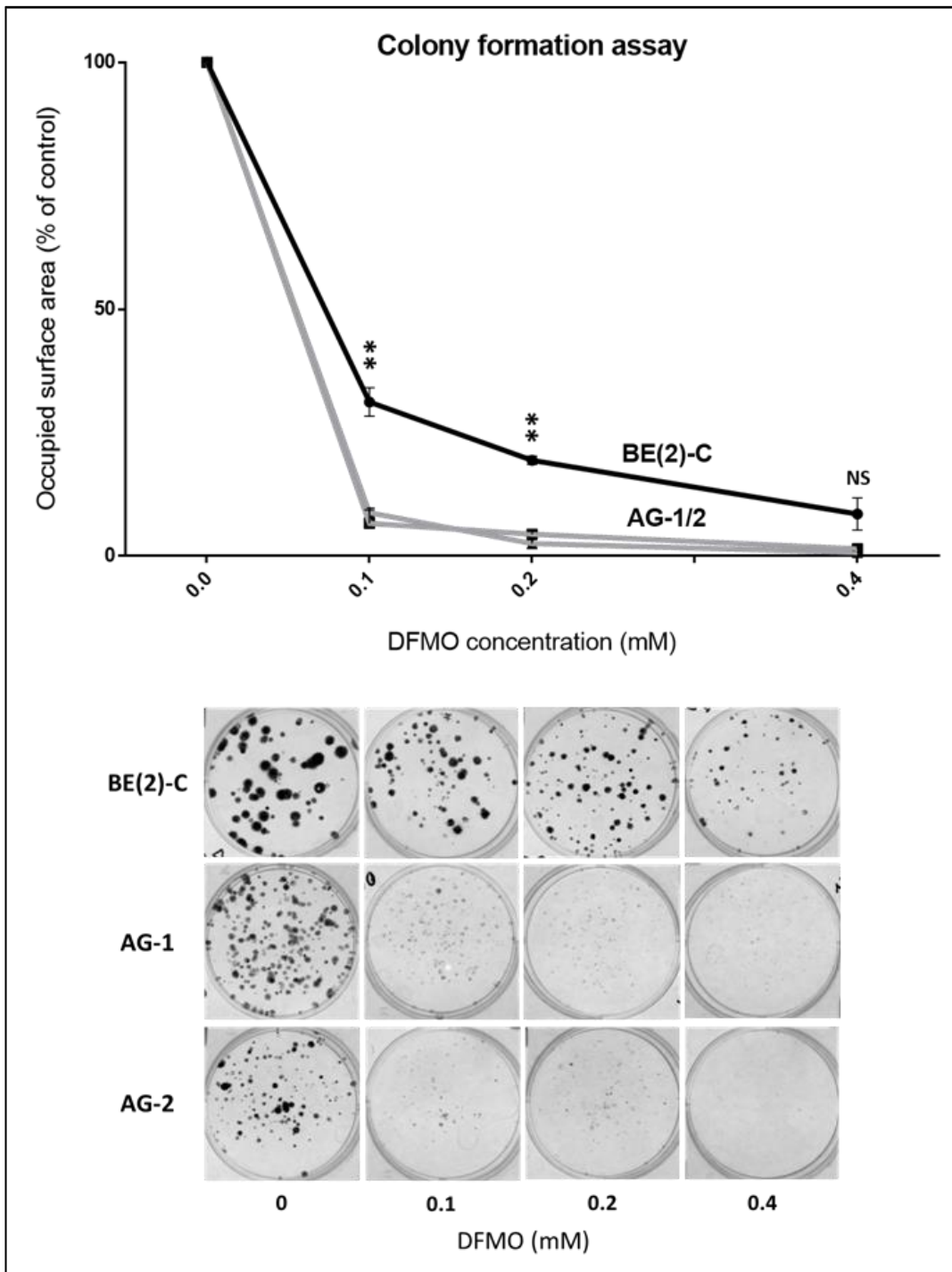


**Figure 22.** Analysis of colony formation of AG cells after treatment with DFMO. Cells were first seeded in a medium containing DFMO at different concentrations (0.0, 0.1, 0.2 and 0.4 mM) and then stained with crystal violet after 10 days. Examples of stained colonies are shown on the bottom. The surface occupied by colonies was measured by *ImageJ* software and presented as percentage of the control condition (0.0 mM DFMO). Statistical significance was measured by t-test (\* =  $P < 0.05$ , \*\* =  $P < 0.01$ , \*\*\* =  $P < 0.001$ ).

In conclusion, CRISPR editing of +316 A/G SNP and *in vitro* analyses demonstrated that the A SNP abolishes *ODC1* expression and, therefore, it impairs tumour cell proliferation and aggressiveness. This result validated the previous observation that correlates the AG and AA genotypes with higher survival of neuroblastoma patients characterized by *MYCN* amplification. In addition, cells with at least one A allele are more sensitive to DFMO, a drug meant for the treatment of aggressive neuroblastoma. In conclusion, the SNP genotype was confirmed to be a potential stratification factor for neuroblastoma that can be exploited for improving prognosis and treatment of this challenging disease.

## **2-RUNX1T1 represents a novel player in neuroblastoma development and progression**

### **2.1-RUNX1T1 is a potential oncosuppressor in neuroblastoma patients**

A preliminary study was conducted to evaluate the relevance of *RUNX1T1* expression in neuroblastoma progression and outcome. Publicly available datasets representing the tumour transcriptome analysis of large cohorts on neuroblastoma patients were examined through the online tool *R2: Genomics Analysis and Visualization Platform*. *Kocak* dataset [76], which is the largest one and includes data from 649 neuroblastoma patients distributed in all risk groups, revealed that high *RUNX1T1* expression in tumour samples significantly correlates with higher event-free survival ( $P = 4.8 \text{ e-}11$ ) (Figure 23). The same correlation between *RUNX1T1* expression and event-free survival was obtained with three other datasets (data not shown), that are *Versteeg* dataset [77] ( $P = 3.3 \text{ e-}03$ ), *TARGET* dataset [78] ( $P = 1.4 \text{ e-}05$ ) and *SEQC* dataset [79] ( $P = 8.9 \text{ e-}12$ ). The cohorts of the three datasets included respectively 88, 249 and 498 patients distributed in all neuroblastoma risk groups. Since the focus of this project is the study of genetic markers and possible therapeutic targets in high-risk neuroblastoma, which is often characterized by *MYCN* amplification, *RUNX1T1* prognostic significance was evaluated in a *MYCN*-related context. When the *Kocak* cohort was divided into subgroups related to *MYCN* status, high *RUNX1T1* expression was found to be significantly prognostic of better outcome in *MYCN*-non amplified patients ( $P = 6.4 \text{ e-}08$ ), but there was not a significant difference in *MYCN*-amplified patients despite a similar trend ( $P = 0.114$ ) (Figure 23). This condition was also observed in *Versteeg* dataset (*MYCN*-non amplified,  $P = 5.5 \text{ e-}03$ ; *MYCN*-amplified,  $P = 0.644$ ), *TARGET* dataset (*MYCN*-non amplified,  $P = 1.1 \text{ e-}05$ ; *MYCN*-amplified,  $P = 0.078$ ) and *SEQC* dataset (*MYCN*-non amplified,  $P = 1.3 \text{ e-}08$ ; *MYCN*-amplified,  $P = 0.010$ ) (Data not shown). The poor significance of *RUNX1T1* expression in outcome of *MYCN*-amplified patients is likely due to the low number of patients included in this risk group, but a causative interaction between *MYCN* and *RUNX1T1* functions cannot be excluded. Interestingly, slightly reduced expression of *RUNX1T1* in *MYCN*-amplified compared to *MYCN*-non amplified patients was consistently found in all datasets (data shown only for *Kocak* dataset in Figure 23). However, a similar reduction was also observed in all datasets for expression of  $\beta$ -*Actin*, here used as control.

### Survival analysis in relation with *RUNX1T1* expression

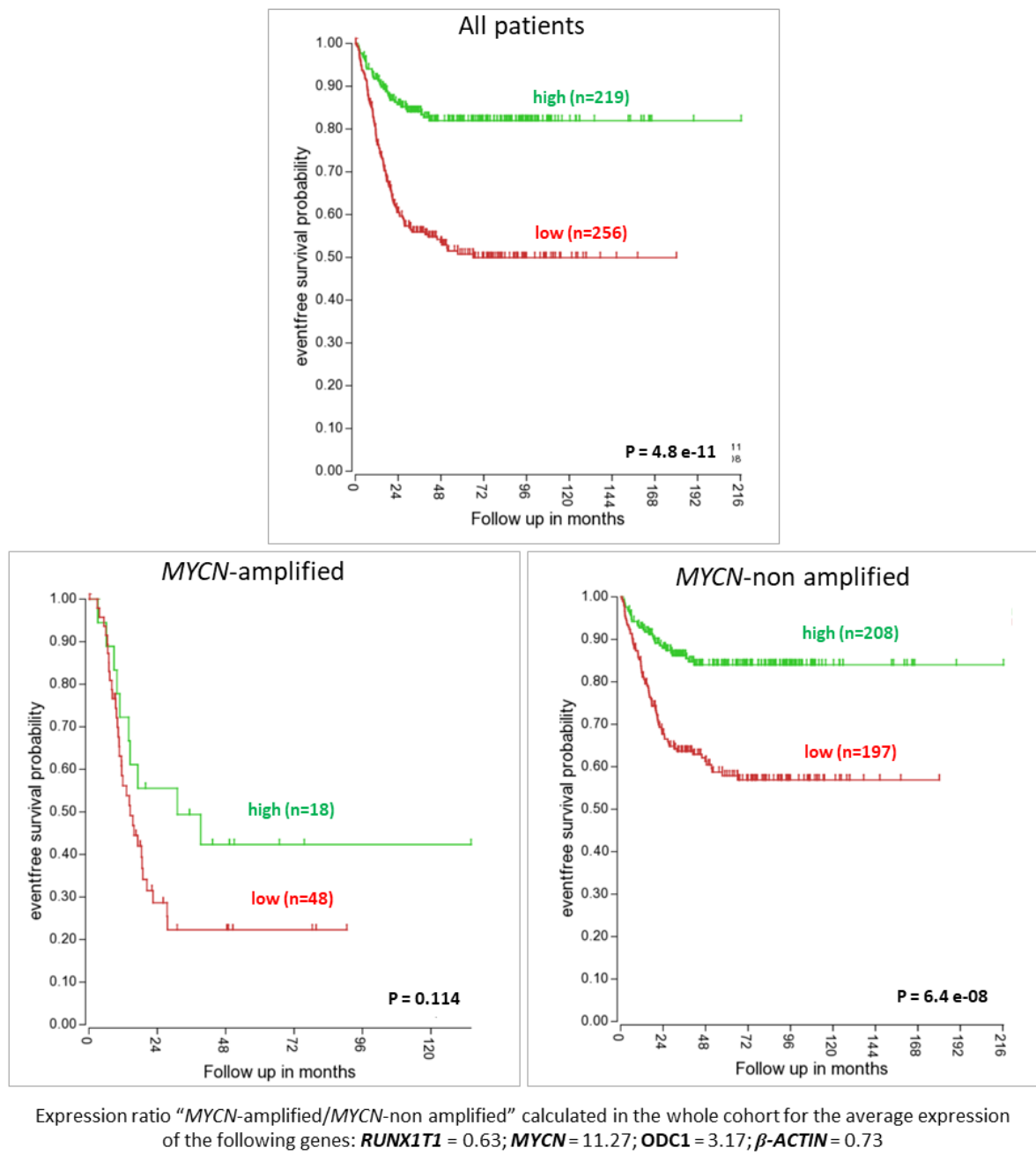


**Figure 23.** Prognostic significance of *RUNX1T1* expression in neuroblastoma samples. Survival rate and *RUNX1T1* expression were analysed in 649 neuroblastoma patients of *Kocak* dataset [76]. The Kaplan Meier curves were obtained through the online tool *R2: Genomics Analysis and Visualization Platform*. The patients were grouped according to *MYCN* status in the bottom curves. The most significant cutoff between high (green) and low (red) *RUNX1T1* expression was chosen by longrank test, and the P value is reported. The average expression ratio between *MYCN*-amplified and *MYCN*-non amplified condition is shown at the bottom of the figure for some representative genes.

This preliminary study suggested a positive correlation between *RUNX1T1* expression and survival in neuroblastoma, thus indicating *RUNX1T1* as a potential oncosuppressor in this disease. Such an evidence is consistent with the tumour suppressor role that was previously demonstrated in glioblastoma, ovarian cancer and pancreatic metastases. Here, survival analysis took into account events including recurrence, progression and death. This implicates that the role of *RUNX1T1* is probably related to aspects such as cancer cell proliferation and differentiation, as well as metastasis formation and invasion. All these functions were already demonstrated to be affected by *RUNX1T1* in many biological systems. However, it cannot be excluded that *RUNX1T1* somehow mediates the interaction between tumour cells and the surrounding environment.

## **2.2-Mutation of *RUNX1T1* gene impairs proliferation and migration, and promotes differentiation in neuroblastoma cells**

**CRISPR-editing of *RUNX1T1* in BE(2)-C cells.** With the aim at evaluating the role of *RUNX1T1* in neuroblastoma development and progression, the gene was knocked-out via CRISPR-editing in BE(2)-C cells. As for the study of *ODC1* gene, this cell line was chosen because it represents a flexible and comprehensive model of aggressive neuroblastoma. At first, deletion of the whole locus of *RUNX1T1* was induced by double Cas9 cleavage, thus producing a null allele (Figure 24A). After PCR screening and sequencing characterization, clonal lines carrying the deletion of a single *RUNX1T1* allele were found with an efficiency of about 10%. PCR screening was performed by using primers that flank the deleted region, thus giving a positive PCR result only if the included 140,000 base pairs are removed. The PCR product was sequenced to confirm the deletion (data not shown). In addition, the gRNA target sites located in the non-deleted allele were sequenced in order to check the presence of any mutation (data not shown). Since no clones with a double null allele were found, clonal cells with a single null allele were newly treated with double CRISPR cleavage. For the second editing, one of the gRNAs previously used was substituted with a gRNA shifted from the first, thus producing a distinct PCR product during the screening (Figure 24A). Although deletion of both alleles was successfully detected by PCR in the transfected cell pool and despite a significant number of

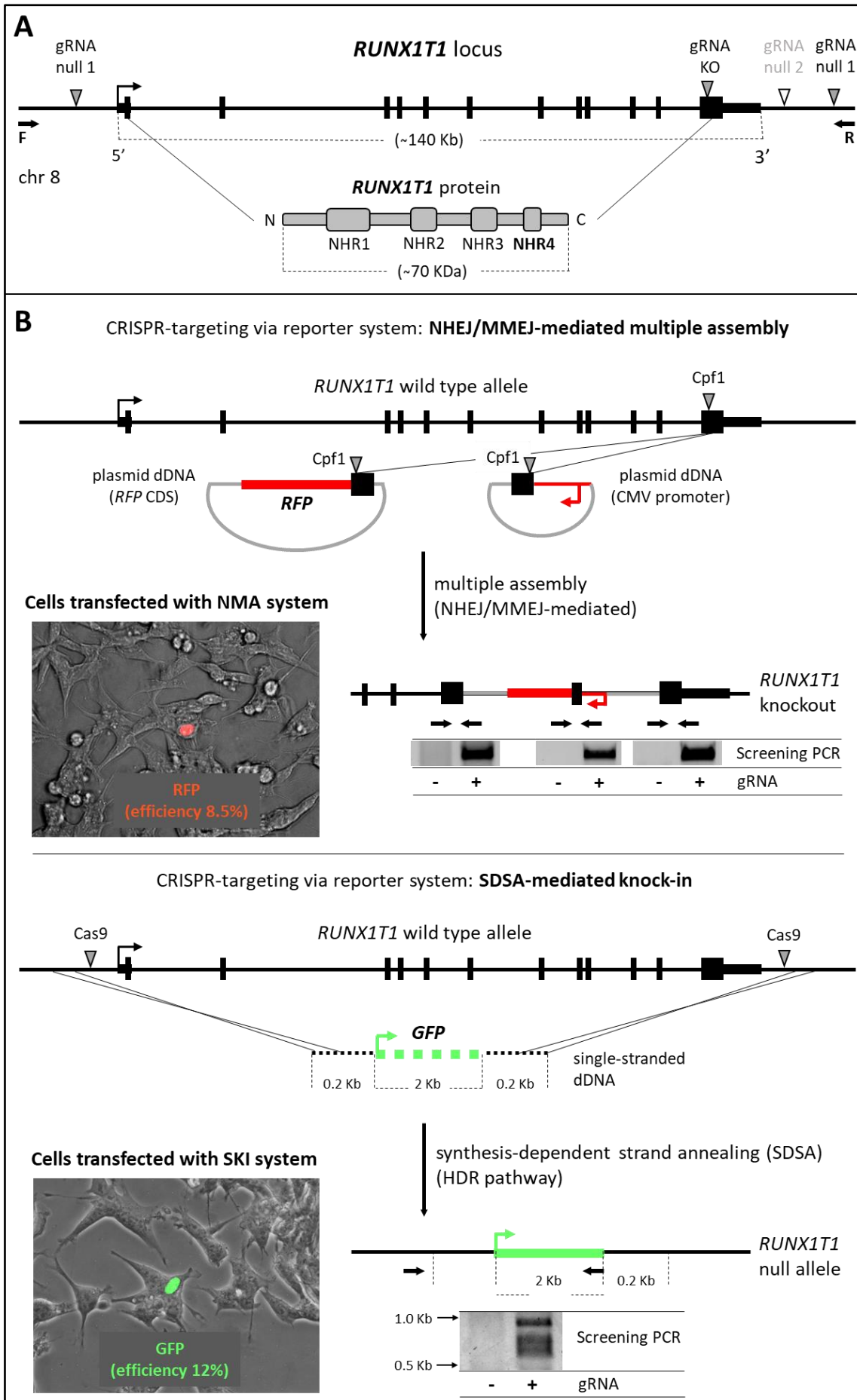
screened clones, it was not possible to isolate any clonal line with a double null allele (data not shown). It was then hypothesized that the complete removal of *RUNX1T1* locus is lethal in neuroblastoma cells.

A further attempt to knockout the second *RUNX1T1* allele in the cells carrying a single null allele was performed via two different reporter systems (Figure 24B). These were developed for the present project based on new advances in CRISPR technology, and they were aimed at tracking and eventually selecting the edited cells. The two strategies were designed to disrupt *RUNX1T1* locus by knocking-in a reporter gene (*GFP* or *RFP*) that gives a positive signal only in case of successful editing, without any background effect. Despite the significant progress of CRISPR technology, no system like this has been described so far. In the first editing strategy, the reporter gene *RFP* was divided into two separate donor plasmids, containing respectively CMV-promoter and *RFP* CDS. Both the CMV-promoter and the *RFP* cassette were flanked by the same sequence, homologous to the coding region of the last exon of *RUNX1T1* gene (Figure 24B). The idea was to assemble the two donors into the last exon of *RUNX1T1* by inducing compatible DNA breaks via CRISPR, and subsequently joining the fragments via NHEJ or MMEJ. This strategy, referred as NHEJ/MMEJ-mediated multiple assembly (or NMA), was intended to produce two simultaneous effects: activation of *RFP* expression in case of correct assembly; *RUNX1T1* knockout by disrupting the sequence coding for the zinc finger, which is proved to be essential for its transcription repression function and is also conserved among all the protein isoforms. The concept of correct assembly order of the two donors, necessary for this strategy, was sustained by a previous work demonstrating precise insertion of DNA fragments through double nickase-Cas9 editing [156]. However, since designing of gRNAs for a double-nick strategy was inconvenient in this case, the alternative Cas protein producing 5 bp-staggered/sticky ends, namely Cpf1, was here employed for precise assembly. Importantly, the donor sequences were designed to insert the *RFP* cassette in the opposite transcription direction of *RUNX1T1*, thereby avoiding RFP synthesis due to formation of a fusion protein. The second editing strategy, characterized by a much simpler design, was based on direct substitution of *RUNX1T1* locus with the gene coding for *GFP* (Figure 24B). The innovative approach, referred as SDSA-mediated knock-in (or SKI), relied on employment of a long single-stranded dDNA containing a reporter gene (*GFP*) flanked by homology arms. A so-designed dDNA was intended to knock-in the reporter cassette via synthesis-dependent strand annealing (SDSA) and, at the same time, to avoid any background effect due to transcription of the dDNA. In support, synthesis and employment of long single-stranded dDNAs for CRISPR editing was previously validated [157, 158]. SKI-editing was performed

by using the same gRNAs employed for deleting *RUNX1T1* gene. Importantly, these gRNAs couldn't target the null allele again and subsequently produce any false positive result, since the target sites were included in the deleted sequence. NMA- and SKI-editing were thereby employed to knockout *RUNX1T1* in clonal cells carrying a single null allele, and fluorescent cells were successfully obtained with an efficiency of about 8.5%, and 12% respectively (Figure 24B). No positive cells were found after NMA-editing when the gRNA was not transfected, therefore demonstrating the absence of background. Differently, rare false positive cells were detected after SKI-editing without gRNA transfection, a result that could be explained by dsDNA contamination during the procedure of ssDNA synthesis. PCR amplification (Figure 24B) and sequencing (data not shown) of the assembled junctions in NMA-edited cells demonstrated that the dDNA components were assembled in the right order, but also that the joining sites included mutations. On the other hand, it was not possible to detect the correct insertion of the *GFP* cassette in SKI-edited cells by screening PCR (Figure 24B). Indeed, the PCR only revealed aberrant insertions characterized by shorter length, a result supposedly due to inefficient PCR-amplification of such external region of *RUNX1T1* locus in *GFP*-labelled cells (data not shown). Although labelled/*RUNX1T1*-KO cells were successfully obtained through the two reporter systems, they were found to be poorly proliferative, and, once selected and isolated by cell sorting, they basically died and were not able to generate clonal lines. These results therefore validated the idea that the complete removal of *RUNX1T1* gene is lethal.

In order to completely abrogate *RUNX1T1* functions in BE(2)-C cells without deleting the whole locus, single Cas9 cleavage was directed toward the sequence coding for the zinc finger, located in the last exon (Figure 24A). Screening of clonal lines was performed via directly sequencing the target region (data not shown). Attention was focused on out-of-frame mutations completely disrupting the NHR4 domain, and then producing a knockout condition. As a result, NHEJ-mediated editing allowed to obtain clonal lines with *indel* mutations on both alleles with 64% efficiency.

In total, five clonal cell lines, edited by either double Cas9 cleavage or NHEJ-mediated editing, were chosen for further analyses (Figure 24C): two lines with a heterozygous null allele (named NU-1 and NU-2); one clone with heterozygous *indel* mutations, one out-of-frame and one in-frame (KO-1); two clones with homozygous out-of-frame mutations (KO-2 and KO-3). Analysis of multiple clonal lines was intended to overcome clonal variability and possible off-target effects due to CRISPR editing.



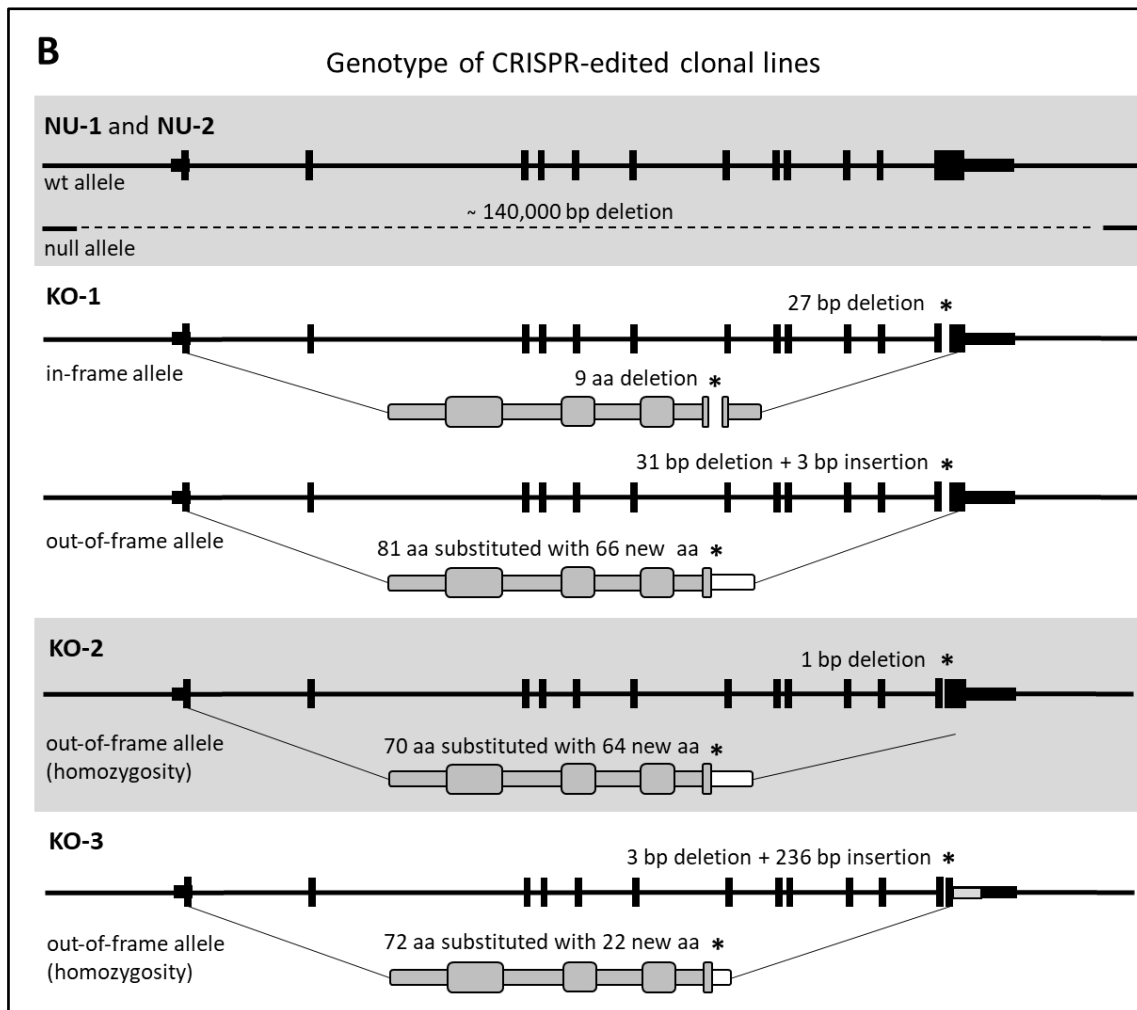


**Figure 24.** CRISPR editing of *RUNX1T1* locus in BE(2)-C cells.

**A.** Representation of *RUNX1T1* locus and the CRISPR-editing strategy. gRNAs *null 1* were used to delete the entire locus in NU-1 and NU-2; gRNA *null 2* and the upstream *null 1* were used to delete the second allele in single-null cells; the gRNA *KO* was used to induce *indel* mutations in KO-1, 2 and 3. **B.** Representation of the two reporter systems used for complete deletion of *RUNX1T1* locus, respectively NMA- (top) and SKI-editing (bottom). The cleavage sites of Cpf1 and Cas9 are indicated by grey triangles, the primers by black arrows. Examples of edited/labelled cells (fluorescence microscope, 40X) and respective editing efficiencies are represented in each panel. The editing efficiency is normalized to transfection efficiency, both measured by flow cytometry. The screening PCR results are represented in each panel (the signs + and - indicate transfection with or without gRNA). **C.** Representation of DNA-sequencing analysis of the mutations characterizing the clonal lines chosen for further analysis. The putative mutations on the amino acid sequence are also indicated.

As expected, qRT-PCR and Western blot analysis of *RUNX1T1* expression revealed that the null clones NU-1 and NU-2 are characterized by approximately halved levels of mRNA and protein compared to BE(2)-C (Figure 25A). This is perfectly consistent with the presence of a

null allele. Differently, *RUNX1T1* mRNA expression in KO-1, -2 and -3 was found to be similar to BE(2)-C, while the Western blot analysis was complicated by the presence of non-specific interactions of the RUNX1T1-specific antibody and by the possible expression of multiple isoforms (Figure 25A). Indeed, RUNX1T1 protein is represented in the wild-type condition by two distinct bands characterized by a little difference in protein size (barely distinguishable in Figure 25A), which is consistent with the size range of most RUNX1T1 protein isoforms. The distinction between isoforms and non-specific bands was possible through Western blot analysis of RUNX1T1 expression in SHEP, a neuroblastoma line that does not express this gene (data not shown). Like NU-1 and NU-2, RUNX1T1 protein is significantly reduced in clone KO-1, while clones KO-2 and KO-3 are characterized by complete absence of the upper band and reduction of the downer band (Figure 25A). In addition, the KO clones, especially KO-3, showed a significant increase in a much lower band, which could represent the mutant protein (shorter than the wild type) but also correspond to a non-specific band (Figure 25A). Interpretation of these results was not obvious. However, since *RUNX1T1* mRNA expression in the KO cells is comparable to the wild type condition (Figure 25A), the significant overall reduction of RUNX1T1 protein in the KO lines is supposedly due to impaired stability. Importantly, the primers utilized for the analysis of *RUNX1T1* mRNA expression via quantitative PCR were complementary to the third last exon, which is common to all mRNA variants and then overcomes the variability due to splicing. Interestingly, only KO-1 retains a significant expression of RUNX1T1 protein among the KO clones (upper band). Also, it is the only KO line to carry an in-frame mutation that, according to a model of protein-structure prediction, preserves the  $\beta$ -strand of NHR4 domain (Figure 25B). Such evidence, together with overall protein reduction in the KO cells, suggests a potential role of the C-terminal domain of RUNX1T1 in protein stability. However, beside all evidences, it is fundamental to the scope of this project to consider that the nonsense mutations of the KO cells undoubtedly impair the transcription regulation activity of RUNX1T1 protein.

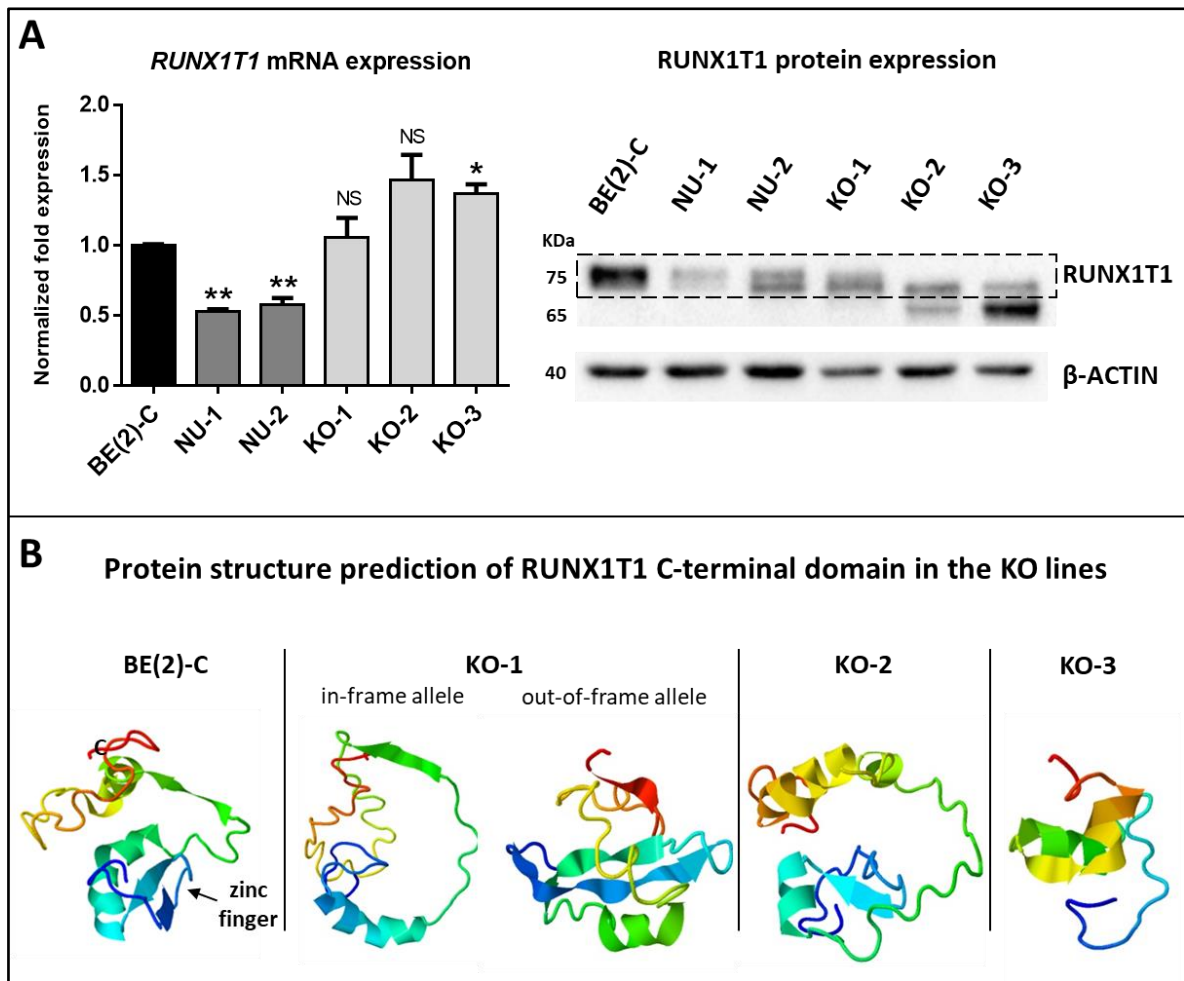


**Figure 25.** Expression analysis of *RUNX1T1* in CRISPR-edited cells.

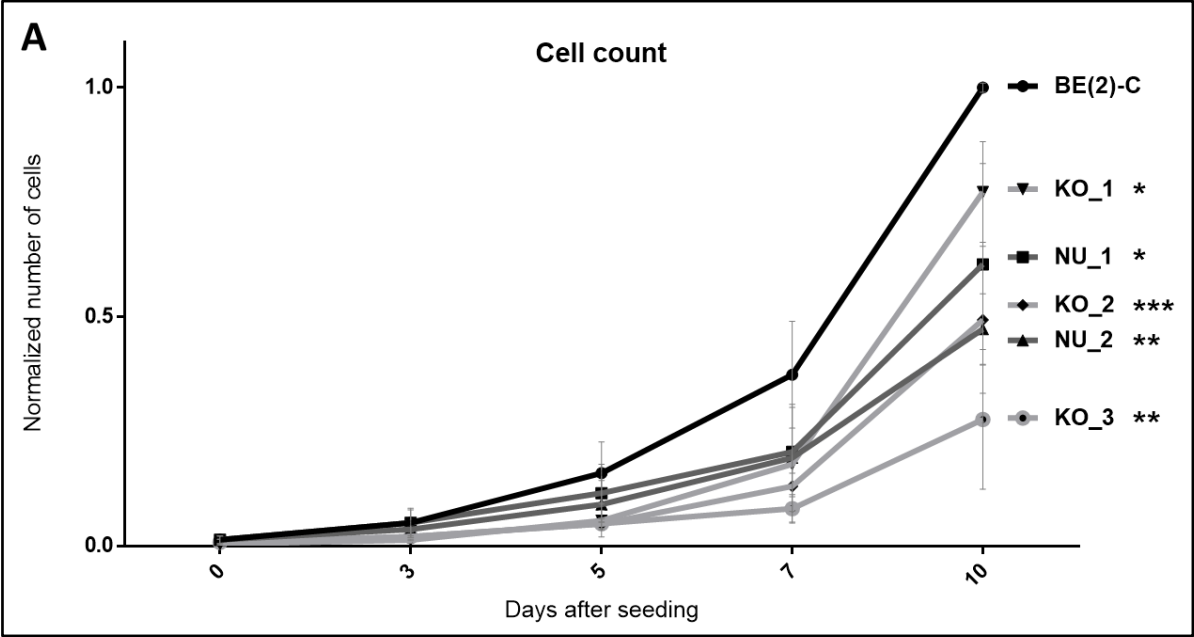
**A.** Expression analysis by qRT-PCR (left) and Western blot with total protein extracts (right) in the CRISPR-edited lines. The bands supposed to correspond to *RUNX1T1* are indicated by a dashed square. Expression of *GUSB* was used for normalization in qRT-PCR, while  $\beta$ -ACTIN was used as housekeeping gene in Western blot. Statistical significance was measured by t-test (\* =  $P < 0.05$ , \*\* =  $P < 0.01$ , \*\*\* =  $P < 0.001$ ). **B.** *In silico* structure prediction of NHR4 and C-term domains of *RUNX1T1* in the KO clones. Protein structure prediction was provided by *I-TASSER*. The N-term side is indicated in blue and the C-term side is indicated in red. The wild type zinc finger is characterized by one  $\alpha$ -helix and two  $\beta$ -strands.

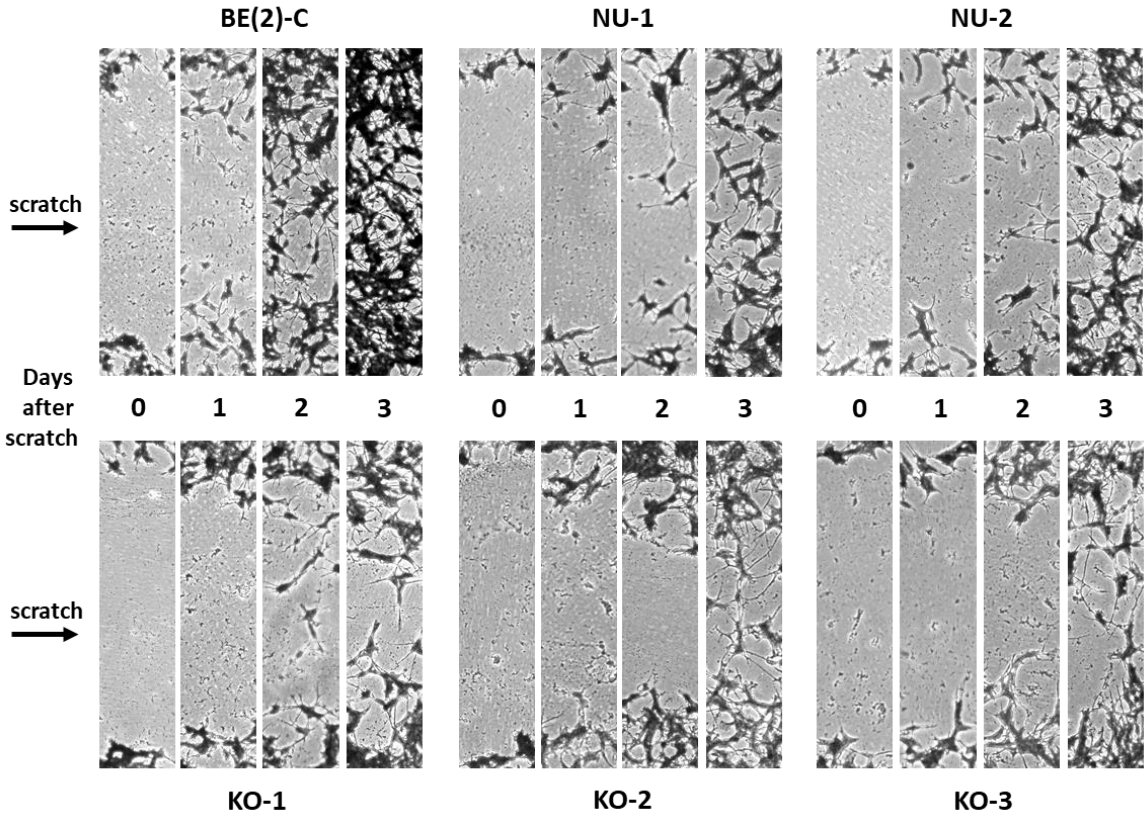
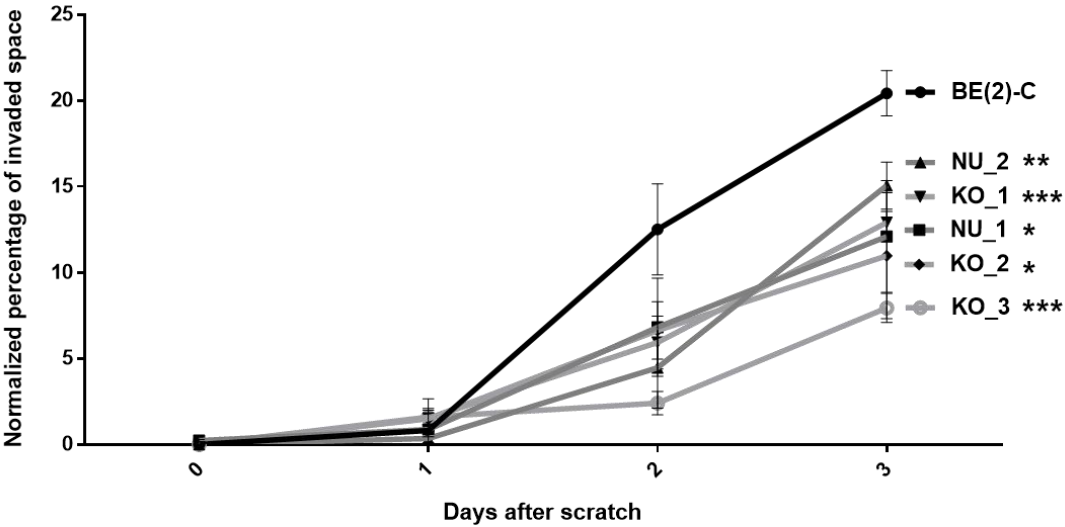
**Phenotypic analysis of *RUNX1T1*-mutated cells.** The five *RUNX1T1*-mutated lines were analysed for the most relevant phenotypic aspects, which are proliferation, migration, differentiation and apoptosis. Proliferation analysis first revealed a significant decrease of proliferation rate in all the mutated lines (Figure 26A). This correlates with the decrease of *RUNX1T1* protein expression characterizing the mutant lines and, especially, the knockout clones KO-2 and KO-3, which showed both the lowest growth rate and the most dramatic

decrease of *RUNX1T1* expression. Interestingly, the effect of *RUNX1T1* mutations on proliferation of clone KO-1 did not appear to be as much significant as for the other clones, which could be supposedly due to rescuing mutations associated with clonal variability. As for proliferation, all the five mutant lines showed impaired migration capacity in wound healing assay (Figure 26B). Also in this case, the lines KO-2 and KO-3 showed the most robust decrease of migration capacity, which is consistent with the complete loss of *RUNX1T1* protein. On the other hand, all the mutant clones showed a higher level of differentiation than the wild type line, with increased number of neurites, more connections between the single cells and larger cell size (Figure 26C). Again, KO-2 and KO-3 showed the highest level of differentiation. Apoptosis was evaluated by Western blot analysis of cleavage and activation of Caspase 3, a main effector of this pathway. In this last case, *RUNX1T1* did not appear to influence apoptosis in the mutant lines, since no Caspase 3 cleavage was detected (data not shown). However, this was not surprising, because BE(2)-C cells are demonstrated to carry a mutation in p53, the most important upstream activator of apoptosis [83]. Altogether, decreased proliferation, impaired migration and increased differentiation of the mutant lines demonstrate that *RUNX1T1* is strongly involved in the main functions of neuroblastoma cells. These results all support an oncogenic role of *RUNX1T1* in neuroblastoma, with a potential effect on both insurgence of the tumour and metastasis spreading. Unexpectedly, the oncogenic role here deduced is in contrast with the oncosuppressor role that was previously evidenced via survival analysis of neuroblastoma patients. This controversy is discussed below and in the following chapters.

Since BE(2)-C is a neuroblastoma line driven by *MYCN*-gene amplification, *MYCN* protein expression was evaluated in order to estimate whether *RUNX1T1* mutations affect expression and/or stability of this oncogene. While the null-allele clones showed only a slight reduction of *MYCN* protein level, the three KO clones appeared to be affected by a more visible decrease (Figure 26D). This result is consistent with the observed phenotype, but the *MYCN* protein level among the KO clones does not perfectly match the amplitude of changes observed in proliferation, migration and differentiation assays. In addition, it is unlikely that *RUNX1T1* is directly involved in the regulation of *MYCN* expression, since it is demonstrated to be a transcription repressor, and KO mutations of *RUNX1T1* should thereby implicate an increased expression of the direct targets. The expression of other two important players of the *MYC* network, namely *MAX* and *MNT*, was then analysed. These are respectively *MYCN*-protein partner and antagonist. Also here, expression of these factors appeared to be impaired in the KO clones (Figure 26D), which is unexpected for *MNT* if considered that its function is notoriously opposed to that of *MYCN*. Indeed, decreased expression of this factor is not

consistent with the phenotype observed in the mutant clones. However, it is clear that *RUNX1T1* mutation has an influence on the Myc/Max/Mad network itself. From one side, this is consistent with the idea that *RUNX1T1* is a transcription regulator with a putative large number of targets. On the other hand, these results confirm the relevant role of *RUNX1T1* in cell functions.



**B****Wound healing assay**

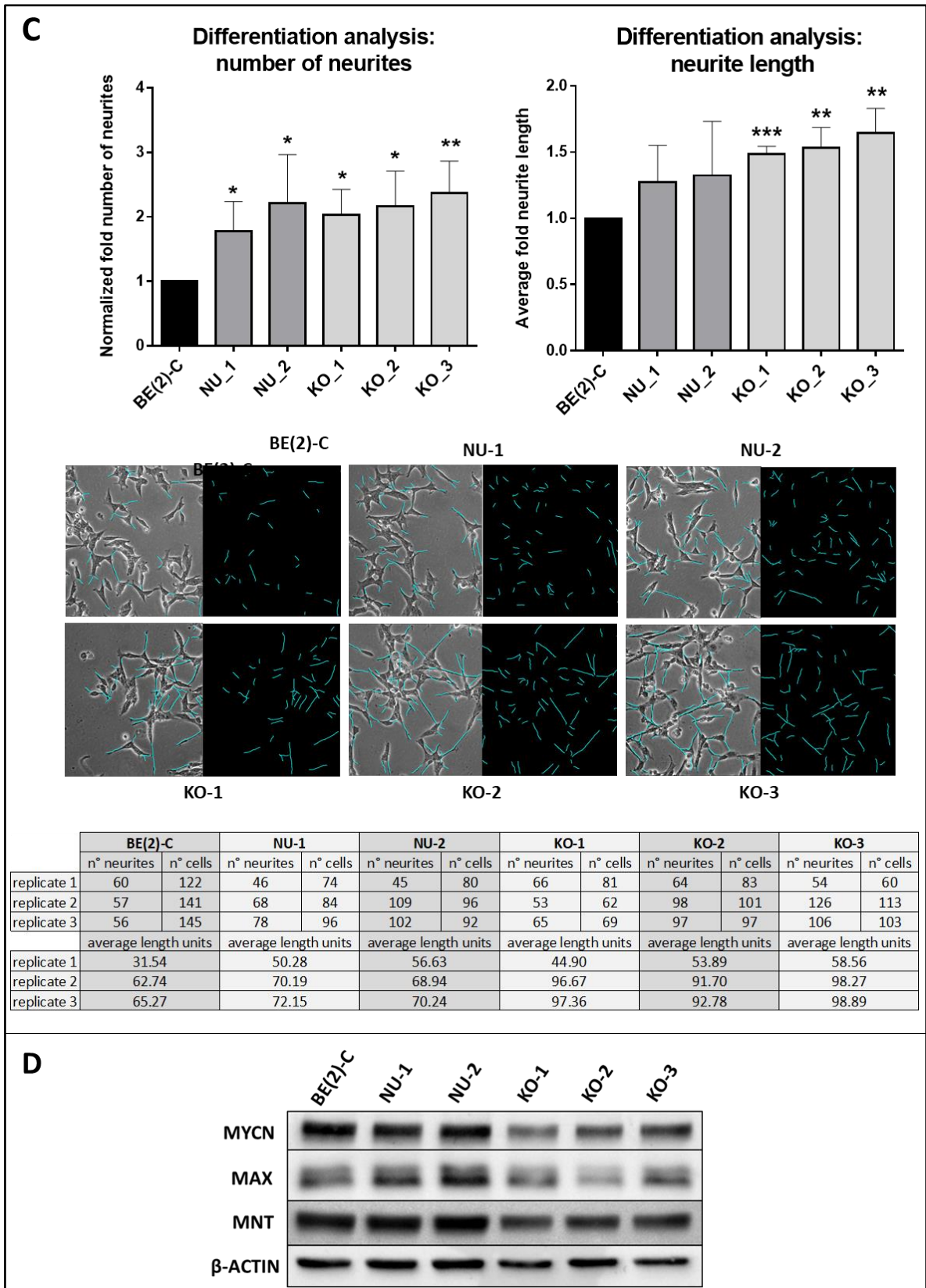


**Figure 26.** Phenotype analysis of *RUNX1T1*-mutated cell lines.

**A.** Cell count performed by *Bürker chamber*. Data are shown as fold change with respect to the number of BE(2)-C cells on day 10. **B.** Wound healing assay. Cells were seeded at 90% confluency and scratched at day 0. Then, cells were stained with crystal violet and analysed by *ImageJ* software at day 0, 1, 2 and 3. Wound repair is represented as percentage of invaded space normalized to day 0. The bottom pictures represent examples of the analysed samples (10X magnification). **C.** Differentiation analysis by *NeuroJ* software. Top-left: analysis of the number of neurites (normalised to the number of cells). Top right: analysis of the average neurite length. Centre: examples of analysed samples (20X magnification); every picture is shown in low contrast (left) and high contrast (right); neurites are highlighted in cyan colour. Bottom: measures of the number of neurites per cell and their average length units. **D.** Expression of MYC-network members by Western blot.  $\beta$ -ACTIN was used as housekeeping gene. Statistical significance was measured by unpaired t-test for experiments in Figure 26A, B and C (\* =  $P < 0.05$ , \*\* =  $P < 0.01$ , \*\*\* =  $P < 0.001$ ).

In order to further demonstrate that *RUNX1T1* promotes cell aggressiveness in neuroblastoma, a rescue assay was performed with the mutant cells. The line with the most dramatic phenotype, KO-3, was stably transfected with a vector expressing wild type *RUNX1T1*. The mouse homologous of *RUNX1T1* was chosen for this task, since the multiple transcript variants (15) of the human gene made the cloning procedure virtually impossible. Indeed, the mouse gene codes for only 3 demonstrated protein isoforms, the longest of which is highly conserved with respect to the human isoforms (97.52% identity) [NCBI assembly GRCm38.p4] and was then cloned for the rescue assay. Colorimetric analysis of the KO-3 cells overexpressing mouse *RUNX1T1* revealed an increased growth rate compared to the cells transfected with an empty vector (Figure 27). This result partially confirms the tumour-promoter role of *RUNX1T1* in neuroblastoma.

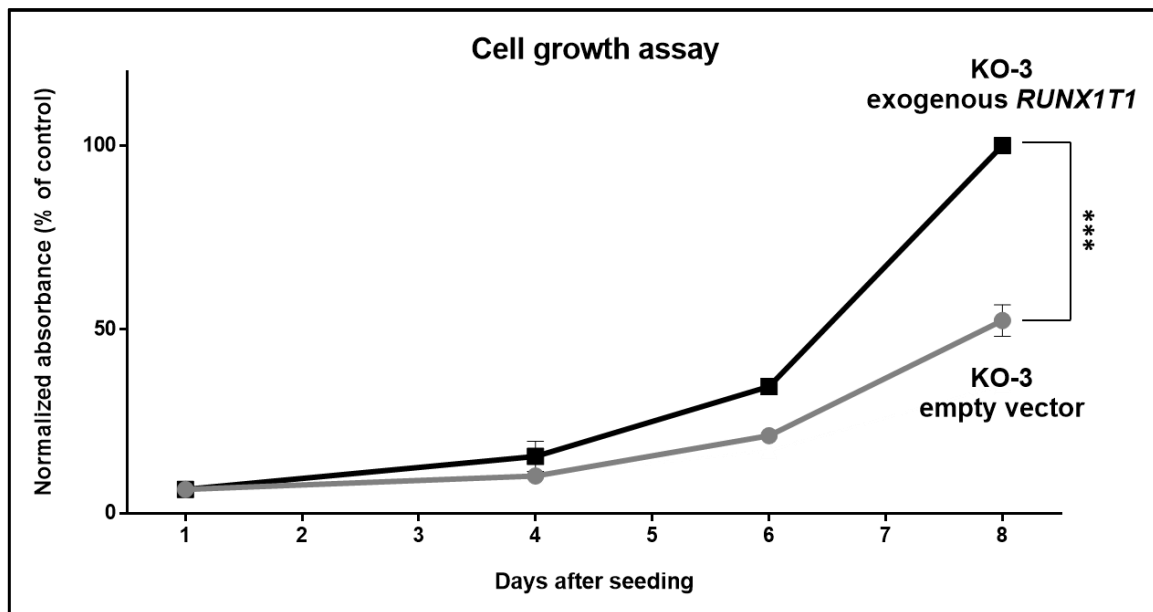


**Figure 27.** Phenotype rescue of *RUNX1T1*-KO cells.

KO-3 cells were stably transfected with either an empty vector or a vector expressing mouse *RUNX1T1*. The growth rate was then measured by crystal-violet colorimetric assay. Absorbance data are shown as percentage with respect to cells transfected with *RUNX1T1* and analysed at day 8. Empty wells were used for normalization. Statistical significance was measured by unpaired t-test (\* =  $P < 0.05$ , \*\* =  $P < 0.01$ , \*\*\* =  $P < 0.001$ ).

Overall, CRISPR-editing of *RUNX1T1* demonstrated that the gene potentially regulates proliferation, migration and differentiation in neuroblastoma cells. All the phenotypic signatures of the mutant cells agree with a tumour-promoter role of *RUNX1T1* in neuroblastoma, a condition previously observed in bladder cancer and malignant mesothelioma. In agreement with the multiple involvement of *RUNX1T1* in distinct development events and insurgence of different types of cancer, the association with relevant cell functions in neuroblastoma also suggests a potential role of this gene in neural crest development. The mutant phenotypes can be partially explained by the reduced MYCN protein expression that characterizes *RUNX1T1*-mutant cells. By the way, the reduction of MYCN expression is not perfectly consistent with cell behaviour. Furthermore, also MAD protein expression was found to be impaired, which is in contrast with the phenotype of the mutant lines. It is therefore possible that *RUNX1T1* function in neuroblastoma is parallel to the Myc/Max/Mad network, and that the influence on expression of MYC-network members is a feedback effect. This, if confirmed, would add more value to *RUNX1T1* role in aggressive neuroblastoma. Interestingly, the oncogenic role of *RUNX1T1* evidenced in neuroblastoma cell cultures is in perfect contrast

with the positive correlation between *RUNX1T1* expression and survival of neuroblastoma patients. Similar to the study concerning *ODCI* gene, this evidence could be explained by considering the different nature of the two examined systems. First, *in vitro* cell cultures are studied in an extremely simplified environment, where factors such as circulating signals, nutrients/oxygen supply, interaction with different tissues and 3D structure are not involved. Nevertheless, *RUNX1T1*, in the role of a modular transcription regulator, potentially affects all these conditions. Second, while analysis of *RUNX1T1* expression and patients' survival was based on RNA samples collected from primary tumours, the *in vitro* experiments were performed with BE(2)-C cells, which derive from neuroblastoma metastases located in the bone marrow. The pattern of genes playing a role in metastasis spreading and invasion are mostly different from those involved in tumour development and growth. Third, it is unlikely to observe a worsening of the tumour phenotype in response to mutations affecting an oncosuppressor in an already aggressive cell line, such as BE(2)-C. All these considerations are even more significant in relation with *RUNX1T1* itself, whose functions are demonstrated to be context dependent. A more intriguing possibility is represented by the complex expression dynamics of *RUNX1T1* gene, which today accounts for 15 demonstrated transcript variants. Indeed, the datasets used for survival analysis rely on microarray expression data, and they might take into account only a few variants of *RUNX1T1*. Differently, the CRISPR-editing procedure performed in this study affects all *RUNX1T1* isoforms.

### **2.3-Mutation of *RUNX1T1* affects signalling pathways involved in neuroblastoma progression and neural crest development**

**Transcriptome analysis of *RUNX1T1*-mutated cells.** The transcriptome of the five CRISPR-edited clonal lines was analysed by RNAseq in order to evaluate which molecular functions are most affected by *RUNX1T1* mutations and, ultimately, to find out which pathways are associated to the tumour-suppression phenotype observed in the mutant lines. RNAseq analysis revealed a total of 829 genes whose expression is at least 2-fold increased/decreased on average among the five mutant lines, with a maximum change of more than 1000-fold in some cases (Figure 28A). Overall, 370 genes were found to be upregulated and 459

downregulated. Only genes whose expression change is consistent among the five lines were taken into consideration, since the phenotype of the CRISPR-edited cells is similarly consistent among the five lines. The large number of genes impaired in the mutant lines and the significant expression change characterizing some of them both support the transcription regulation function of *RUNX1T1*. Furthermore, the upregulated genes, but not the downregulated ones, showed an expression change pattern that generally matches the type of mutation of *RUNX1T1*, with the highest change often found in the KO lines. This supports the model of *RUNX1T1* protein being part of a transcriptional repression complex. Cross-analysis between the RNAseq and three publicly-available transcriptome datasets obtained from large cohorts of neuroblastoma patients (*Versteeg* [77], *TARGET* [78], *NRC* [84]) revealed that a significant number of genes are strong predictors of prognosis in neuroblastoma (Figure 28A). More specifically, 75 predictors of survival were found to be upregulated, while 63 death predictors were found to be downregulated, all consistent with the decreased aggressiveness of the mutant lines. In addition, the percentage of survival predictors among the upregulated genes is significantly larger than the percentage of death predictors among the downregulated genes (20.3% against 13.7%), suggesting that the direct function of *RUNX1T1* in neuroblastoma could be maintaining the cells in an undifferentiated/aggressive state by repressing the expression of tumour suppressors. Notably, one of the most significant survival predictors that is upregulated in the mutant clones is *NTRK1*, a strong marker of both neural crest differentiation and high survival in neuroblastoma [3]. *SEMA6D* is another regulator of neural crest differentiation to be found among the upregulated survival predictors. This is a semaphorin that, like *SEMA3D* (also found among the upregulated genes), is demonstrated to regulate neural crest cell migration [85]. On the other hand, *ALK* is one of the downregulated genes to be identified as a death predictor. This is consistent with the occurrence of activating mutations of *ALK* gene in a significant number of familial neuroblastomas [1-3]. All these evidences support the idea of a neuroblastoma-specific involvement of *RUNX1T1* in tumour development and progression. On the other hand, some survival predictors were also found among the downregulated genes, and *vice versa* for death predictors. This finding, in evident contrast with the phenotype of the mutant lines, is consistent with the oncosuppressor role of *RUNX1T1* that was evidenced in neuroblastoma patients. This apparent contradiction nonetheless supports the concept that *RUNX1T1* is a wide-range transcription regulator with a context-dependent function.

In order to identify neuroblastoma-associated pathways that are affected by *RUNX1T1* mutations, the set of 829 genes was analysed by gene ontology (Figure 28B). At first, a significant number of genes was found to be associated with neural cell differentiation (80

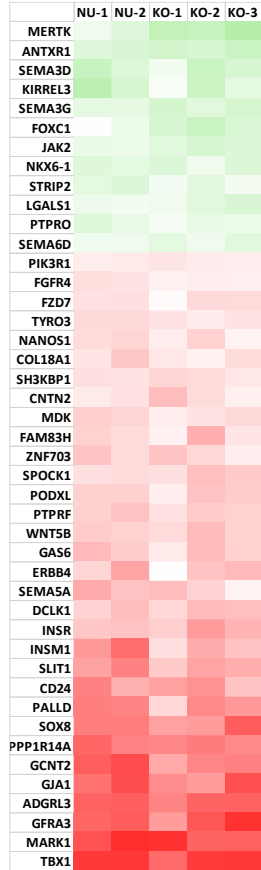
genes), cell migration (44 genes), cell proliferation (25 genes) and cell adhesion (39 genes). Also, 16 genes were identified as regulators of neural crest cell migration and differentiation (*IGF2*, *FGF2*, *FGF10*, *FGF20*, *CDH6*, *SOX9*, *PIK3R1*, *MSX2*, *MYB*, *SEMA5A*, *SEMA6D*, *ERBB4*, *SEMA3G*, *SEMA3D*, *TBX1*, and *SOX8*). Such finding was not unexpected, since the most evident phenotypic signatures of the mutant lines are, indeed, decreased proliferation and migration, and increased differentiation. Even apoptosis was found to be represented by a significant number of genes (42), indicating a potential role of *RUNX1T1* in this function despite no apoptotic activity was detected in the mutant lines. Furthermore, the whole set of genes is not enriched for the known targets of MYCN, not even the most important and best characterized ones [13]. This evidence supports the idea that *MYCN* regulation network has not an obvious role in determining the phenotype of *RUNX1T1*-mutated cells. Gene ontology analysis then revealed several signalling pathways that are represented by a significant number of genes (Figure 28C). These are PI3K-Akt (25 genes), Wnt (22 genes), cAMP-PKA (20 genes), MAPK-Erk (19 genes), Rap1 (17 genes), Notch (15 genes), cGMP-PKG (14 genes), and Hippo pathway (12 genes). All these pathways are supposedly altered in the mutant clones, and this, if confirmed, would extensively demonstrate the wide range of action of *RUNX1T1*. In support, *RUNX1T1* mutation affects the expression of many secreted signals (i.e. *FGF2*, *FGF10*, *FGF20*, *EFNA2*, *EFNA4*, *IGF2*) that potentially regulate several interconnected pathways at the same time. Some of these pathways are known to play a role in neuroblastoma development and neural crest differentiation. Wnt pathway, as instance, is a known regulator of neural crest differentiation, and it is demonstrated to drive proliferation and/or differentiation in neuroblastoma cells in a context-dependent manner [86, 87]. Upregulation of Wnt pathway inhibitors (*DKK1*, *DKK2*, *NPHP3*, *DACT3*), as well as downregulation of two important activator signals (*WNT3*, *WNT5B*), a receptor (*FZD7*), an upstream activator (*MARK1*) and a downstream effector (*TNIK*), altogether suggest a downregulation of the entire pathway in association with mutation of *RUNX1T1*. This perfectly correlates with decreased proliferation rate of the mutant lines, but not with increased differentiation. PI3K-Akt, another pathway massively represented among the altered genes, is a well-established driver of tumorigenesis, and its activation correlates with poor outcome in neuroblastoma. It is also involved in neural crest differentiation [88, 89]. Consistent with the weak aggressiveness of the clonal lines, the pathway appears to be impaired when *RUNX1T1* is mutated, an evidence sustained by decreased expression of a central activator of the pathway, *PIK3R*, and of a typical transcription target, *MYB*. In addition, a previous study demonstrated that inhibition of PI3K-Akt pathway leads to destabilization of MYCN protein [90], a condition already observed in the mutant cells (see

Figure 26D). MAPK-Erk pathway, also identified by ontology analysis, regulates multipotency maintenance of neural crest cells, even though little is known about its involvement in neuroblastoma development and progression [91]. However, MAPK-Erk is a convergence point of several other signalling pathways, and expression of a significant number of related factors is impaired in the mutant lines. This suggests that the pathway could be directly involved in the mutant phenotype. Hippo pathway was recently demonstrated to mediate neural crest differentiation and, also, to positively correlate with poor outcome in neuroblastoma [92, 93]. In contrast with the observed phenotype, it appears to be activated in the mutant cells, as the repressor *CRB2* is downregulated and both the main effector *YAPI* and the transcriptional target *BBC3* are upregulated. Rap1 signalling is demonstrated to drive neuroblastoma cell proliferation via ALK-mediated activation of the pathway [94]. Again, this is consistent with downregulation of *ALK* expression in the mutant lines. The last signalling pathway that is represented among the altered genes, Notch, is specifically involved in neural crest development, while its activation is demonstrated to block the growth of neuroblastoma cells [95, 96]. At last, RNAseq and gene ontology analysis allowed to evaluate some aspects of *RUNX1T1* regulation network that might be relevant for tumour progression in a physiological context. As instance, 9 genes were found to be implicated in cellular response to hypoxia, including the fundamental regulator *HIF3A* (data not shown). Response to hypoxia is commonly accepted to be an important factor in neuroblastoma progression, since low oxygenation stimulates tumour vascularization and growth in size [116]. Also, 9 genes were found to be involved in regulation of inflammatory response, suggesting that *RUNX1T1* might influence the immune response against neuroblastoma (data not shown).

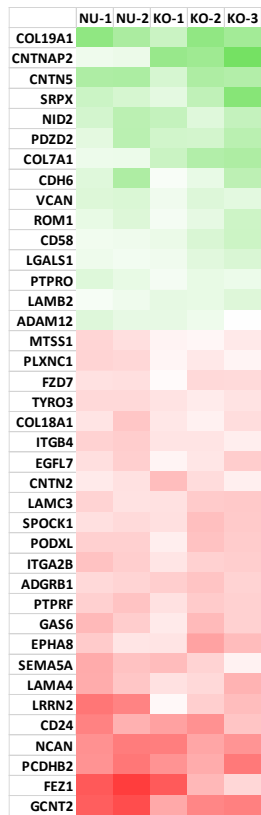


**B**

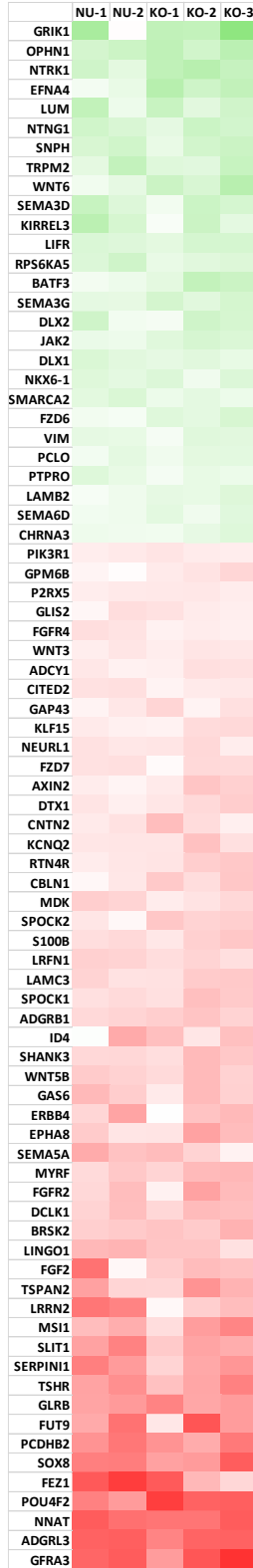
**Cell migration**



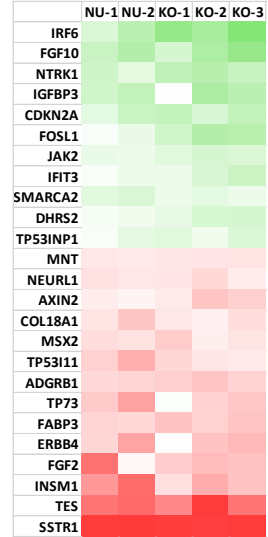
**Cell adhesion**



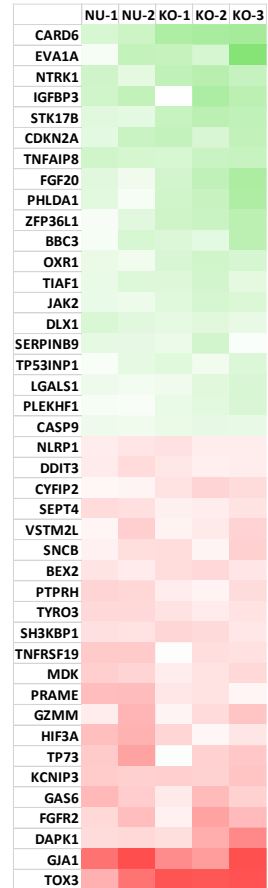
**Neural differentiation**



**Proliferation**



**Apoptosis**



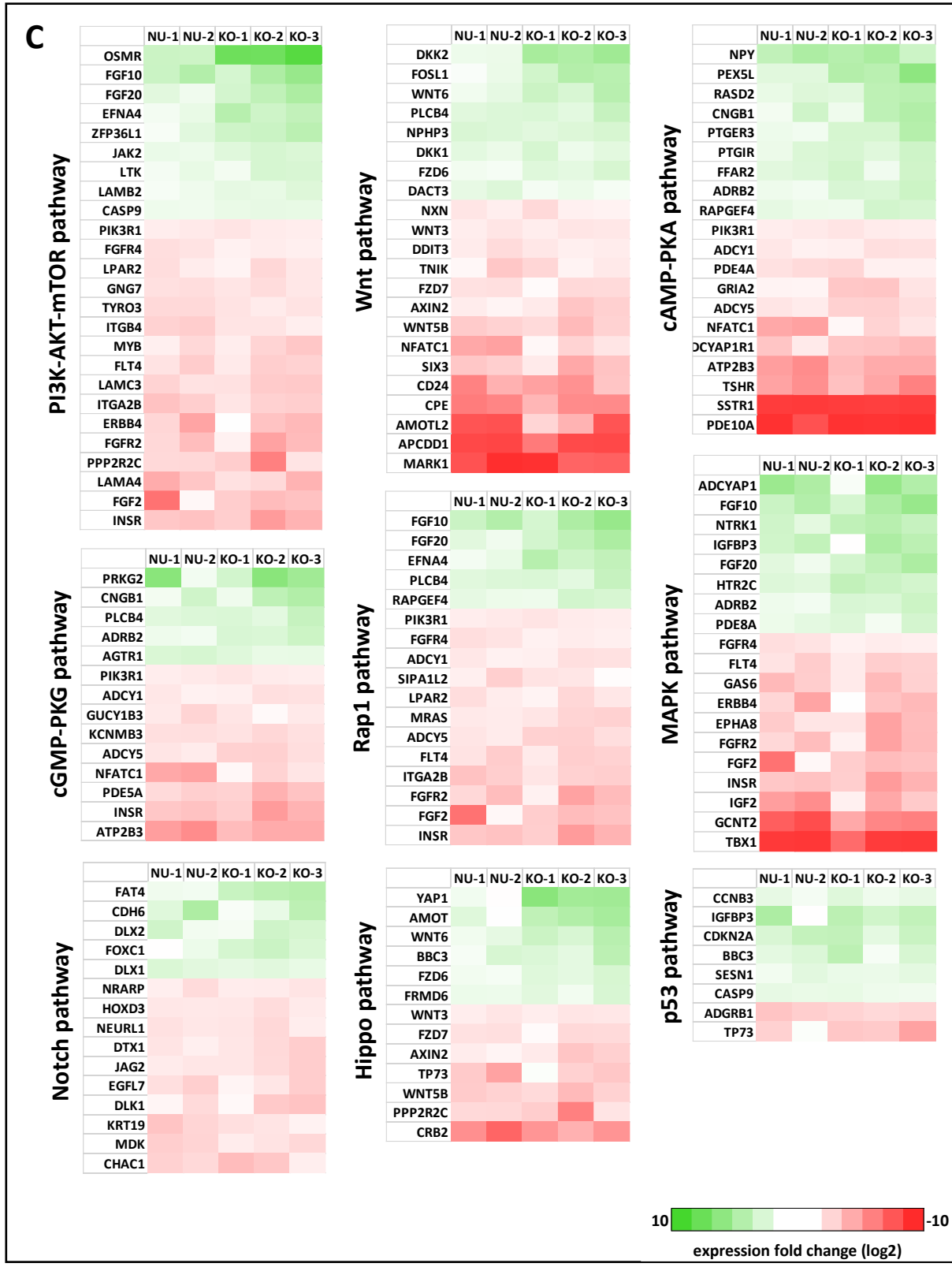


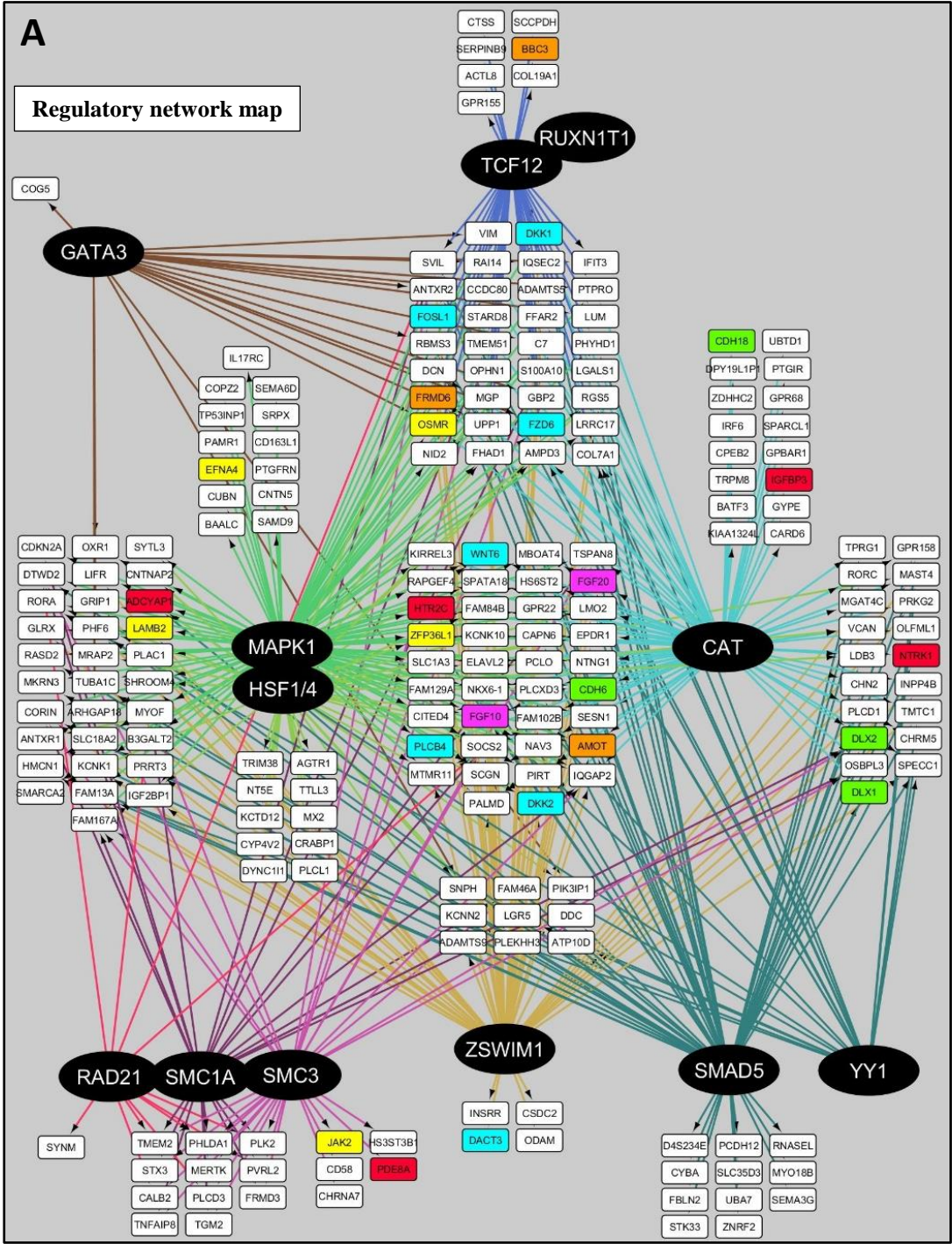
**Figure 28.** Transcriptome analysis of *RUNX1T1*-mutated cells.

- A.** RNAseq analysis of the most deregulate genes in NU-1, NU-2, KO-1, KO-2 and KO-3. Upregulated tumour suppressors and downregulated death predictors are labelled in yellow.
- B.** Gene ontology analysis of deregulated genes that are involved in principal cell functions.
- C.** Gene ontology analysis of deregulated genes that are involved in significant signalling pathways. In all figures, expression fold change is relative to BE(2)-C cells, and the lines NU-1, NU-2, KO-1, KO-2 and KO-3 are represented in each column from left to right.

**Prediction of *RUNX1T1* regulon.** The spectrum of phenotype signatures characterizing the clonal lines are likely orchestrated by the signalling pathways that are supposedly affected by *RUNX1T1* mutations. It is reasonable to assume that *RUNX1T1* protein itself, as part of a transcription repression complex, regulates the expression of factors directly involved in one, or more, of these pathways, while the remaining signalling pathways are consequently affected via a hierarchical mechanism. The pathways that are directly influenced by *RUNX1T1* activity could be highly interesting for targeted therapy in neuroblastoma, since the phenotype observed in the mutant lines could be reproduced, and even improved, by using pathway-specific drugs. However, identification of the direct targets of *RUNX1T1* is complicated by the inability of the protein to bind DNA. The current model indeed establishes that *RUNX1T1*, and the related repression complex, is recruited on target genes through interaction with primary transcription factors. So far, only a few of these *RUNX1T1* co-regulators have been described, but no one in the context of neuroblastoma. Thus, in order to predict which transcription factors are most likely responsible of *RUNX1T1*-mediated transcription regulation in neuroblastoma, a regulon-prediction tool (*iRegulon*) was used to examine the set of genes whose expression is altered in the mutant lines. The software tool associates canonical DNA motifs, found in the target genes, with putative transcription factors. The software operates on a collection of thousands of ChIP-seq databases accounting for a total of about 10,000 canonical binding motifs. Since disruption of *RUNX1T1* activity is supposed to cause upregulation of the direct targets, only the 370 upregulated genes were taken for analysis. The search for DNA motifs was limited to 500 bp around the TSS in order to make the analysis stringent. Prediction of the regulation network revealed a series of 12 putative transcription factors (*TCF12*, *MAPK1*, *CAT*, *HSF1*, *HSF4*, *GATA3*, *RAD21*, *SMC1A*, *SMC3*, *ZSWIM1*, *SMAD5*, and *YY1*) that potentially regulate a significant number of genes among the 370 (Figure 29A). Some of these genes share common binding motifs and are therefore regulated by the same factors. Interestingly, the expression of none of the 12 transcription factors is significantly altered in *RUNX1T1*-mutated lines, hence indicating two possible circumstances: impairment of *RUNX1T1* activity affects stability of

these proteins; loss of *RUNX1T1* protein affects the function of an eventual protein-protein interaction. With the aim at investigating the second possibility, interaction between *RUNX1T1* and the 12 putative transcription factors was evaluated via *STRING* software, an online tool that predicts protein-protein interactions through databases of experimental evidences. Surprisingly, *RUNX1T1* was found to directly interact with *TCF12*, interaction that was previously demonstrated in 293T cells [97]. *TCF12* is a basic helix-loop-helix (bHLH) protein that can bind the canonical E-box sequence (CANNTG). Prediction of putative targets by *iRegulon* revealed that *TCF12* could directly regulate the expression of genes involved in Wnt and Hippo pathways. More specifically, it was associated to upregulation of *DKK1* and *FRMD6*, respectively an inhibitor of Wnt and an activator of Hippo pathway. Also *BBC3*, a downstream inducer of apoptosis, was found to be a potential regulation target. *TCF12* is known to be involved in neuronal differentiation [98], and it can also promote pluripotency maintenance in osteoblasts [99]. The mechanism through which it regulates osteoblast differentiation is mediated by MAPK-Erk and BMP signalling pathways, which are overall downregulated by *TCF12* [100]. This is consistent with the finding that MAPK-Erk pathway is potentially altered in the CRISPR clones. A further study demonstrated that high *TCF12* expression in colorectal cancer promotes cell migration, invasion and metastasis via directly downregulating E-cadherin expression [101]. On the other hand, downregulation of E-cadherin is essential for epithelial-to-mesenchymal-transition (EMT) and consequent migration of neural crest cells [7, 10, 102]. In addition, two cadherins (*CDH6* and *CHD18*) are upregulated in the mutant lines, although they are not predicted to be directly regulated by *TCF12*; however, *TCF12* appeared to directly bind *CDH18* locus when the region queried was *iRegulon* is 10 kb around the TSS (data not shown). Notably, different studies demonstrated that the cadherin effect on cell motility is not strictly mechanic, since cadherin-mediated cell contact regulates a series of signalling pathways that include PI3K-Akt, Wnt, Hippo and, indeed, MAPK-Erk [103]. According to all these evidences, a possible model explaining the phenotypic signatures of the CRISPR lines implicates that impairment of *TCF12* activity by *RUNX1T1* mutation might affect signalling pathways such as Wnt, Hippo and MAPK-Erk (Figure 29B). All these pathways potentially regulate proliferation and differentiation. Additionally, the effect on expression of cadherins might impair cell adhesion and motility, and it might also generate a feedback effect on the previous signalling pathways (Figure 29B). As last consideration, analysis of the regulation network of either the 370 upregulated or the 459 downregulated genes in *RUNX1T1*-mutated cells did not detect enriched genes putatively regulated by factor of the Myc/Max/Mad network, including *MYCN* (data not shown for the downregulated genes). This further supports the idea

that the role of *RUNX1T1* in neuroblastoma development and progression is independent from the main oncodriver of this tumour, *MYCN*. Analysis of the downregulated genes also revealed a significant number of putative targets of *ARNT* (data not shown), a fundamental regulator of hypoxia-response pathway together with *HIF* factors. Such evidence, consistent with the previous observation made in the gene ontology analysis, confirms a potential role of *RUNX1T1* in hypoxia response in a physiological context.



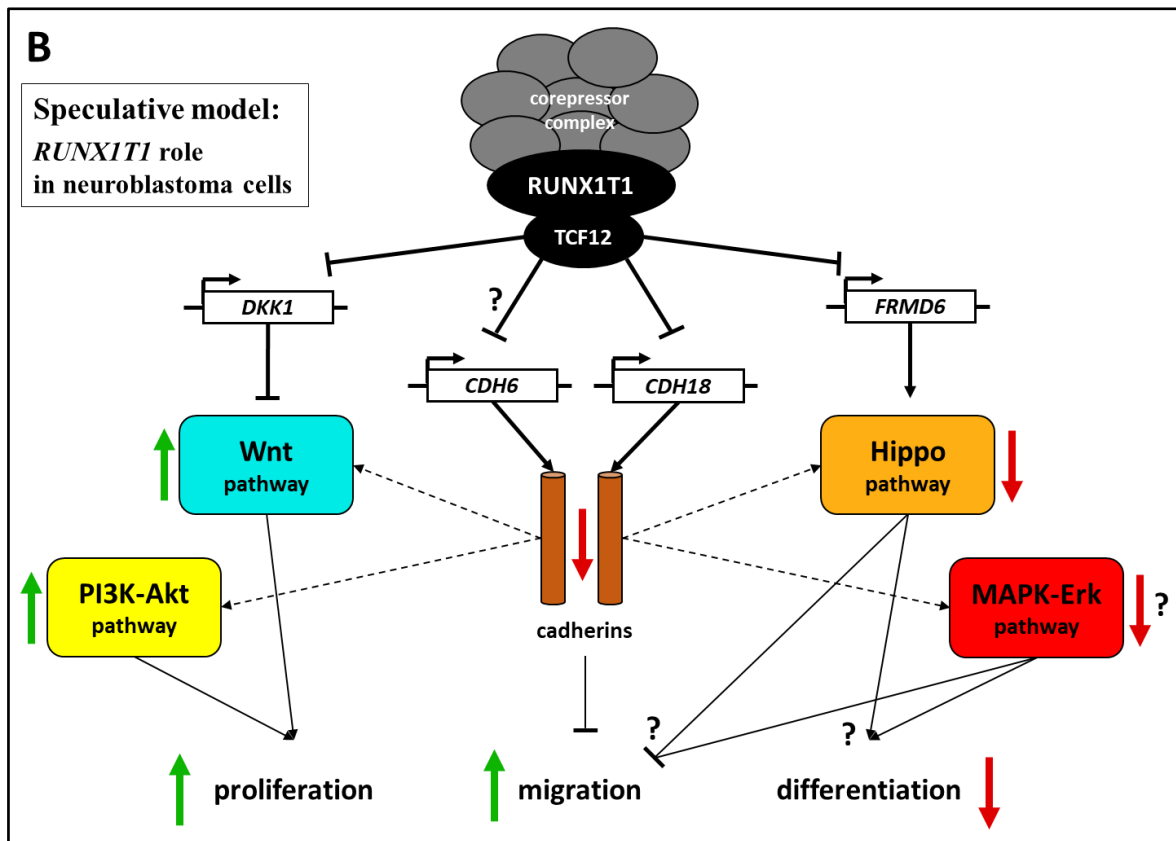


**Figure 29.** Prediction of *RUNX1T1* regulatory network in BE(2)-C cells.  
**A.** Prediction by *iRegulon* of the transcription factors regulating the 370 genes upregulated in the mutant lines. The black-labelled and the white-labelled nodes respectively represent transcription regulators and targets. Regulation connections are indicated by arrows. Overlapping transcription factors are interactors (found by *STRING*). Genes involved in PI3K-Akt pathway are labelled in yellow, Wnt in light blue, MAPK-Erk in red, Hippo in orange, Notch in green, and multifunctional growth factors in purple. **B.** Speculative model of *RUNX1T1* regulation of pathways and mechanisms that are relevant for neuroblastoma cell behaviour. Green and red arrows respectively indicate up- and down-regulation.

Transcriptome analysis of mutant cells with a heterozygous null allele of *RUNX1T1* (NU-1 and NU-2) and *RUNX1T1*-knockout cells (KO-1, KO-2 and KO-3) revealed a large number of genes whose expression is significantly affected. This result is perfectly in line with the transcription regulation function that is attributed to *RUNX1T1*. A significant number of genes was found to be predictors of neuroblastoma outcome, with *RUNX1T1* potentially downregulating survival predictors (75 in total) and indirectly upregulating death predictors (63 in total). This result confirms the tumour-promoter role of *RUNX1T1* in the context of aggressive neuroblastoma cells. As expected, gene ontology analysis of the RNAseq data revealed a significant number of genes involved in proliferation, migration, differentiation and

apoptosis, confirming the relevant role of *RUNX1T1* in neuroblastoma cell behaviour. Some of these genes are also known to be involved in neural crest development, a finding consistent with the switchable function of *RUNX1T1* between embryo development and tumour progression. Gene ontology analysis also revealed that several impaired genes belong to important signalling pathways (PI3K-Akt, Wnt, cAMP-PKA, MAPK-Erk, Rap1, cGMP-PKG, Hippo, Notch). The assumed inhibition of Wnt and PI3K-Akt pathways is consistent with poor aggressiveness of the mutant lines, but not activation of Hippo. However, RNAseq data are not enough to evaluate the activity of such pathways, and every deduction is purely speculative. Certainly, the large number of pathways potentially affected indicate that *RUNX1T1*-mediated regulation of cell behaviour is likely conveyed by these signalling mechanisms. In support of this, *RUNX1T1* mutation affects many secreted signals that potentially regulate several interconnected pathways at the same time. Such evidence could also explain why it is possible to obtain and detect cells with double-null alleles by CRISPR editing, but it's not possible to isolate single clonal lines (see chapter 2.2). A more accurate analysis of the RNAseq data allowed to predict the transcription-regulation network that is impaired in the mutant lines. Interestingly, *TCF12*, a known interactor of *RUNX1T1*, was found to potentially regulate a significant number of genes, some of which involved in relevant signalling pathways. It was therefore modelled that *RUNX1T1* protein, via interaction with *TCF12*, regulates a series of genes, including also cadherins, which are involved in MAPK-Erk, PI3K-Akt, Wnt and Hippo pathways, thus influencing proliferation, migration and differentiation of neuroblastoma cells. This model, if experimentally confirmed, could provide a new base for understanding the molecular mechanisms behind neuroblastoma development and progression, and for developing novel therapy strategies.

### **3-CRISPR-targeting of *MYCN* amplification is a potential therapeutic strategy in neuroblastoma**

The third and last part of this project was aimed at evaluating the therapeutic potential of targeting *MYCN* amplification through CRISPR-editing in aggressive neuroblastoma cells. The strategy was intended to impair cell proliferation and, at the same time, promote apoptosis via two parallel mechanisms, which are *MYNC* knockout and induction of a large-scale DNA damage. A couple of gRNAs, with target sites flanking *MYCN* coding-sequence, was designed to delete the entire included region following Cas9 cleavage (Figure 30A). The dual Cas9-cut was then supposed to be converted into an extended DNA damage in case of *MYCN* amplification. This strategy was tested in six different cell lines, which included three *MYCN*-amplified lines (IMR32, CHP134 and BE(2)-C), two *MYNC*-non amplified lines (SHEP and SHSY5Y) and a non-neuroblastoma cell line (293T). The experiment was performed by transfecting cells with the indicated couple of gRNAs and a Cas9 variant fused to GFP, so to evaluate the number of transfected/fluorescent cells in the total population over time and, therefore, their survival. The percentage of fluorescent cells was measured by flow cytometry at days 2 and 5 post-transfection, a time frame that was supposed to be appropriate for estimating any relevant effect. Consistently with the initial idea, flow cytometry analysis revealed that survival of *MYCN*-amplified lines IMR32 and CHP134 is significantly impaired by Cas9 treatment. On the contrary, the treatment resulted completely ineffective in all the *MYCN*-non amplified lines, including 293T (Figure 30B). These results clearly proved the efficacy of impairing cell proliferation via Cas9-targeting of *MYCN* amplification. In addition, high specificity of the system for *MYCN*-amplified cells was evidenced, indicating that the effect on survival might be mainly due to cell-cycle arrest as a consequence of DNA damage. In order to confirm this assumption, a comparison between proliferation decrease and *MYCN* expression is necessary, but it was not possible to estimate the second factor due to the relative low number of transfected cells. Curiously, Cas9 treatment was found to be completely ineffective in BE(2)-C cells, which are characterized by *MYCN* amplification (Figure 30B). This result can be explained by the presence of an inactivating mutation in *p53*, thus making these cells unable to correctly activate cell-cycle arrest and apoptosis [83]. The condition of BE(2)-C cells therefore supported the idea of a mechanism mainly based on response to DNA

damage. Indeed, some effect on proliferation was expected to be induced by impairment of *MYCN* expression, but it was not observed. This might indicate either a sort of compensating mechanism occurring in this line, or that the Cas9 system is not able to significantly reduce *MYCN* expression. Either possibilities remain to be verified. Unfortunately, the survival data were overall affected by great variability, which is probably due to low transfection efficiency. However, more replicates were analysed in order to make the results more reliable. As a control, deletion of *MYCN* gene in the six cell lines was evaluated via PCR with a couple of primers flanking the target region (Figure 30A). Only *MYCN*-amplified cells showed a clear positive result, while the PCR product was barely detectable in the others. Despite the result was not positive for all the lines, it demonstrated the efficiency of the editing system. Indeed, the PCR product was expected to be weak also for the *MYCN*-amplified cells due to low transfection rate, but the positive result indicated that Cas9 deleted a huge number of *MYCN* copies in these cells. Given that the experiment was intended to provide a proof of principle and no further analysis were performed, off-target activity of the editing system was not investigated.

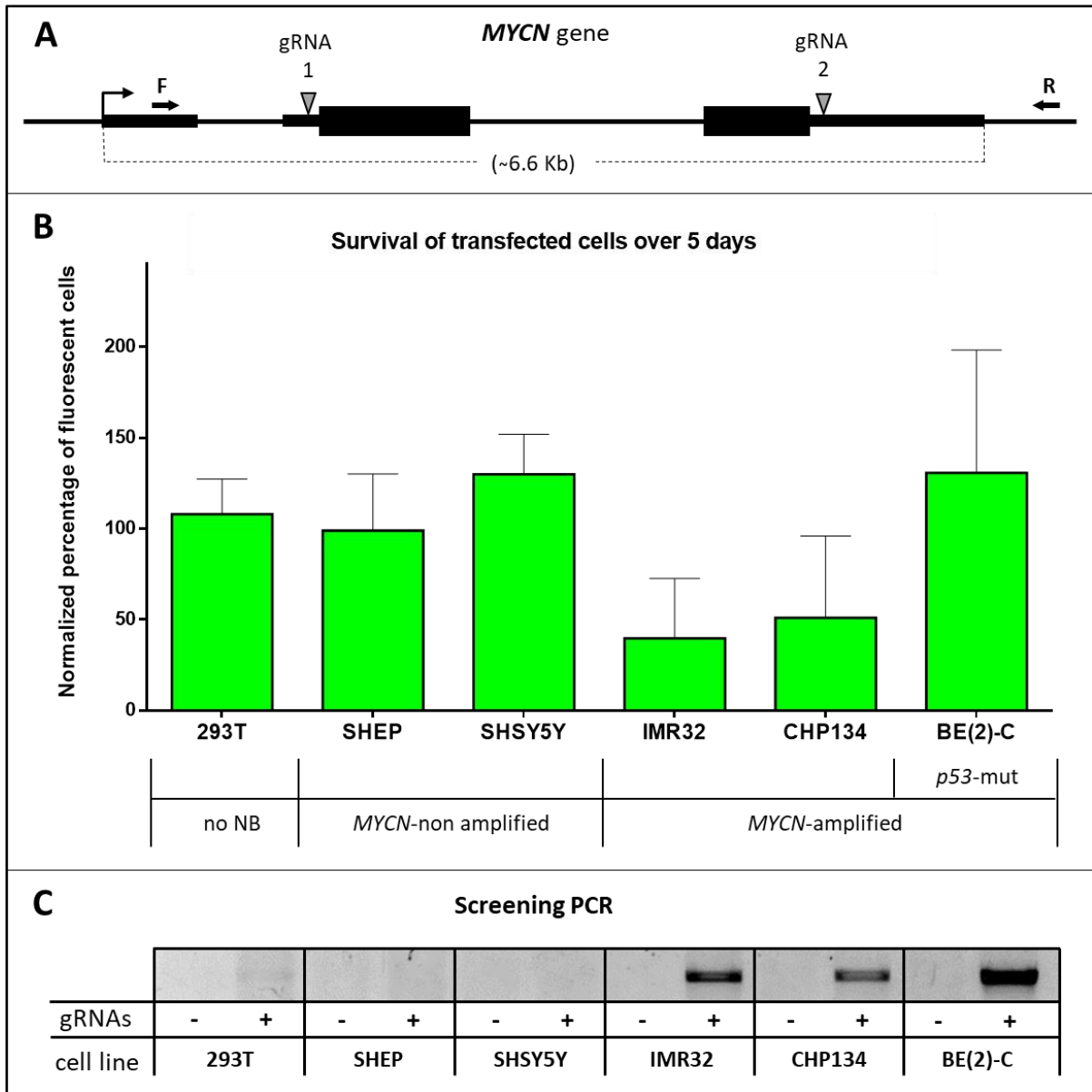


**Figure 30.** Survival analysis of cell lines treated with the *MYCN*-targeting system. **A.** Representation of human *MYCN* gene. The gRNAs used for deleting the gene are indicated as gRNA1 and 2, while the primers used for screening are indicated as F and R. **B.** Survival analysis via flow cytometry of cells transfected with the Cas9-GFP system. The number of cells survived after 5 days post-transfection is represented as percentage in relation to day 2. The value is normalized on fluorescence measurements of cells transfected without gRNAs (negative control). No NB = non-neuroblastoma type; *p53*-mut = mutation in *p53*. **C.** Screening PCR of cell pools transfected with the Cas9 system. The PCR product, obtained with the primers indicated in figure 30A, represents successful deletion of *MYCN* gene. The signs + and – respectively represent transfection with or without the couple of gRNAs.

Despite a relevant variability of survival data, the experiment overall demonstrated the great potential of a Cas9-based system designed to target *MYCN* amplification with the aim at

impairing proliferation of aggressive neuroblastoma cells. The system is supposed to work by decreasing *MYCN* expression and, at the same time, by inducing a large-scale DNA damage in a chromothripsis-like process. However, the second mechanism seemed to prevail, a condition evidenced by high specificity of the system for *MYCN*-amplified cells and, also, by the result obtained in BE(2)-C cells. This finding, also supported by a recent work describing Cas9-induced apoptosis, makes the strategy even more specific for aggressive neuroblastoma. Provided that this targeting system requires further investigation and improvement, the results obtained in this project established a proof of principle for the development of a novel promising therapy.

## *Conclusions and future perspectives*

**+316 A/G SNP genotype affects *ODCI* expression in neuroblastoma cells, and can be potentially employed as prognostic factor in remissive patients.** The SNP genotype was previously found to influence *ODCI* expression and tumour outcome in colorectal and breast cancer, although none of these studies examined *ODCI* expression in relation to the SNP genotype *in vivo*. Distinct experiments demonstrated that the A SNP is associated with improved regulation activity of transcription factors such as *c-MYC*, *MAX* and *MADI* toward *ODCI* promoter. The opposite functions of these factors (i.e. *c-MYC* is a transcription activator, *MADI* a repressor) make the role of *ODCI* SNP context-dependent. The same studies indeed demonstrated that the A SNP is associated with worse prognosis and/or recurrence in colorectal and breast cancer, but also that it is associated with decreased recurrence in colorectal cancer patients that take aspirin as chemoprevention. Interestingly, a recent study demonstrated that aspirin impairs *c-MYC* expression in colon cancer cells, therefore confirming the strong dependence of the SNP function on the pattern of expressed factors [115]. The current study demonstrated that the A SNP correlates with favourable outcome in neuroblastoma. This condition is even more significant for patients with amplified *MYCN*, where the presence of at least one A allele is prognostic of survival. No difference in *ODCI* expression was found in relation with the SNP genotype in primary tumour samples, a result that does not surprise if it is considered that no other study demonstrated it. It is assumed that such evidence is likely due to the complexity of neuroblastoma tumours, where *ODCI* expression might be heterogeneously regulated and play a role only in specific frames. Besides, total polyamine content is directly responsible of tumour progression, and it could represent a more reliable factor to be studied in relation with the SNP genotype in the future. In a second part, CRISPR-editing of aggressive/*MYCN*-amplified neuroblastoma cells demonstrated, for the first time, that the A allele is associated with significantly reduced, almost absent, *ODCI* expression. Consequently, also proliferation was found to be impaired in CRISPR-edited cells. It was therefore concluded that, in *MYCN*-amplified neuroblastoma, the A allele counteracts *MYCN*-mediated activation of *ODCI* expression and then plays a protective role against tumour progression.

Chromatin analysis of *ODCI* promoter revealed that, consistent with impaired gene expression, acetylation of H3-histone is also robustly decreased in association with the A SNP, therefore indicating silent chromatin. No further factors involved in chromatin-remodelling were investigated, and the exact regulation mechanism remains undiscovered. However, according to the current model of chromatin-modification dynamics, the status of histone residues oscillates between stable states through the activity of specific enzymes, which are

HAT and HDAC for acetylation [73-75]. It can be thereby deduced that loss of H3 acetylation observed in CRISPR-edited cells is likely due to HDAC-associated factors that preferentially bind E-boxes close to the A SNP instead of G, and *vice versa* for HAT-associated factors. Previous studies demonstrated that c-MYC and MAD1 proteins preferentially bind the A SNP in colorectal and breast cancer cells. Accordingly, the findings in *MYCN*-amplified neuroblastoma cells suggest that transcription inhibitors such as MAD1 and MNT could preferentially bind the A SNP, thus excluding *MYCN* factor. On the other hand, absence of such affinity for the G SNP could allow *MYCN* to fully activate *ODCI* expression in this condition. However, this possible explanation ignores that high *MYCN* levels, typically characterizing aggressive cells, could overwhelm other factors in regulating the A allele, which is not the case. Therefore, an alternative model might be represented by the structural differences between c-MYC and *MYCN* proteins. Indeed, the two amino acid sequences share only a few crucial regions of high homology, while the interspaced sequences are significantly different and might contain an *affinity-switch* domain. Such domain could make *MYCN* more active in the presence of the G SNP, on the contrary of c-MYC. In addition to this alternative, also the transcription-repression function of *MYCN* deserves to be considered. It is indeed demonstrated that *MYCN* carries out HDAC-mediated repression of non-canonical target genes through indirect binding to DNA and interaction with transcription factors such as SP1 and MIZ1. It is therefore possible that, in the event of an involvement of such *MYCN*-interactors in *ODCI* regulation, the A SNP influences their activity and, eventually, inverts the function of *MYCN* itself. In order to evaluate all the proposed possibilities, and to better characterized the SNP role in *ODCI* expression, chromatin immunoprecipitation experiments should be performed for factors such as *MYCN*, MAX, MAD1, MNT, MIZ1 and SP1 in CRISPR-edited cells. Furthermore, the specific affinity of *MYCN* (and c-MYC) toward the two forms of the SNP should be investigated through electrophoretic shift mobility assay.

The aim of this part of the project was to evaluate the prognostic significance of *ODCI* +316 A/G SNP in neuroblastoma. The relevance of this study relies on a novel neuroblastoma therapy targeting *ODCI* via the specific inhibitor DFMO. This is currently in phase 3 clinical trial for treatment of colon, bladder and skin cancer, while it is in phase 2 trial for prostate, cervical, gastric and oesophageal cancer [*ClinicalTrials.gov*]. Since the finding of *ODCI* involvement in neuroblastoma development and progression, DFMO is considered a promising therapeutic strategy for treatment of this tumour too. More precisely, a phase 2 clinical trial was recently completed, while five other studies are currently ongoing, with the aim to evaluate the application of DFMO as maintenance therapy for reoccurring neuroblastoma in remissive

patients. In this context, *ODCI* SNP could represent a stratification factor for prognosis of relapsing tumours. In support of this, the presence of at least one A allele is here demonstrated to be prognostic of poorly aggressive cells *in vitro*, and favourable outcome *in vivo*. The A SNP is also demonstrated to make neuroblastoma cells more sensitive to DFMO. Such findings gain in importance if considered that: about half of the total population carries at least one A allele (GG 56%, AG 37%, AA 7%); these results are relative to *MYCN*-amplified/aggressive neuroblastoma typically characterized by poor survival (< 30%). In addition, it is important to mention that, in the clinical context, genotyping the SNP is potentially more feasible than directly evaluating *ODCI* expression, also prognostic of outcome. In the prospect of a clinical application, the results obtained in this study obviously need to be further confirmed. As instance, the molecular mechanism behind the SNP influence on *ODCI* expression should be better defined. Also, the *in vitro* experiments were performed on a single cell line, BE(2)-C, while multiple lines should be analysed in order to overcome the significant genetic heterogeneity of neuroblastoma, and to obtain more reliable data. In this view, improving CRISPR technology would be decisive, since it is affected by the following limitations: low efficiency of HDR-mediated editing (2.5% of transfected cells); long and expensive clone-screening procedure; variability of the clonal lines; necessity to analyse more clonal lines in order to bypass clonal variability. At last, genotyping of patients that are currently undergoing clinical trial for DFMO application could provide new information about the response to treatment in relation with the SNP genotype. In conclusion, this study, on the condition of being further confirmed, has the potential to make *ODCI* +316 A/G SNP a new prognosis standard for maintenance treatment of relapsing neuroblastoma through DFMO.

***RUNX1T1* plays a fundamental role in neuroblastoma development and progression, and represents an interesting object of study for targeted therapy.** *RUNX1T1* is a transcription repressor with a poorly defined regulation network and, at the same time, a multifunctional role in development and cancer. It is well demonstrated to interact with a repressor complex that includes SIN3A, NCOR1, SMRT and different types of HDAC. The current model establishes that *RUNX1T1* protein recruits the repressor complex on the promoter of target genes through indirect binding to DNA, which is mediated by auxiliary factors that are not completely defined. As far as it is known, the expression pattern of these auxiliary factors is tissue/culture-dependent, therefore making the regulation network of *RUNX1T1* extremely flexible depending on the context. Expectedly, *RUNX1T1* is also demonstrated to be a versatile transcription factor with an incisive role in a wide range of

physiological events and disease conditions. It is involved in adipogenesis, angiogenesis, and development of gut, pancreas and glial cells. High *RUNX1T1* expression is associated with poor outcome in bladder cancer and malignant mesothelioma, while it is demonstrated to suppress progression of glioblastoma, ovarian cancer and pancreatic metastases. In such a biological landscape, the second objective of this project was to investigate, for the first time, the involvement of *RUNX1T1* in development and progression of neuroblastoma. Survival analysis of large cohorts of patients revealed that high *RUNX1T1* expression in primary tumours is prognostic of favourable outcome. This finding suggests an oncosuppressor role of *RUNX1T1* in neuroblastoma, which is consistent with observations in glioblastoma, ovarian cancer and pancreatic metastases. On the contrary, CRISPR-mediated deletion/knockout of *RUNX1T1* in aggressive neuroblastoma cells demonstrated that the gene promotes proliferation and migration, as well as it inhibits differentiation. This, likewise, is consistent with previous studies indicating a developmental function of *RUNX1T1*. The results obtained *in vivo* and *in vitro* appear to be in opposition, a finding that could be explained according to the differences between the two biological systems: in primary tumours, cells live in a 3D structure, where microenvironment and cell-cell interactions are obviously different from those characterizing cell cultures; *in vivo*, tumour cells also interact with other tissues and signals deriving from these; the cells analysed *in vitro* (BE(2)-C) derive from metastases, which supposedly have a different molecular background from non-metastasising cells of the primary tumours. By the way, the opposite results obtained in the two biological systems also suggest a double-face role of *RUNX1T1* in neuroblastoma. This concept of double-function is partially demonstrated by RNAseq analysis of CRISPR-edited cells. *RUNX1T1* was found to affect mechanisms relevant in the context of a solid tumour, such as hypoxia response and inflammation regulation. Impairment of these two systems is already known to be important for neuroblastoma progression. On the other hand, speculative reconstruction of *RUNX1T1* regulon suggests that this factor potentially interacts with TCF12 in neuroblastoma cells and, consequently, regulates a series of genes implicated in signalling pathways such as PI3K-Akt, Wnt, Hippo and MAPK-Erk. These pathways regulate genes that are notoriously involved in modulation of cell behaviour, and some of them are also known to be involved in neural crest differentiation. In addition, *RUNX1T1* is found to potentially regulate both death and survival predictors in cell cultures. Overall, these results depict a transcription factor with a modular regulation network that is potentially involved in distinct aspects of neuroblastoma.

Additional studies and experiments are necessary in order to confirm the model. First of all, interaction between *RUNX1T1* and TCF12 proteins should be demonstrated in neuroblastoma

cells via co-immunoprecipitation analysis. In support, a previous study already demonstrated that the two proteins interact through the N-terminal domain NHR1 of *RUNX1T1*. If the interaction is confirmed, *TCF12* involvement in neuroblastoma events should be further investigated. For example, CRISPR-editing could be used to evaluate whether *TCF12* knockout produces the same phenotype of *RUNX1T1* knockout. Similar to the first part of this project, a significant improvement of CRISPR technology would allow to study both *RUNX1T1* and *TCF12* on multiple cell lines, thus dealing with the troublesome heterogeneity of neuroblastoma lines. ChIPseq analysis, then, would reveal the entire targetome of *TCF12* and *RUNX1T1* in neuroblastoma cells for the first time. As a second approach, activity of the pathways PI3K-Akt, Wnt, Hippo and MAPK-Erk should be confirmed via analysis, in the mutant cells, of the principal downstream regulators, in terms of protein expression and/or phosphorylation of the modulating residues. Also, rescue experiments in the mutant cells would demonstrate the importance of this pathways for neuroblastoma cell behaviour, and their role in *RUNX1T1* regulon. At last, *RUNX1T1* functions should be investigated and demonstrated *in vivo*. Xenotransplantation of neuroblastoma cells carrying either wild-type or mutated *RUNX1T1* (or possibly *TCF12*) should be performed in mice in order to evaluate the role in invasion and metastasis formation. Also, model mice spontaneously developing neuroblastoma could be used to evaluate *RUNX1T1* involvement in tumour development and progression. For this purpose, the transgenic mouse carrying exogenous expression of *MYCN* under *tyrosine hydroxylase* promoter, and spontaneously developing neuroblastoma, would represent a suitable model [117].

The finding, and eventual demonstration, of a new player of the neuroblastoma landscape represents an important opportunity for development of novel targeted therapies and therapeutic approaches. This would be even more relevant if *RUNX1T1* involvement in neuroblastoma is confirmed in a *MYCN*-amplification context, where survival is still significantly poor. Transcription factors, such as *RUNX1T1* and *TCF12*, are unlikely targets for therapy. Their structure usually results unsuitable for drug design, and impairment of their activity often involves significant side effects. However, the entire regulation network of *RUNX1T1* could represent a valuable target itself. A multimodal therapy should be designed in order to target multiple pathways via multiple drugs. In the case of neuroblastoma, the therapy should be directed toward those pathways and processes that, overall and synergistically, regulate neuroblastoma development and progression. Such kind of strategy potentially works in a tumour-specific manner, and potentially allows to keep low dosages of the single drugs to prevent adverse effects. In addition, a multi-drug therapy should prevent the tumour to develop

resistance. PI3K-Akt, for example, is found to be deregulated in *RUNX1T1*-mutant cells and it is one of the best known pathways to be involved in neuroblastoma. Different members of the pathway represent possible therapeutic targets and some of them are currently under study for neuroblastoma treatment [118, 122], while a PI3K-specific drug, *Idelalisib*, is already approved for clinical treatment of leukemia [U.S. Food and Drug Administration]. Wnt pathway, also impaired in *RUNX1T1*-mutant cells, is demonstrated to play a role in neuroblastoma development, and it is also known as a therapeutic target in different types of cancer. Wnt-specific drugs for treatment of neuroblastoma are not currently available, although inhibition of the pathway is already considered as a promising strategy [123]. Furthermore, some Wnt inhibitors, including *Niclosamide*, *Sulindac* and *Pyrvinium*, are FDA-approved for treatment of specific tumours, while a huge number of similar drugs is currently under trial [119, U.S. Food and Drug Administration]. Despite the absence of experimental data in neuroblastoma, drugs targeting Hippo and MAPK-Erk pathways are also under trial for treatment of some tumours [120, 121], and a translational application in neuroblastoma is plausible. In conclusion, a deeper knowledge of *RUNX1T1* regulation-network in neuroblastoma could provide a new foundation for the study and development of therapeutic strategies intended to cure the most aggressive form of neuroblastoma.

**CRISPR technology represents an important research and therapy advancement for neuroblastoma and, possibly, several other malignancies.** CRISPR technology was employed in this project with a large spectrum of functions to pursue distinct research targets, thus providing the chance to explore the ultimate advances of this technology and to assess novel strategies. In the study of *ODCI* SNP, improvements and alternative editing systems of CRISPR editing were tested. The canonical Cas9 was demonstrated to have higher HDR-editing efficiency than double-nCas9 cleavage, although induction of DNA nicks is commonly accepted to have low off-target rate. In the light of this evidence, novel Cas9 variants with no off-target activity and unaltered throughput, such as HypaCas9 [137], represent an optimal strategy for efficient and reliable HDR-editing. Also, application of a single-stranded donor DNA and an HDR-enhancing drug (RS-1) were found to greatly improve the recombination rate, therefore defining a standard for this editing function. On the other hand, the experiments related to *RUNX1T1* clearly confirmed the outstanding performance of NHEJ-mediated editing in inducing knockout mutations or large deletions. Indeed, the rates of successful editing were about 60 and 10% respectively, and bi-allelic KO mutations were not rare. In this part of the project, two innovative editing strategies were also developed, referred as NHEJ/MMEJ-

mediated multiple assembly (or NMA) and SDSA (synthesis-dependent strand annealing)-mediated knock-in (or SKI). Intended to track the cells that are successfully edited, they were designed to knock-in a reporter gene into a target locus and to avoid any false positive signal due to random insertion or transcription of the donor DNA. In a future perspective, efficient detection and isolation of edited cells could be performed through systems like these, which can even be applied to HDR-editing if sequential reporter insertion and HDR-mediated removal are employed. Such an approach could potentially facilitate the editing procedure and exclude the need of multiple clonal lines. Certainly, further improvements and validations are required.

In the last part of the present project, a novel CRISPR-based therapeutic strategy was designed to target the most important neuroblastoma oncogene, *MYCN*. Amplification of *MYCN* gene is found in almost all aggressive neuroblastoma and represents a strong marker of poor survival. Transcription regulation activity of *MYCN* protein is directly responsible of aggressive cell behaviour, characterized by high proliferation rate, poor differentiation and apoptosis repression. Despite the critical role of this genetic lesion in development and progression of aggressive tumours, no successful therapy targeting *MYCN* has been developed so far. The third part of this project was therefore aimed at providing a proof of principle for the development of a novel, more efficient, therapeutic system. The approach here described is based on targeting the multiple oncogene copies that characterize *MYCN*-amplified tumours through Cas9-mediated cleavage. This is expected to knockout *MYCN* itself and, in addition, to generate a wide-spread DNA damage, eventually inducing the cell to proliferation arrest and apoptosis. Experimental results demonstrated that the system is considerably efficient and highly specific toward *MYCN*-amplified cells. Some evidences also suggested that impairment of cell survival might be principally due to response to DNA damage instead of *MYCN* knockout, a finding that is consistent with a recent work demonstrating that Cas9 activity induces *p53*-mediated apoptosis. This, if further confirmed, would validate the extreme specificity of this strategy and, additionally, would distinguish it from previous similar approaches that resulted to be unproductive, such as RNA interference. Notably, a therapeutic strategy based on this kind mechanism can be potentially applied to all those tumours affected by amplification of oncogenes, a recurrent event in cancer [154]. Since this project was not proposed for a deeper characterization of this targeting system, further analyses are now necessary to ultimately develop a concrete therapeutic strategy. First, the system should be tested and verified in additional, multiple cell lines, including both *MYCN*-amplified and -non amplified cells. Second, transfection efficiency needs to be improved, thus providing more reliable data and, also, enough material for further molecular analyses. Accordingly, cells could

be transfected with already assembled RNPs, which are demonstrated to be highly transfectable in a wide range of cell types. So, if Cas9 is fused to a fluorescent protein, then the cells can be sorted and their viability can be easily assessed, as well as molecular features such as expression of *MYCN* or other factors involved in the DNA-damage response. Application of RNPs is already demonstrated to be suitable for *in vivo* application, thus validating the therapy potential. However, the most appropriate delivery system should be evaluated according to the target [167], which, in the case of aggressive neuroblastoma, could be represented by metastases in relapsing patients. Viral-delivered Cas9, for example, could represent a valid alternative to RNPs, since some viruses show an interesting specificity toward neuroblastoma cells [168-170]. As third and last consideration, the clinical aspect of this strategy should be further improved. For example, clinical safety could be increased through application of new Cas9 variants with no off-target activity, or even via targeting strategies that do not induce *MYCN* knockout in wild type cells. Also, the Cas9-induced effect could be enhanced by co-application of apoptosis-inducer drugs such as *Nutlin*, which is already studied for treatment of aggressive neuroblastoma [155]. Importantly, apoptosis-inducer drugs that bypass *p53* function could be fundamental in tumours with mutations occurring in this oncosuppressor. In conclusion, if the efficacy of the system is validated, the innovative therapeutic approach proposed in this study could represent a realistic opportunity to treat neuroblastoma and, potentially, a significant number of other malignancies.

## *Materials and methods*

**Analysis of survival and *ODCI* SNP genotype in neuroblastoma patients.** All the survival and *ODCI* expression data were provided by the laboratory of Michelle Haber, Children Cancer Institute of Sydney. The study was performed with primary tumour samples of 839 neuroblastoma patients belonging to three different cohorts: the USA cohort, comprising patients enrolled between 1994 and 1998 by the Children's Oncology Group and previously studied [104]; the Australian cohort, comprising patients who were diagnosed in Australia and New Zealand from 1985 to 2000, also previously studied [105]; the European cohort, including patients from two different centres (NRC and SIOPEN). For SNP genotyping, DNA was extracted from tumour samples as previously described [106]. Real-time PCR, coupled to SNP-specific probes labelled with FAM or VIC. Primer and probe sequences were as follows: ODC-G316A-F 5'-CCGGGCACGTGTGC-3'; ODC-G316A-R 5'-GAAGCGGCGCCTCAAG-3'; ODC-G probe 5'-CTGCGGAGACACG-3'; ODC-A probe 5'-CCTGCAGAGACACG-3'. For *ODCI* expression quantification, RNA was extracted using TRIZOL reagent (*Life Technologies*) and reverse transcribed with MMLV reverse transcriptase (*Life Technologies*) according to the manufacturer's protocols. Gene expression was quantified by qRT-PCR using FAM labelled TaqMan Gene Expression Assays (Applied Biosystems) on a 96 × 96 Integrated Fluidics Circuit (IFC) (BioMark HD System, *Fluidigm*). Data were normalised to a panel of control genes: *HPRT1*, *GUSB*, *PPIA*, *HMBS*, and *SDHA*. The used Taqman assays were *ODCI* Hs00159739\_m1, *HPRT1* Hs99999909\_m1, *GUSB* Hs99999908\_m1, *PPIA* Hs99999904\_m1, *HMBS* Hs00609296\_g, *SDHA* Hs00188166\_m1. Statistical significance between two groups was determined with an unpaired two-tailed Student's t-test.

**Analysis of survival and *RUNX1T1* expression in neuroblastoma patients.** The study was performed through the online tool *R2: Genomics Analysis and Visualization Platform* [107]. Event-free survival and *RUNX1T1* expression data were obtained from four publicly available datasets of transcriptome analysis, namely *Kocak* [76], *Versteeg* [77], *SEQC* [79] and *TARGET* [78]. All the datasets are built on microarray analysis except for *TARGET*, which is built on *Illumina* sequencing analysis. Patients were distributed between *RUNX1T1*-high and *RUNX1T1*-low expression groups via the *R2* function *Kaplan Scan*, which sorts the expression data based on statistical testing and long-rank test. The statistical significance of the different survival values between high and low-expression groups was calculated by unpaired two-tailed Student's t-test. The average expression data of the genes *RUNX1T1*, *MYCN*, *ODCI* and  $\beta$ -*ACTIN* were provided by the platform and shown as ratio between the *MYCN*-amplified and the *MYCN*-non amplified condition. Only for *Versteeg* dataset, the median gene expression was

adopted instead of the average, which was not available. For the datasets built on microarray analysis, the data represented by the probe-set with the highest average expression was selected for each one of the analysed genes.

**Cell cultures.** The lines BE(2)-C, Tet21N, IMR-32, SH-SY-5Y, SHEP, CHP-134, SK-N-FI, SK-N-AS, SK-N-DZ, NBL5 and 293T were cultured in DMEM- high glucose (*Sigma Aldrich*) + 10% FBS (*Gibco*), while NB-69, LAN-1 and KELLY were cultured in RPMI (*Sigma Aldrich*) + 10% FBS. All the clonal lines derived from BE(2)-C (AG-1, AG-2, NU-1, NU-2, KO-1, KO-2 and KO-3) were cultured in DMEM-high glucose + 10% FBS. All cultures were maintained with penicillin and streptomycin (*Gibco*).

**CRISPR editing.** The following vectors from Feng Zhang's laboratory (*Addgene*) were employed: PX459, coding for SpCas9; PX462, coding for nCas9 D10A; PX458, coding for GFP-fused SpCas9; pHbCpf1-PY016, encoding for Cpf1. The Cpf1-coding cassette was cloned into the PX459 vector prior to editing as previously described [159]. The gRNAs were designed with the online tool *BlueHeron*, and the relative off-targets were predicted through *CasOT* software. The gRNA used for Cpf1-editing was designed, and the respective off-targets were predicted, through the online tool *CCTop-Offtarget*. Selection of the best gRNAs was driven by low number of off-targets, high number of *seed region*-mismatches in the most probable off-targets and location of the most probable off-targets in non-coding regions. The gRNAs were purchased as complementary oligonucleotides (*Sigma Aldrich*) and cloned into the CRISPR vectors. The cloning procedure was provided by Feng Zhang's laboratory. The following oligonucleotides were used: *ODCI* SNP editing via canonical Cas9, gatcgCGCCGGCCTGCGGAGACACGg (F), aaaacCGTGTCTCCGCAGGCCGGCGc (R); *ODCI* SNP editing via dual-nCas9, gatcgCCGCCGGAGACGCCGGCCCGg (up, F), aaaacCGGGCCGGCGTCTCCGGCGGc (up, R), gatcgGAGCCAGGCGCTGACGGGCGg (down, F), aaaacCGCCCGTCAGCGCCT-GGCTCc (down, R); *RUNX1T1* locus deletion (first allele, upstream site), gatcgGCAGACGCCGCCTGTGACAGg (F), aaaacCTGTACAGGC-GGCGTCTGc (R); *RUNX1T1* locus deletion (first allele, downstream site) gatcgTACCTCCTTGGTTGTGTGGCg (F), aaaacGCCACACAACCAAGGAGGTAc (R); *RUNX1T1* locus deletion (second allele, downstream site), gatcgAACCTAACTGTCCAAA-GTGg (F), aaaacCACTTTGGACAGT-TAGGGTTc (R); Reporter knock-in via Cpf1-editing, caccgTAATTTCTACTAAGTGTAG-ATcCAGCACAAAGACTGGGAGAAGCtttttt (F), aaacaaaaaaGCTTCTCCAGTCTTTG-TGCTGgATCTACACTTAGTAGAAATTAc (R);

NHEJ editing of the last exon of *RUNX1T1*, gatcgGGCAAAATGAGCCA-CAGTATg (F) aaaacATACTGTGGCTCATTTTGGCCc (R); *MYCN* CDS deletion (upstream site), caccgCGCCCCGTTTCGTTTTAATAC (F), aaacGTATTAAAACGAACGGGGCGc (R); *MYCN* CDS deletion (downstream site), caccgACCCAGAGCCGAACTCGACA (F), aaacTGTCGAGTTCGGCTCTGGGTc (R). Two different donors were used for HDR-mediated editing of *ODCI* SNP. The double-stranded donor (682 bp) was amplified from genomic DNA of NBL5 cells (AA genotype). The following primers were used for PCR amplification: TGGCGACCCGCCGGTGCTAT (F), CTGAAGGCGCCAAGGCCGG (R). The single-stranded donor (ssODN) was purchased from *Sigma Aldrich* as a purified oligonucleotide with the following sequence: 5'-CCGGGGCGGGCTGCGGGCCCCGGG-CCCCGGGCACGTGTGCGGCGCGCCTCGCCGGCCTGCGGAGACACGTGGTCGCCGAGCGGGCCACGACCTTGAGGCGCCGCTTCCTCCC GGCCCCGGG-3'. A phosphothioate bond was added between the 3'-last and the second-last nucleotide in order to prevent degradation of the ssODN. For editing of the wild type allele of *RUNX1T1* in the clonal line carrying a null allele, two plasmidic dDNAs and one single-stranded dDNA were used in respectively NHEJ/MMEJ-mediated multiple assembly (NMA) and SDSA-mediated knock-in (SKI). Sequences for NMA donors were amplified from the pGIPZ\_tRFP-PURO vector and BE(2)-C genomic DNA. The following primers were used: homology region flanking the CMV promoter, ttctagaTGCTTTCTTCTGCCTTCTCCTT (F), ttgagctcTGGTGCTTCTCCAGT (R); *RFP* cassette, aagagctcATCCACGCTGTTTT (F), aaacatgCAATTCAACAGGCAT (R); homology region flanking the *RFP* cassette, ttgagctcTTTGCCAGCACAAAGA (F), ttctagaGTCTAGCGAGGGGTTGTCTCT (R). Both the CMV-promoter and the *RFP*-CDS plasmids were built with the p3XFLAG-CMV-10 backbone. Sequences for the SKI donor were amplified from pGIPZ\_tGFP-PURO vector and BE(2)-C genomic DNA. The following primers were used: *GFP* cassette, aagagctcATCCACGCTGTTTT (F), aagaattcCAATTCAACAGGC-ATCT (R); upstream flanking region, ttcatatgCAGATGTCTCCACCTC (F), ttaagcttGCTCACTCTCG-AGGAAG (R); downstream flanking region, ttgaattcGAGATTGT-ACATGGGGA (F), aatctagaATATTTATTGAGCGCGGTTG (R). The entire donor sequence (about 2500 bp) was cloned into the p3XFLAG-CMV-10 vector, amplified by PCR and single-stranded donors were obtained via subsequent single-primer PCR. The product was then digested with *SacI* enzyme (*New England Biolabs*) and extracted from agarose gel to remove the original double-stranded DNA. Cells were transfected in 24-well plates at 70% cell confluency. Transfections were principally performed with Lipofectamine 3000 (*Thermo Fisher Scientific*) according to the manufacturer's protocol. Transfections for *MYCN*-

amplification targeting where performed with Lipofectamine 2000 (*Thermo Fisher Scientific*) according to the manufacturer's protocol. As a general rule, cells were transfected with 800 ng DNA/well. For *ODCI* SNP editing, all types of dDNA were constantly transfected in a quantity of 1 pmol/well, while the quantities of CRISPR vectors were adapted considering 800 ng/well as the maximum amount. The drugs SCR7 and RS-1 were applied right after transfection at the concentration of 1  $\mu$ M and 7.5  $\mu$ M respectively. For *RUNX1T1* locus deletion, the couple of CRISPR vectors coding for different gRNAs was co-transfected into the same well in equal quantities. For *RUNX1T1* editing via NMA and SKI, all vectors and dDNAs were co-transfected in equal quantities. Transfected cells were incubated for 72 hours prior to any further action. In order to generate single clonal lines in *ODCI* and *RUNX1T1* editing, cells were treated with 1 $\mu$ g/ml puromycin for 1 week and then directly spooled into 96-well plates (1.5 cells every 2 wells).

**Screening and genotyping of CRISPR-edited clones.** The following primers were used for screening of CRISPR-edited cells: allele-specific PCR for screening of AG/AA colonies in *ODCI* editing, GACCCGCCGGTGCTATAAGTA (F), GGCGACCACGTGTCCCT (A-specific, R), GGCGACCACGTGTCACC (G-specific, R); sequencing of *ODCI* SNP, TGGCGACCCGCCGGTGCTAT (F), CTGAAGGCGCCAAGGCCGG (R); sequencing of the most probable off-target in *ODCI* SNP editing, CCGTATACCTCCCACGTCAT (F), CAGAAAGACCTGGAAGCCG (R); screening and sequencing of *RUNX1T1* locus deletion, GGAAAGTGGTCGTCTTGGGT (F), AACCATCGTCAACCACCACA (R); sequencing of the single target sites of the gRNAs used for *RUNX1T1* deletion, TGAGCGACAAGTACAGCCTG (R, coupled to the previous forward), GCCTGACCCAAGTTGCCTAT (F, coupled to the previous reverse); screening and sequencing of NMA-editing junctions, TGTGTCTGACTATTGTGGTATAGG (up, F), aaacatagCAATTCAACAGGCAT (up, R), ttctagaTTACACCTTCCTCTTCTTCTTG (mid, F), GTAAAACGACGGCCAGT (mid, R), aaacatagCAATTCAACAGGCAT (down, F), CCCTCTGTGTTTTACTACCACCT (down, R); screening and sequencing of *RUNX1T1*-knockout clones, TGTGTCTGACTATTGTGGTATAGG (F), CCCTCTGTGTTTTACTACCACCT (R); screening of SKI-editing, GGAAAGTGGTCGTCTTGGGT (F), TTTCTAGATTACACCTTCCTCTTCTTCTTG (R); screening of *MYCN* deletion, GCTGGGGTTCTTCTCCAAAG (F), GGCAAGCAAAGCTGTCTCAT (R). As a general rule, allele-specific primers for *ODCI* SNP screening were designed according to the following parameters [108]: the SNP has to be positioned at the 3' end of the primer; the third-last nucleotide of the primer has to carry a mismatch that can be

either CA or TG regardless the SNP type, with the aim to increase the stringency. For screening of cell pools transfected for *ODCI* SNP and *RUNXIT1* editing, a total of 500 ng of genomic DNA was used for PCR. For screening of cell pools transfected with NMA, SKI and *MYCN*-targeting systems, 1000 ng of genomic DNA was used for PCR. Where necessary, PCR products were sequenced via *Macrogen* service. Sequencing results were aligned and analysed through the online tool *Clustal Omega*.

**Primer design.** All primers were designed with the support of *Primer3Plus*, *IDT OligoAnalyzer* and *UCSC-PCR*. The criteria for primer design were: length between 17 and 27 nt; CG content < 60%; melting temperature 60°C; melting temperature of secondary structure < 40°C; homodimer formation  $\Delta G > -9$  Kcal/mol; heterodimer formation  $\Delta G > -9$  Kcal/mol.

**DNA extraction, PCR and cloning procedures.** Genomic DNA of the neuroblastoma cell lines was extracted with PerfectPure DNA Cultured Cell Kit (*5 Prime*) according to the manufacturer's protocol for the cell lines. Genomic DNA of CRISP-transfected cells was extracted with the following procedure: suspension of cells in lysis solution (10 mM TrisHCL pH 8.0, 0.5 mM EDTA, 0.1% SDS, 100 mM NaCl, 0.2 mg/ml Proteinase K *Roche*) in a ratio of 1 ml every million cells, with 100 cells being the minimum suitable number; lysate cells were incubated at 55°C for 3 h and Proteinase K was then inhibited at 85°C for 30 min; one volume of isopropanol was added and the solution was incubated at room temperature for 10 min; the samples were centrifuged at maximum speed for 30 min at 4°C; the pellet was washed with 0.5 ml of 70% ethanol two times; after the centrifuge, the samples were let drying at room temperature and then resuspended with water. Genomic DNA was quantified via Nanodrop (*Thermo Fisher Scientific*) and used for PCR amplification. Screening PCR was performed by AmpliTaq Gold 360 Master Mix (*Thermo Fisher Scientific*) following the manufacturer's protocol. PCR for cloning was performed with Herculase II Fusion DNA polymerase (*Agilent*) and the manufacturer's protocol was followed. Enzymes provided by *New England Biolabs* were used for cloning. The PCR products were purified from agarose gel by Gel Extraction Kit (*Qiagen*), while the plasmids were purified by MINI-Prep Kit (*Machery Nagel*).

**Flow cytometry and cell sorting.** Prior to cytometry and sorting, cells were resuspended in PBS solution with 1% FBS and strained through 0.7  $\mu$ m membrane. S3e Cell Sorter (*BioRad*) was used. In analysis of the Cas9-system targeting *MYCN* amplification, fluorescent cells were counted 2 and 5 days after transfection. A total of 50,000 cells was analysed for each sample.

For sorting of NMA- and SKI-edited cells, a minimum of 1000 cells was sorted and seeded into 48-well plates.

**Gene expression analysis by qRT-PCR.** Total RNA was extracted from cells via Trizol solution (*Sigma Aldrich*) following the manufacturer's protocol. Purified RNA was treated with DNA-free kit (*Thermo Fisher Scientific*) and cDNA was obtained with iScript Reverse Transcription Supermix (*BioRad*) as the manufacturers suggest. For qRT-PCR, the following primers were used: *ODC1*, TGCTGCCTCTACGTTCAATG (F), GTTCTGGAATTGCTGC-ATGA (R); *MYCN*, GATGCACCCCCACAGAAGAA (F), CTCCGAGTCAGAGT-TTCGGG (R); *c-MYC*, CGTCCTCGGATTCTCTGCTCTC (F), GCTGCGTAGTTGTGCTGATGT (R); *MAX*, GGACTCGGCTTGTTGTTGTC (F), TTGAAACCTCGGTTGCTCTT (R); *MNT*, CAGTGGATGGACGTACTGGA (F), TCCTCCTCCATATCCTCGTC (R); *RUNX1T1*, CACATCGGGAATTCCTTCAC (F), TCGCTTCACCTCATTACAG (R); *GUSB*, AGCCTGGAGCAAGACAGTGG (F), ATACAGATAGGCAG-GGCGTTCG (R). qRT-PCR was performed with SYBR Green (*BioRad*) with the following quantities: 5 ng cDNA for each sample, 0.5  $\mu$ M primers, 2X SYBR Green, total volume 15  $\mu$ l. qRT-PCR samples were run and analysed on CFX96 Thermal Cycler (*BioRad*). At least 3 replicates of the experiment were performed.

**Gene expression analysis by Western blot.** Total protein content was extracted from cells by standard RIPA solution (150 mM NaCl, 0.5% sodium deoxycholate, 1% Np40, 1 mM PMSF, 0.1% SDS, 50 mM Tris-HCl, 2% cComplete), with a ratio of 20  $\mu$ l every million cells. Cells were washed with PBS solution before lysis. Cell lysates were incubated in ice for 20 min, sonicated at high intensity for 10 min with Bioruptor® Plus (*Diabgenode*), and the supernatant was collected after 30 min centrifuge at maximum speed. Protein samples were quantified by BCA assay (*Thermo Fisher Scientific*) as suggested by the manufacturer. Samples were run in 10% acrylamide gel in a quantity of 60  $\mu$ g per sample, and then transferred to a nitrocellulose membrane. The membrane was blocked with 4% milk solution (20 mM Tris-HCl, 150 mM NaCl) and the following antibodies were: *ODC1*, *Abcam* ab126590 (1:800); *RUNX1T1*, *Proteintech* 15494 (1:800); *MYCN*, *Santa Cruz* B8.4.B (1:1000); *MAX*, *Santa Cruz* C-17; *MNT*, *Santa Cruz* G-2;  $\beta$ -ACTIN, *Sigma* a2066 (1:1000); anti-rabbit IgG, *Jackson* (1:2000); anti-mouse IgG, *Jackson* (1:2000). The membranes were developed with ECL solution (*BioRad*) and analysed via ChemiDoc MP system (*BioRad*). At least 3 replicates of the experiment were performed.

**Protein structure prediction.** The 3D structure of the C-terminal domain of RUNX1T1 in the knockout clones was predicted via the online tool *I-TASSER* [109]. The input amino acid sequences were deduced from DNA-sequencing of the mutations. As output, the model with the highest C-score was selected.

**ChIP.** A total of 10 million cells were collected for each immunoprecipitation. The anti-acetyl-histone H3 antibody (06-599, *Merk*) was used in a quantity of 5 µg for each precipitation. A total of 80 µl slurry beads Protein A Sepharose 4B (*Thermo Fisher Scientific*) were prepared for each precipitation as follows: beads were centrifuged at 1700 g for 2 min at room temperature and washed 3 times on rotation with 0.9 ml RIPA Wash solution (150 mM NaCl, 0.5% sodium deoxycholate, 1% Np40, 1 mM PMSF, 0.1% SDS, 50 mM Tris-HCl); after washing, the beads were resuspended in RIPA Wash with 1/2 initial slurry volume; beads were blocked with 1 µg BSA (for each precipitation) for 5 h at 4°C on rotation; after coating, beads were washed 3 times with 0.9 ml RIPA Wash as previously described (centrifuge at 4°C); the beads were resuspended in RIPA Wash with ½ initial slurry volume. Collected cells were treated as follows: cells were washed with PBS solution, resuspended in 10 ml DMEM + 10% FBS and fixed with 1% formaldehyde for 10 min at room temperature on rotation; formaldehyde was inhibited with 0.125 M glycine for 10 min at room temperature on rotation; fixed cells were centrifuged at 850 g for 10 min at 4°C; the pellet was washed 2 times with PBS solution in ice; nuclei were extracted with 0.5 ml Lysis Buffer (5 mM Pipes pH 8, 85 mM KCl, 0.5% NP40, 1 mM PMSF, 2% cOmplete) by pipetting 20 times and incubating in ice for 10 min; nuclei were centrifuged at 1700 g for 10 min at 4°C; the pellet was resuspended in 0.2 ml RIPA Sonic-Buffer (150 mM NaCl, 1% NP40, 1 mM PMSF, 2% cOmplet, 1% SDS, 50 mM Tris-HCl) by pipetting 20 times; the lysate was sonicated by Biorupture NextGen (*Diagenode*) with 10 cycles at high power for 6 times and 10 cycles at low power for 2 times (each cycle being composed of 30 sec on and 30 sec off); sonicated samples were centrifuged at maximum speed for 15 min at 4°C; the supernatant was collected and added with RIPA Wash without SDS in order to reach a final concentration of 0.5% SDS; the samples was pre-cleared by incubating with 30 µl coated beads for 30 min at 4°C on rotation; the beads were removed by centrifuging at 1700 g for 5 min at 4°C; 10% of the volume was taken as input and added with RIPA Wash in order to reach a volume of 70 µl, while the remaining volume was added with RIPA Wash without SDS in order to reach a final concentration of 0.125% SDS; the solution was incubated with 5 µg antibody overnight at 4°C on rotation; 40 µl coated beads were added to each samples and these were incubated for 30 min at room temperature on rotation; the beads

were taken and washed 3 times with 0.8 ml RIPA Wash, 4 times with 0.8 ml Washing Buffer (1% sodium deoxycholate, 1% NP40, 500 mM LiCl, 100 mM Tris-HCl) and 2 times with 1 ml TE Buffer (10 mM Tris-HCl, 1 mM EDTA) as previously described (centrifugations with TE Buffer were performed at 2200 g); 70 µl of TE Buffer was added to the washed beads; the input and the beads were incubated with 10 µl 10 mg/ml RNase A (*Sigma Aldrich*) for 45 min at 37°C on shaking; the samples were added with 20 µl Proteinase K Buffer (50 mM EDTA, 500 mM NaCl, 100 mM Tris-HCl) and 6 µl 19 mg/ml Proteinase K (*Roche*), and incubated for 6 h (or overnight) at 65°C on shaking; samples were centrifuged at 3500 g for 4 min at 4°C and the supernatant (106 µl) was transferred to Phase-Lock Gel Tubes (*5Prime*); the samples were added with 106 µl phenol/chloroform/isoamyl alcohol (24:24:1), shaken and centrifuged at maximum speed for 3 min at room temperature; the resulting supernatant was added with 106 µl chloroform/isoamyl alcohol (24:1), shaken and centrifuged again; the supernatant was collected and added with 1/10 volume of 3 M pH 5.2 sodium acetate, 1 µl glycogen and 2.5 volumes of ethanol; the DNA was precipitated at -80°C for 30 min; the samples were centrifuged at maximum speed for 30 min at 4°C and the pellet was then washed with 1 ml 70% ethanol; DNA was resuspended in 60 µl; the input sample was quantified and checked by agarose gel. The following primers were used for real-time PCR: +316 A/G SNP, TTCTGCCCCCGTCTTCACAG (F), CCGAAGGGTTGGGAAAGAGG (R); -15,000 bp region, AGACTCTCCCTGGCCAAGAT (F), AGCTCTCACCTCCAGATTGC (R); E-box 1, ATCACTTCCAGGTCCCTTGC (F), GAGAGCGGAAAAGGGAAATC (R); exon 9, AATCAACCCAGCGTTGGACA (F), CAGAGCCCGTCTGTTCCTTT (R);  $\beta$ -ACTIN, GCAGAAGAGAGAACCAGTGAGAA (F), GAGAAGATGACCCAGGTGAGTG (R); Quantitative real-time PCR was performed via CFX96 Thermal Cycler (*BioRad*) with 1 µl DNA sample (either input or precipitated sample) and 5 µl SsoAdvance Universal SYBR® Green Supermix (*BioRad*), in a total volume of 10 µl. At least 3 replicates of the experiment were performed.

**Dual-reporter assay.** The following sequence of *ODC1* promoter was selected: CGGGCTGGCTGCGGGCCCCGGGCCCCGGGCACGTGTGCGGCGCGCCTCGCCGGC CTGC(G/A)GAGACACGTGGTTCGA. The two possible sequences were synthesised as couples of oligonucleotides (*Sigma Aldrich*). The oligonucleotides were annealed and cloned into pGL3 Basic Promoter Vector (*Promega*). Cloning enzymes and buffers were provided by *New England Biolabs*. The Renilla-TK Vector (*Promega*) was used as an internal control. Tet21N cells were cultured with tetracycline (*Sigma Aldrich*) for one week and a total of

100,000 cells was seeded in 24-well plates. Cells were transfected 24 h post-seeding with both pGL3 Basic Promoter Vector (with either G or A SNP, 12.5 ng/well) and Renilla-TK Vector (400 ng/well), and Lipofectamine LTX Reagent (*Thermo Fisher Scientific*) was used according to the manufacturer's protocol. Cells analysed in high-MYCN condition were deprived of tetracycline during transfection. Cells were analysed 24 h post-transfection with Dual-Luciferase Reporter Assay System (*Promega*) according with manufacturer's instructions. Luminescence was measured via Tube Luminometer GLOMAX® 20/20 (*Promega*). Luciferase luminescence measures were normalized to renilla luminescence. At least 3 replicates of the experiment were performed.

**BrdU assay.** Cells were seeded in 96-well plates (500 cells/well). At every time-point (up to 8 days), cell proliferation was analysed by bromodeoxyuridine (BrdU) incorporation assay (*Roche*), according to the manufacturer's protocol. BrdU was added at a concentration of 10  $\mu$ M to cells 24 h prior to analysis, and incorporation of BrdU was quantified by ELISA using Victor3 Multilabel Plate Reader (*Perkin Elmer*). At least 3 replicates of the experiment were performed.

**Colony formation assay.** Cells were seeded in 6-well plates at a concentration of 500 cells/well and, 5 hours later, treated with 0 mM, 0.1 mM, 0.2 mM or 0.4 mM DFMO. After 10 days, colonies were washed with PBS, fixed and stained with crystal violet solution (0.5% crystal violet, 50% methanol) for 30 min, washed with water and let drying for 3 days. Pictures of the wells were taken via ChemiDoc MP system (*BioRad*). The total surface area occupied by the colonies was determined using *ImageJ* software [110]. Colonies smaller than 50 cells were excluded from analysis. At least 3 replicates of the experiment were performed.

**Cell count assay.** Cell count was performed with a standard Bürker chamber. A total of 10,000 cells was seeded in 6-well format for each condition at day 0. Cells were harvested, treated with Trypan Blue (*Sigma*) and counted at day 3, 5, 7 and 10. At least 3 replicates of the experiment were performed.

**Wound healing assay.** Cells were seeded in 6-well plates. At a confluency of about 80-90%, the wells were scratched with a 200  $\mu$ l pipette tip. At day 0, 1, 2 and 3, cells were washed with PBS, fixed and stained with crystal violet solution (0.5% crystal violet, 50% methanol) for 30 min, washed with water and let drying for 3 days. Pictures of the wound were take via

microscope (10X magnification) by using a *NIKON Digital Sight DS-U2* camera and *NIS Elements F 3.0* software. The percentage of wound space invaded by cells was measured by *ImageJ* software [110] and normalized to day 0 (used as blank sample). At least 3 replicates of the experiment were performed.

**Cell differentiation analysis.** Cells were seeded in 6-well plates with a number of 10,000/well. After 3 days (enough to let the cells to differentiate and to avoid them to grow in overlapping clusters) images were taken via microscope (20X magnification) by using *NIKON Digital Sight DS-U2* camera and *NIS Elements F 3.0* software. The images were analysed with *NeuronJ* in order to count and measure the neurites of each single cell [111]. At least 3 replicates of the experiment were performed.

**Rescue assay.** The coding sequence of mouse *RUNX1T1* gene (NM\_001111027.2, GRCm38.p4) was cloned into p3XFLAG-CMV-10 vector, downstream of the 3xFLAG sequence. Cloning enzymes and buffers were provided by *New England Biolabs*. Empty and *RUNX1T1*-expressing vectors were transfected into KO-3 cell with Lipofectamine 2000 Reagent (*Thermo Fisher Scientific*) following the manufacturer's protocol. Stably transfected cells were selected and cultured with 0.2 mg/ml G418 Sulfate (*Thermo Fisher Scientific*). Cells were seeded in 24-well plates in a concentration of 2000 cells/well. At day 1, 4, 6 and 8, cells were washed with PBS, fixed and stained with crystal violet solution (0.2% crystal violet, 20% methanol) for 10 min, washed with water and let drying for 3 days. Fixed samples were then resuspended in 0.2 ml 5% SDS and shaken for 2 h at room temperature. Absorbance (570 nm) of the resuspended solution was measured by Victor3 Multilabel Plate Reader (*Perkin Elmer*). Empty wells stained with crystal violet were used as blank samples. At least 3 replicates of the experiment were performed.

**RNAseq and *in silico* analysis.** Total RNA was extracted from cells via Trizol solution (*Sigma Aldrich*) following the manufacturer's protocol. The library for RNA sequencing was prepared according to TruSeq RNA Sample Preparation v2 Guide (*Illumina*). The libraries were analysed through NextSeq 500 v2 MID output flowcell, 79bp x2 (*Illumina*). The result was aligned to h38 genome assembly and examined for SNVs and chromosomal rearrangements. Non-expressed genes were excluded from analysis. RNAseq data were first analysed with *DAVID Bioinformatics Resources 6.8* for functional annotation [112]. Only genes with average  $\log_2$  (fold change)  $\geq +1$  or  $\leq -1$  among the 5 clones (percentage error  $\leq 75\%$ ) were chosen for analysis

and the following annotation categories were considered: GOTERM\_BIOLOGICAL\_PROCESS, KEGG\_PATHWAY. *iRegulon*, an application of *Cytoscape* software, was used to reconstruct the transcription regulation network of the upregulated genes identified in the clonal lines [113]. The following settings were used for analysis: 10K motif collection, 1120 ChIP-seq tracks, putative region centred 500 bp around TSS, enrichment score threshold 3.0, ROC threshold for AUC calculation 0.03, rank threshold 5000. Only transcription factors that are found to be expressed in clonal lines by RNAseq were taken into consideration. *STRING 10.5* was used to analyse protein interaction between the transcription factors identified by *iRegulon* and RUNX1T1 [114]. Only interactions experimentally proved were taken into consideration. Interactions between the predicted transcription factors were used to delineate the transcription regulation network.

**Statistical analysis.** All statistical analyses were performed with at least 3 replicated via unpaired two-tailed Student's t-test. The software *Graphpad Prism* was used for analysis.

## *Bibliography*

- [1] Chrystal U Louis, and Jason M Shoheit, MD. Neuroblastoma: Molecular Pathogenesis and Therapy. *Annu Rev Med*, 2015 ; 66: 49–63. doi:10.1146/annurev-med-011514-023121.
- [2] Nai-Kong V. Cheung and Michael A. Dyer. Neuroblastoma: developmental biology, cancer genomics and immunotherapy. *Nature Reviews Cancer*, volume 13, June 2013, 397.
- [3] Manrong Jiang, Jennifer Stanke, and Jill M. Lahti. The Connections Between Neural Crest Development and Neuroblastoma. *Curr Top Dev Biol*, 2011 ; 94: 77–127. doi:10.1016/B978-0-12-380916-2.00004-8.
- [4] Garrett M. Brodeur, Robert C. Seeger, Ann Barrett, Frank Berthold, Robert P. Castleberry, Giulio D'Angio, Bruno De Bernardi, Audrey E. Evans, Marie Favrot, Arnold I. Freeman, Gerald Haase, Olivier Hartmann, F. Ann Hayes, Larry Helson, John Kemshead, Fritz Lampert, Jacques Ninane, Haruo Ohkawa, Thierry Philip, C.R. Pinkerton, Jon Pritchard, Tadashi Sawada, Stuart Siegel, E. Ide Smith, Yoshiaki Tsuchida, and P.A. Voute. International Criteria for Diagnosis, Staging, and Response to Treatment in Patients With Neuroblastoma. *Journal of Clinical Oncology*, Vol 6, No 12 (December), 1988: pp 1874-1881.
- [5] Susan L. Cohn, Andrew D.J. Pearson, Wendy B. London, Tom Monclair, Peter F. Ambros, Garrett M. Brodeur, Andreas Faldum, Barbara Hero, Tomoko Iehara, David Machin, Veronique Mosseri, Thorsten Simon, Alberto Garaventa, Victoria Castel, and Katherine K. Matthay. The International Neuroblastoma Risk Group (INRG) Classification System: An INRG Task Force Report. *Journal of Clinical Oncology*, volume 27, number 2, January 10 2009.
- [6] Yoshiko Takahashi, Douglas Sipp, Hideki Enomoto. Tissue Interactions in Neural Crest Cell Development and Disease. *Science*, 23 august 2013, vol 341.
- [7] Chandra S. Mayanil. Transcriptional and Epigenetic Regulation of Neural Crest Induction during Neurulation. *Developmental Neuroscience* 2013;35:361–372.
- [8] Yoshio Wakamatsu, Yuko Watanabe, Harukazu Nakamura and Hisato Kondoh. Regulation of the neural crest cell fate by N-myc: promotion of ventral migration and neuronal differentiation. *Development* 124, 1953-1962 (1997).
- [9] Jill L. Reiter and Garrett M. Brodeur. High-Resolution Mapping of a 130-kb Core Region of the MYCN Amplicon in Neuroblastomas. *Genomics* 32, 97–103 (1996).
- [10] Miller Huang and William A. Weiss. Neuroblastoma and MYCN. *Cold Spring Harb Perspect Med* 2013; 3:a014415.
- [11] RR Olsen, JH Otero, J García-López, K Wallace, D Finkelstein, JE Rehg, Z Yin1, Y-D Wang and KW Freeman. MYCN induces neuroblastoma in primary neural crest cells. *Oncogene* (2017) 36, 5075–5082.

- [12] Emma Bell, Lindi Chen, Tao Liu, Glenn M. Marshall, John Lunec, Deborah A. Tweddle. MYCN oncoprotein targets and their therapeutic potential. *Cancer Letters* 293 (2010) 144–157.
- [13] Chia-Lang Hsu, Hsin-Yi Chang, Jen-Yun Chang, Wen-Ming Hsu, Hsuan-Cheng Huang, Hsueh-Fen Juan. Unveiling MYCN regulatory networks in neuroblastoma via integrative analysis of heterogeneous genomics data. *Oncotarget*, Vol. 7, No. 24, 2016.
- [14] Bernhard Luscher. Function and regulation of the transcription factors of the Myc/Max/Mad network. *Gene* 277 (2001) 1–14.
- [15] William P. Tansey. Mammalian MYC Proteins and Cancer. *New Journal of Science* Volume 2014, Article ID 757534, 27 pages.
- [16] Samuele Gherardi, Emanuele Valli, Daniela Erriquez and Giovanni Perini. MYCN-mediated transcriptional repression in neuroblastoma: the other side of the coin. *Frontiers in Oncology* March 2013, Volume 3, Article 42.
- [17] Anthony E. Pegg. Regulation of Ornithine Decarboxylase. *The Journal of Biological Chemistry* vol. 281, n°. 21, pp. 14529–14532, May 26, 2006.
- [18] Anthony E. Pegg. Mammalian Polyamine Metabolism and Function. *IUBMB Life*. 2009 September; 61(9): 880–894. doi:10.1002/iub.230.
- [19] A. J. M. Walhout, J. M. Gubbels, R. Bernards<sup>1</sup>, P. C. van der Vliet and H. Th. M. Timmers. c-Myc/Max heterodimers bind cooperatively to the E-box sequences located in the first intron of the rat ornithine decarboxylase (ODC) gene. *Nucleic Acids Research*, 1997, Vol. 25, No. 8, 1493–1501.
- [20] T. G. O'Brien. The Induction of Ornithine Decarboxylase as an Early, Possibly Obligatory, Event in Mouse Skin Carcinogenesis. *Cancer Research*, 36, 2644-2653, July 1976.
- [21] Eugene W. Gerner and Frank L. Meyskens Jr. Polyamines and cancer: old molecules, new understanding. *Nature Reviews, Cancer*, volume 4, October 2004.
- [22] Thresia Thomas, T. J. Thomas. Polyamine metabolism and cancer. *J.Cell.Mol.Med.* Vol 7, No 2, 2003 pp. 113-126.
- [23] Yutaka Hoshino, Shinya Terashima, Yasushi Teranishi, Masanori Terashima, Michihiko Kogure, Takuroh Saitoh, Fumihiko Osuka, Seigo Kashimura, Zenichiroh Saze, Mitsukazu Gotoh. Ornithine decarboxylase activity as a prognostic marker for colorectal cancer. *Fukushima Journal of Medical Science*, 2007 Volume 53 Issue 1 Pages 1-9.
- [24] Peter P. Grimminger, Paul M. Schneider, Ralf Metzger, Daniel Vallböhmer, Kathleen D. Danenberg, Peter V. Danenberg, Arnulf H. Hölscher, Jan Brabender. Ornithine Decarboxylase mRNA Expression in Curatively Resected Non–Small-Cell Lung Cancer. *Clinical Lung Cancer*, Vol. 11, No. 2, 114-119, 2010.

- [25] Wensheng Deng, Xian Jiang, Yu Mei, Jingzhong Sun, Rong Ma, Xianxi Liu, Hui Sun, Hui Tian and Xueying Sun. Role of ornithine decarboxylase in breast cancer. *Acta Biochim Biophys Sin* (2008): 235-243.
- [26] Jonas A. Nilsson, Ulrich B. Keller, Troy A. Baudino, Chunying Yang, Sara Norton, Jennifer A. Old, Lisa M. Nilsson, Geoffrey Neale, Debora L. Kramer, Carl W. Porter, and John L. Cleveland. Targeting ornithine decarboxylase in Myc-induced lymphomagenesis prevents tumor formation. *Cancer Cell*, May 2005, vol. 7.
- [27] Rajiv R. Mohan, Anjana Challa, Sanjay Gupta, David G. Bostwick, Nihal Ahmad, Rajesh Agarwal,<sup>2</sup> Susan R. Marengo, Saeid B. Amini, Francisco Paras, Gregory T. MacLennan, Martin I. Resnick, and Hasan Mukhtar. Overexpression of Ornithine Decarboxylase in Prostate Cancer and Prostatic Fluid in Humans. *Clinical Cancer Research*, vol. 5, 143–147, January 1999.
- [28] Amy Clifford, David Morgan, Stuart H. Yuspa, Alejandro Peralta Soler, and Susan Gilmour. Role of Ornithine Decarboxylase in Epidermal Tumorigenesis. *Cancer Research*, 55. 1681-1686. April 15. 1995.
- [29] Michael D. Hogarty, Murray D. Norris, Kimberly Davis, Xueyuan Liu, Nicholas F. Evageliou, Candace S. Hayes, Bruce Pawel, Rong Guo, Huaqing Zhao, Eric Sekyere, Joanna Keating, Wayne Thomas, Ngan Ching Cheng, Jayne Murray, Janice Smith, Rosemary Sutton, Nicola Venn, Wendy B. London, Allen Buxton, Susan K. Gilmour, Glenn M. Marshall, and Michelle Haber. ODC1 Is a Critical Determinant of MYCN Oncogenesis and a Therapeutic Target in Neuroblastoma. *Cancer Res* 2008; 68: (23). December 1, 2008.
- [30] Dirk Geerts, Jan Koster, David Albert, Dana-Lynn T. Koomoa, David J. Feith, Anthony E. Pegg, Richard Volckmann, Huib Caron, Rogier Versteeg, and André S. Bachmann. The polyamine metabolism genes ornithine decarboxylase and antizyme 2 predict aggressive behaviour in neuroblastomas with and without MYCN amplification. *Int J Cancer*. 2010 May 1; 126(9): 2012–2024.
- [31] Laura D. Gamble, Michael D. Hogarty, Xueyuan Liu, David S. Ziegler, Glenn Marshall, Murray D. Norris and Michelle Haber. Polyamine pathway inhibition as a novel therapeutic approach to treating neuroblastoma. *Frontiers in Oncology*, November 2012, Volume 2, Article 162.

- [32] Nicholas F. Evageliou, Michelle Haber, Annette Vu, Theodore W. Laetsch, Jayne Murray, Laura D. Gamble, Ngan Ching Cheng, Kangning Liu, Megan Reese, Kelly A. Corrigan, David S. Ziegler, Hannah Webber, Candice S. Hayes, Bruce Pawel, Glenn M. Marshall, Huaqing Zhao, Susan K. Gilmour, Murray D. Norris, and Michael D. Hogarty. Polyamine Antagonist Therapies Inhibit Neuroblastoma Initiation and Progression. *Clinical Cancer Research*, March 24, 2016.
- [33] Mary C. Fitzgerald, Margaret A. Flanagan. Characterization and Sequence Analysis of the Human Ornithine Decarboxylase Gene. *DNA*, vol. 8, n° 9, 10 Jun 2009.
- [34] Yongjun Guo, Robin B. Harris, Dan Rosson, David Boorman, and Thomas G. O'Brien. Functional Analysis of Human Ornithine Decarboxylase Alleles. *Cancer Research*, 60, 6314–6317, November 15, 2000.
- [35] David L.C. Solomon, Bruno Amati and Hartmut Land. Distinct DNA binding preferences for the c-Myc/Max and Max/Max dimers. *Nucleic Acids Research*, 1993, Vol. 21, No. 23.
- [36] A.J.M. Walhout, P.C. van der Vliet, H.Th.M. Timmers. Sequences flanking the E-box contribute to cooperative binding by c-Myc/Max heterodimers to adjacent binding sites. *Biochimica et Biophysica Acta* 1397 1998. 189–201.
- [37] Mari'a Elena Marti'nez, Thomas G. O'Brien, Kimberly E. Fultz, Naveen Babbar, Hagit Yerushalmi, Ning Qu, Yongjun Guo, David Boorman, Janine Einspahr, David S. Alberts, and Eugene W. Gerner. Pronounced reduction in adenoma recurrence associated with aspirin use and a polymorphism in the ornithine decarboxylase gene. *PNAS*, June 24, 2003, vol. 100, no. 13, 7859–7864.
- [38] Richard A. Hubner, Kenneth R. Muir, Jo-Fen Liu, Richard F.A. Logan, Matthew J. Grainge, Richard S. Houlston, and the Members of the UKCAP Consortium. Ornithine Decarboxylase G316A Genotype Is Prognostic for Colorectal Adenoma Recurrence and Predicts Efficacy of Aspirin Chemoprevention. *Clin Cancer Res*, 2008;2303 14(8) April 15, 2008.
- [39] Jason A. Zell, Argyrios Ziogas, Natalia Ignatenko, Jane Honda, Ning Qu, Alexander S. Bobbs, Susan L. Neuhausen, Eugene W. Gerner, and Hoda Anton-Culver. Associations of a Polymorphism in the Ornithine Decarboxylase Gene with Colorectal Cancer Survival. *Clin Cancer Res*, 2009;15(19) October 1, 2009.
- [40] Jason A. Zell, Christine E. McLaren, Wen-Pin Chen, Patricia A. Thompson, Eugene W. Gerner, Frank L. Meyskens. Ornithine Decarboxylase-1 Polymorphism, Chemoprevention With Eflornithine and Sulindac, and Outcomes Among Colorectal Adenoma Patients. *J Natl Cancer Inst* 2010;102: 1513–1516.

- [41] Linping Xu, Jianping Long, Peng Wang, Kangdong Liu, Ling Mai and Yongjun Guo. Association between the ornithine decarboxylase G316A polymorphism and breast cancer survival. *Oncology Letters* 10: 485-491, 2015.
- [42] J. Nathan Davis, Laura McGhee, Shari Meyers. The ETO (MTG8) gene family. *Gene* 303 (2003) 1–10.
- [43] Stefano Rossetti, Andre´ T. Hoogeveen, and Nicoletta Sacchi. The MTG proteins: chromatin repression players with a passion for networking. *Genomics* 84 (2004) 1 –9.
- [44] Johanna K. Wolford, Michal Prochazka. Structure and expression of the human MTG8/ETO gene. *Gene* 212 (1998) 103–109.
- [45] Yoshinobu Odaka, Anirudh Mally, Liza T Elliott, and Shari Meyers. Nuclear import and subnuclear localization of the proto-oncoprotein ETO (MTG8). *Oncogene* (2000) 19, 3584 ± 3597.
- [46] Jinsong Zhang, Bruce A. Hug, Eric Y. Huang, Clarice W. Chen, Vania Gelmetti, Marco Maccarana, Saverio Minucci, Pier Giuseppe Pelicci, and Mitchell A. Lazar. Oligomerization of ETO Is Obligatory for Corepressor Interaction. *Molecular and Cellular Biology* 156–163.2001 Jan. 2001, p. 156–163.
- [47] Daniela Hildebrand, Jens Tiefenbach, Thorsten Heinzl, Manuel Grez, and Alexander B. Maurer. Multiple Regions of ETO Cooperate in Transcriptional Repression. *The Journal of Biological Chemistry*, Vol. 276, No. 13, Issue of March 30, pp. 9889–9895, 2001.
- [48] ETO, a Target of t(8;21) in Acute Leukemia, Makes Distinct Contacts with Multiple Histone Deacetylases and Binds mSin3A through Its Oligomerization Domain. *Molecular and Cellular Biology*, Oct. 2001, p. 6470–6483 Vol. 21, No. 19.
- [49] Ari M. Melnick, Jennifer J. Westendorf, Adam Polinger, Graeme W. Carlile, Sally Arai, Helen J. Ball, Bart Lutterbach, Scott W. Hiebert, and Jonathan D. Licht. The ETO Protein Disrupted in t(8;21)-Associated Acute Myeloid Leukemia Is a Corepressor for the Promyelocytic Leukemia Zinc Finger Protein. *Molecular and Cellular Biology*, Mar. 2000, p. 2075–2086 Vol. 20, No. 6.
- [50] Laura McGhee, Josh Bryan, Liza Elliott, H. Leighton Grimes, Avedis Kazanjian, J. Nathan Davis, and Shari Meyers. Gfi-1 Attaches to the Nuclear Matrix, Associates With ETO (MTG8) and Histone Deacetylase Proteins, and Represses Transcription Using a TSA-Sensitive Mechanism. *Journal of Cellular Biochemistry* 89:1005–1018 (2003).

- [51] Nathalie Chevallier, Connie M. Corcoran, Christine Lennon, Elizabeth Hyjek, Amy Chadburn, Vivian J. Bardwell, Jonathan D. Licht, and Ari Melnick. ETO protein of t(8;21) AML is a corepressor for Bcl-6 B-cell lymphoma oncoprotein. *Blood*, 15 February 2004, volume 103, number 4.
- [52] Youzhong Yuan, Liming Zhou, Toshihiro Miyamoto, Hiromi Iwasaki, Nari Harakawa, Christopher J. Hetherington, Sebastien A. Burel, Eric Lagasse, Irving L. Weissman, Koichi Akashi, and Dong-Er Zhang. AML1-ETO expression is directly involved in the development of acute myeloid leukemia in the presence of additional mutations. *PNAS*, 10398–10403, August 28, 2001, vol. 98 u no. 18.
- [53] Jonathan D. Wood, Frederick C. Nucifora, Jr., Kui Duan, Chuanyi Zhang, Jianxiang Wang, Yujin Kim, Gabriele Schilling, Nicoletta Sacchi, Johnson M. Liu, and Christopher A. Ross. Atrophin-1, the Dentato-rubral and Pallido-luysian Atrophy Gene Product, Interacts with ETO/MTG8 in the Nuclear Matrix and Represses Transcription. *The Journal of Cell Biology*, Volume 150, Number 5, September 4, 2000 939–948.
- [54] Daniela Salat, Robert Liefke, Jo'rg Wiedenmann, Tilman Borggrefe, and Franz Oswald. ETO, but Not Leukemogenic Fusion Protein AML1/ETO, Augments RBP-J/SHARP-Mediated Repression of Notch Target Genes. *Molecular and Cellular Biology*, May 2008, p. 3502–3512 Vol. 28, No. 10.
- [55] Alain C. Borczuka, Jianming Peib, Robert N. Taubc, Brynn Levyd, Odelia Nahumd, Jinli Chend, Katherine Chena, and Joseph R. Testab. Genome-wide analysis of abdominal and pleural malignant mesothelioma with DNA arrays reveals both common and distinct regions of copy number alteration. *Cancer Biology and Therapy*, 2016, Vol. 17, N. 3, 328–335.
- [56] Zhenyu Zhong, Mengxin Lv & Junxia Chen. Screening differential circular RNA expression profiles reveals the regulatory role of circTCF25-miR-103a-3p/miR-107-CDK6 pathway in bladder carcinoma. *Scientific Reports*, 2016, 6:30919 | DOI: 10.1038/srep30919.
- [57] Kun Tu Yeh, Tze Ho Chen, Hui Wen Yang, Jian Liang Chou, Lin Yu Chen, Chia Ming Yeh, Yu Hsin Chen, Ru Inn Lin, Her Young Su, Gary C.W. Chen, Daniel E. Deatherage, Yi Wen Huang, Pearly S. Yan, Huey Jen Lin, Kenneth P. Nephew, Tim H. M. Huang, Hung Cheng Lai and Michael W.Y. Chan. Aberrant TGFb/SMAD4 signaling contributes to epigenetic silencing of a putative tumor suppressor, RunX1T1, in ovarian cancer. *Epigenetics* 6:6, 727-739; June 2011.

- [58] Fengkun Du, Yan Li, Wensheng Zhang, Shubha P. Kale, Harris McFerrin, Ian Davenport, Guangdi Wang, Elena Skripnikova, Xiao-Lin Li, Nathan J. Bowen, Leticia B. McDaniels, Yuan Xiang Meng, Paula Polk, Yong Yu Liu, and Qian Jin Zhang. Highly and moderately aggressive mouse ovarian cancer cell lines exhibit differential gene expression. *Tumour Biol.* 2016 August; 37(8): 11147–11162.
- [59] Artem D. Berezovsky, Laila M. Poisson, David Cherba, Craig P. Webb, Andrea D. Transou, Nancy W. Lemke, Xin Hong, Laura A. Hasselbach, Susan M. Irtenkauf, Tom Mikkelsen and Ana C. deCarvalho. Sox2 Promotes Malignancy in Glioblastoma by Regulating Plasticity and Astrocytic Differentiation. *Neoplasia*, Volume 16 Number 3 March 2014 pp. 193–206.
- [60] Aejaz Nasir, MD, MPhil, FCAP, James Helm, MD, PhD, Leslie Turner, MD, Dung Tsa Chen, PhD, Jonathan Strosberg, MD, Naiel Hafez, MD, Evita B. Henderson Jackson, MD, Pamela Hodul, MD, Marilyn M. Bui, MD, PhD, Nelly A. Nasir, MD, Ardeshir Hakam, MD, Mokenge P. Malafa, MD, Timothy J. Yeatman, MD, Domenico Coppola, MD, and Larry K. Kvols, MD. RUNX1T1: A Novel Predictor of Liver Metastasis in Primary Pancreatic Endocrine Neoplasms. *Pancreas.* 2011 May ; 40(4): 627–633.
- [61] Justin J. Rochford, Robert K. Semple, Matthias Laudes, Keith B. Boyle, Constantinos Christodoulides, Claire Mulligan, Christopher J. Lelliott, Sven Schinner, Dirk Hadaschik, Meera Mahadevan, Jaswinder K. Sethi, Antonio Vidal Puig, and Stephen O’Rahilly. ETO/MTG8 Is an Inhibitor of C/EBP Activity and a Regulator of Early Adipogenesis. *Molecular and Cellular Biology*, Nov. 2004, p. 9863–9872 Vol. 24, No. 22.
- [62] Xu Zhao, Ying Yang, Bao Fa Sun, Yue Shi, Xin Yang, Wen Xiao, Ya Juan Hao, Xiao Li Ping, Yu Sheng Chen, Wen Jia Wang, Kang Xuan Jin, Xing Wang, Chun Min Huang, Yu Fu, Xiao Meng Ge, Shu Hui Song, Hyun Seok Jeong, Hiroyuki Yanagisawa, Yamei Niu, Gui Fang Jia, Wei Wu, Wei Min Tong, Akimitsu Okamoto, Chuan He, Jannie M Rendtlew Danielsen, Xiu Jie Wang, Yun Gui Yang. FTO-dependent demethylation of N6-methyladenosine regulates mRNA splicing and is required for adipogenesis. *Cell Research* (2014) 24:1403 -1419.
- [63] Hongbin Zhang, Meiping Guan, Kristy L Townsend, Tian Lian Huang, Ding An, Xu Yan, Ruidan Xue, Tim J Schulz, Jonathon Winnay, Marcelo Mori1, Michael F Hirshman, Karsten Kristiansen, John S Tsang, Andrew P White, Aaron M Cypess, Laurie J Goodyear & Yu Hua Tseng. MicroRNA-455 regulates brown adipogenesis via a novel HIF1an-AMPK-PGC1a signaling network. *EMBO reports*, Vol 16, No 10, 2015.

- [64] Kaiping Deng, Caifang Ren, Zifei Liu, Xiaoxiao Gao, Yixuan Fan, Guomin Zhang, Yanli Zhang, Ei Samahy MA, Feng Wang, and Peihua You. Characterization of RUNX1T1, an Adipogenesis Regulator in Ovine Preadipocyte Differentiation. *Int. J. Mol. Sci.* 2018, 19, 1300.
- [65] Nimmi Baby, Yali Li, Eng Ang Ling, Jia Lu, S. Thameem Dheen. Runx1t1 (Runt-Related Transcription Factor 1; Translocated to, 1) Epigenetically Regulates the Proliferation and Nitric Oxide Production of Microglia. *PLOS ONE*, February 2014, Volume 9, Issue 2, e89326.
- [66] Tzyy Nan Huang and Yi Ping Hsueh. Brain-specific transcriptional regulator T-brain-1 controls brain wiring and neuronal activity in autism spectrum disorders. *Frontiers in Neuroscience*, 1 November 2015, Volume 9, Article 406.
- [67] Zou Linqing, Jin Guohua, Li Haoming, Tao Xuele, Qin Jianbing, Tian Meiling. Runx1t1 Regulates the Neuronal Differentiation of Radial Glial Cells From the Rat Hippocampus. *Stem Cells Translational Medicine*, 2015; 4:110–116.
- [68] Savita Sankar, Dhananjay Yellajoshiyula, Bo Zhang, Bryan Teets, Nicole Rockweiler & Kristen L. Kroll. Gene regulatory networks in neural cell fate acquisition from genomewide chromatin association of Geminin and Zic1. *Scientific Reports*, 2016, 6:37412, DOI: 10.1038/srep37412.
- [69] Franco Calabi, Richard Pannell, and Gordana Pavloska. Gene Targeting Reveals a Crucial Role for MTG8 in the Gut. *Molecular and Cellular Biology*, Aug. 2001, p. 5658–5666 Vol. 21, No. 16.
- [70] Cecil M. Benitez, Kun Qu, Takuya Sugiyama, Philip T. Pauerstein, Yinghua Liu, Jennifer Tsai, Xueying Gu, Amar Ghodasara, H. Efsun Arda, Jiajing Zhang, Joseph D. Dekker, Haley O. Tucker, Howard Y. Chang, Seung K. Kim. An Integrated Cell Purification and Genomics Strategy Reveals Multiple Regulators of Pancreas Development. *PLOS Genetics*, October 2014, Volume 10, Issue 10, e1004645.
- [71] Ko-Hsun Liao, Shing Jyh Chang, Hsin Chuan Chang, Chen Li Chien, Tse Shun Huang, Te Chia Feng, Wen Wei Lin, Chuan Chi Shih, Muh Hwa Yang, Shung Haur Yang, Chi Hung Lin, Wei Lun Hwang, Oscar K. Lee. Endothelial angiogenesis is directed by RUNX1T1-regulated VEGFA, BMP4 and TGF- $\beta$ 2 expression. *PLOS ONE*, June 22, 2017.
- [72] Jonah Riddell, Roi Gazit, Brian S. Garrison, Guoji Guo, Assieh Saadatpour, Pankaj K. Mandal, Wataru Ebina, Pavel Volchkov, Guo Cheng Yuan, Stuart H. Orkin, and Derrick J. Rossi. Reprogramming committed murine blood cells to induced hematopoietic stem cells with defined factors. *Cell*. 2014 April 24; 157(3): 549–564.
- [73] Tianyi Zhang, Sarah Cooper, & Neil Brockdorff. The interplay of histone modifications – writers that read. *EMBO reports*, Vol 16, No 11, 2015.

- [74] Swagatam Mukhopadhyay, Anirvan M. Sengupta. The Role of Multiple Marks in Epigenetic Silencing and the Emergence of a Stable Bivalent Chromatin State. *PLOS Computational Biology*, 1 July 2013, Volume 9, Issue 7.
- [75] Yael Katan-Khaykovich and Kevin Struhl. Dynamics of global histone acetylation and deacetylation in vivo: rapid restoration of normal histone acetylation status upon removal of activators and repressors. *Genes & Development*, 16, 743–752, 2002.
- [76] H Kocak, S Ackermann, B Hero, Y Kahlert, A Oberthuer, D Juraeva, F Roels, J Theissen, F Westermann, H Deubzer, V Ehemann, B Brors, M Odenthal, F Berthold and M Fischer. Hox-C9 activates the intrinsic pathway of apoptosis and is associated with spontaneous regression in neuroblastoma. *Cell Death and Disease* (2013) 4.
- [77] Jan J. Molenaar, JanKoster, Danny A. Zwijnenburg, Peter van Sluis, Linda J. Valentijn, Ida van der Ploeg, Mohamed Hamdi, Johan van Nes, Bart A. Westerman, Jennemiek van Arkel, Marli E. Ebus, Franciska Haneveld, Arjan Lakeman, Linda Schild, Piet Molenaar, Peter Stroeken, Max M. van Noesel, Ingrid Øra, Evan E. Santo, Huib N. Caron, Ellen M. Westerhout & Rogier Versteeg. Sequencing of neuroblastoma identifies chromothripsis and defects in neuritogenesis genes. *Nature* 29 March 2012, Vol 483, 589.
- [78] Trevor J. Pugh, Olena Morozova, Edward F. Attiyeh, Shahab Asgharzadeh, Jun S. Wei, Daniel Auclair, Scott L. Carter, Kristian Cibulskis, Megan Hanna, Adam Kiezun, Jaegil Kim, Michael S. Lawrence, Lee Lichenstein, Aaron McKenna, Chandra Sekhar Pdamallu, Alex H. Ramos, Erica Shefler, Andrey Sivachenko, Carrie Sougnez, Chip Stewart, Adrian Ally, Inanc Birol, Readman Chiu, Richard D. Corbett, Martin Hirst, Shaun D. Jackman, Baljit Kamoh, Alireza Hadj Khodabakshi, Martin Krzywinski, Allan Lo, Richard A. Moore, Karen L. Mungall, Jenny Qian, Angela Tam, Nina Thiessen, Yongjun Zhao, Kristina A. Cole, Maura Diamond, Sharon J. Diskin, Yael P. Mosse, Andrew C. Wood, Lingyun Ji, Richard Sposto, Thomas Badgett, Wendy B. London, Yvonne Moyer, Julie M. Gastier-Foster, Malcolm A. Smith, Jaime M. Guidry Auvil, Daniela S. Gerhard, Michael D. Hogarty, Steven J. M. Jones, Eric S. Lander, Stacey B. Gabriel, Gad Getz, Robert C. Seeger, Javed Khan, Marco A. Marra, Matthew Meyerson, and John M. Maris. The genetic landscape of high-risk neuroblastoma. *Nat Genet.* 2013 March, 45(3): 279–284.
- [79] David P Kreil, Christopher E Mason, and Leming Shi. A comprehensive assessment of RNA-seq accuracy, reproducibility and information content by the Sequencing Quality Control consortium. *Nat Biotechnol.* 2014 September, 32(9): 903–914.
- [80] Patrick D. Hsu, Eric S. Lander, and Feng Zhang. Development and Applications of CRISPR-Cas9 for Genome Engineering. *Cell* 157, June 5, 2014.

- [81]** Jennifer A. Doudna and Emmanuelle Charpentier. The new frontier of genome engineering with CRISPR-Cas9. *Science*, 28 November 2014, vol 346, issue 6213.
- [82]** Jeffrey D. Sander and J. Keith Joung. CRISPR-Cas systems for genome editing, regulation and targeting. *Nat Biotechnol*, 2014 April, 32(4): 347–355.
- [83]** David Goldschneider, Emilie Horvilleur, Louis-Francois Plassa, Marine GuillaudBataille, Karine Million, Evelyne Wittmer-Dupret, Gise`le Danglot, Hughes de The´, Jean Be´nard1, Evelyne May5, and Se´tha Douc-Rasy. Expression of C-terminal deleted p53 isoforms in neuroblastoma. *Nucleic Acids Research*, 2006, Vol. 34, No. 19 5603–5612, 2006.
- [84]** Nancy E. Kohl, Naotoshi Kanda, Rhona R. Schreck, Gail Bruns, Samuel A. Latt, Fred Gilbert, Frederick W. Alt. Transposition and amplification of oncogene-related sequences in human neuroblastomas. *Cell*, Volume 35, Issue 2, Part 1, December 1983, Pages 359-367.
- [85]** Sei Kuriyama and Roberto Mayor. Molecular analysis of neural crest migration. *Phil. Trans. R. Soc. B* (2008) 363, 1349–1362, 2008.
- [86]** Marianna Szemes, Alexander Greenhough, Zsombor Meleg, Sally Malik, Aysen Yuksel, Daniel Catchpoole, Kelli Gallacher, Madhu Kollareddy, Ji Hyun Park and Karim Malik. Wnt Signalling Drives Context-Dependent Differentiation or Proliferation in Neuroblastoma. *Neoplasia*, Volume 20 Number 4 April 2018 pp. 335–350.
- [87]** Ewa Maj, Lutz Künneke, Elisabeth Loesch, Anita Grund, Juliane Melchert, Tomas Pieler, Timo Aspelmeier, Annette Borchers. Controlled levels of canonical Wnt signaling are required for neural crest migration. *Developmental Biology* 417 (2016) 77–90.
- [88]** Susanne Fransson, Frida Abel, Per Kogner, Tommy Martinsson and Katarina Ejeskär. Stage-dependent expression of PI3K/Akt-pathway genes in neuroblastoma. *International Journal of Oncology* 42: 609-616, 2013.
- [89]** Daniela Opel, Christopher Poremba, Thorsten Simon, Klaus-Michael Debatin, and Simone Fulda. Activation of Akt Predicts Poor Outcome in Neuroblastoma. *Cancer Res* 2007; 67: (2). January 15, 2007.
- [90]** Louis Chesler, Chris Schlieve, David D. Goldenberg, Anna Kenney, Grace Kim, Alex McMillan, Katherine K. Matthey, David Rowitch, and William A. Weiss. Inhibition of Phosphatidylinositol 3-Kinase Destabilizes Mycn Protein and Blocks Malignant Progression in Neuroblastoma. *Cancer Res*. 2006 August 15.
- [91]** Lauren Geary, Carole LaBonne. FGF mediated MAPK and PI3K/Akt Signals make distinct contributions to pluripotency and the establishment of Neural Crest. *eLife* 2018, 7:e33845.

- [92] Christopher J. Hindley<sup>1</sup>, Alexandra Larisa Condurat, Vishal Menon, Ria Thomas, Luis M. Azmitia, Jason A. Davis & Jan Pruszk. The Hippo pathway member YAP enhances human neural crest cell fate and migration. *Scientific Reports*, DOI: 10.1038/srep23208, 6:23208, 2016.
- [93] Chao Yang, Juan Tan, Jun Zhu, Shan Wang, Guanghui Wei. YAP promotes tumorigenesis and cisplatin resistance in neuroblastoma. *Oncotarget*, 2017, Vol. 8.
- [94] Schönherr C, Yang HL, Vigny M, Palmer RH, Hallberg B. Anaplastic lymphoma kinase activates the small GTPase Rap1 via the Rap1-specific GEF C3G in both neuroblastoma and PC12 cells. *Oncogene*. 2010 May 13;29(19):2817-30.
- [95] Yoshio Wakamatsu, Thomas M. Maynard and James A. Weston. Fate determination of neural crest cells by NOTCH-mediated lateral inhibition and asymmetrical cell division during gangliogenesis. *Development* 127, 2811-2821 (2000).
- [96] Peter E. Zage, Riitta Nolo, Wendy Fang, John Stewart, Guillermo Garcia-Manero, and Patrick A. Zweidler-McKay. Notch Pathway Activation Induces Neuroblastoma Tumor Cell Growth Arrest. *Pediatric Blood Cancer*. 2012 May ; 58(5): 682–689.
- [97] Michael J. Plevin, Jinsong Zhang, Chun Guo, Robert G. Roeder, and Mitsuhiko Ikura. The acute myeloid leukemia fusion protein AML1-ETO targets E proteins via a paired amphipathic helix-like TBP-associated factor homology domain. *PNAS*, 10242–10247, July 5, 2006, vol. 103, no. 27.
- [98] M. Uittenbogaard, A. Chiaramello. Expression of the bHLH transcription factor Tcf 12 (ME1) gene is linked to the expansion of precursor cell populations during neurogenesis. *Gene Expression Patterns* 1 (2002) 115–121.
- [99] Simone Mesman and Marten P. Smidt. Tcf12 Is Involved in Early Cell-Fate Determination and Subset Specification of Midbrain Dopamine Neurons. *Frontiers in Molecular Neuroscience*. November 2017, Volume 10, Article 353.
- [100] Siqi Yi, Miao Yu, Shuang Yang, Richard J. Miron, Yufeng Zhang. Tcf12, A Member of Basic Helix-Loop-Helix Transcription Factors, Mediates Bone Marrow Mesenchymal Stem Cell Osteogenic Differentiation In Vitro and In Vivo. *Stem Cells*, 2017, 35:386–397.
- [101] Chun-Chung Lee, Wei-Shone Chen, Chia-Chi Chen, Li-Li Chen, Yi-Shing Lin, Chi-Shuan Fan, and Tze-Sing Huang. TCF12 Protein Functions as Transcriptional Repressor of E-cadherin, and Its Overexpression Is Correlated with Metastasis of Colorectal Cancer. *Journal of Biological Chemistry*, volume 287, number 4, January 20, 2012.

- [102] Elena Scarpa, Andra's Szabo', Anne Bibonne, Eric Theveneau, Maddy Parsons, Roberto Mayor. Cadherin Switch during EMT in Neural Crest Cells Leads to Contact Inhibition of Locomotion via Repolarization of Forces. *Developmental Cell* 34, 421–434, August 24, 2015.
- [103] Olga Klezovitch, Valeri Vasioukhin. Cadherin signaling: keeping cells in touch. *F1000 Research*, 2015, 4.
- [104] Michelle Haber, Janice Smith, Sharon B. Bordow, Claudia Flemming, Susan L. Cohn, Wendy B. London, Glenn M. Marshall, and Murray D. Norris. Association of High-Level MRP1 Expression With Poor Clinical Outcome in a Large Prospective Study of Primary Neuroblastoma. *Journal of Clinical Oncology*, Volume 24, Number 10, April 1 2006.
- [105] Marina Pajica, Jayne Murraya, Glenn M. Marshalla, Susan P.C. Coleb, Murray D. Norrisa and Michelle Habera. ABCC1 G2012T single nucleotide polymorphism is associated with patient outcome in primary neuroblastoma and altered stability of the ABCC1 gene transcript. *Pharmacogenetics and Genomics* 2011, 21:270–279.
- [106] Norris MD, Haber M, Gilbert J, Kavallaris M, Marshall GM, Stewart BW. N-myc gene amplification in neuroblastoma determined by the polymerase chain reaction. *Prog Clin Biol Res* 385: 27-33 (1994).
- [107] R2: Genomics Analysis and Visualization Platform (<http://r2.amc.nl>).
- [108] Jing Liu, Shunmou Huang, Meiyu Sun, Shengyi Liu, Yumei Liu, Wanxing Wang, Xiurong Zhang, An improved allele-specific PCR primer design method for SNP marker analysis and its application. *Plant Methods* 2012, 8:34.
- [109] Jianyi Yang, Renxiang Yan, Ambrish Roy, Dong Xu, Jonathan Poisson & Yang Zhang. The I-TASSER Suite: protein structure and function prediction. *Nature Methods*, vol.12 n<sup>o</sup>.1, January 2015.
- [110] Caroline A Schneider, Wayne S Rasband & Kevin W Eliceiri. NIH Image to ImageJ: 25 years of image analysis. *Nature Methods* volume 9, pages 671–675 (2012).
- [111] Paul Cottrell, Sohail Ahmed, Catherine James, James Hodson, Peter J. McDonnell, Saaeha Rauz, and Geraint P. Williams. Neuron J is a Rapid and Reliable Open Source Tool for Evaluating Corneal Nerve Density in Herpes Simplex Keratitis. *IOVS*, November 2014, Vol. 55, No. 11, 7313.
- [112] Huang DW, Sherman BT, Lempicki RA. Bioinformatics enrichment tools: paths toward the comprehensive functional analysis of large gene lists. *Nucleic Acids Res.* 2009;37(1):1-13.

- [113] Rekin's Janky, Annelien Verfaillie, Hana Imrichova, Bram Van de Sande, Laura Standaert, Valerie Christiaens, Gert Hulselmans, Koen Hertzen, Marina Naval Sanchez, Delphine Potier, Dmitry Svetlichnyy, Zeynep Kalender Atak, Mark Fiers, Jean-Christophe Marine, Stein Aerts. iRegulon: From a Gene List to a Gene Regulatory Network Using Large Motif and Track Collections. *PLOS Computational Biology*, July 2014, Volume 10, Issue 7, e1003731.
- [114] Damian Szklarczyk, Andrea Franceschini, Stefan Wyder, Kristoffer Forslund, Davide Heller, Jaime Huerta-Cepas, Milan Simonovic, Alexander Roth, Alberto Santos, Kalliopi P. Tsafou, Michael Kuhn, Peer Bork, Lars J. Jensen, and Christian von Mering. STRING v10: protein–protein interaction networks, integrated over the tree of life. *Nucleic Acids Research*, 2015, Vol. 43.
- [115] Guoqiang Ai & Rakesh Dachineni & Pratik Muley & Hemachand Tummalala & G. Jayarama Bhat. Aspirin and salicylic acid decrease c-Myc expression in cancer cells: a potential role in chemoprevention. *Tumor Biol.* (2016) 37:1727–1738.
- [116] Sven Pålman & Sofie Mohlin. Hypoxia and hypoxia-inducible factors in neuroblastoma. *Cell Tissue Res* (2018) 372:269–275.
- [117] William A. Weiss, Ken Aldape, Gayatri Mohapatra, Burt G. Feuerstein, and J. Michael Bishop. Targeted expression of MYCN causes neuroblastoma in transgenic mice. *The EMBO Journal* Vol.16 No.11 pp.2985–2995, 1997.
- [118] Mike-Andrew Westhoff, Georg Karpel-Massler, Oliver Brühl, Stefanie Enzenmüller, Katia La Ferla-Brühl, Markus D Siegelin, Lisa Nonnenmacher and Klaus-Michael Debatin. A critical evaluation of PI3K inhibition in Glioblastoma and Neuroblastoma therapy. *Molecular and Cellular Therapies* 2014, 2:32.
- [119] Nithya Krishnamurthy, Razelle Kurzrock. Targeting the Wnt/beta-catenin pathway in cancer: Update on effectors and inhibitors. *Cancer Treatment Reviews* 62 (2018) 50–60.
- [120] June Sung Bae, Sun Mi Kim, Ho Lee. The Hippo signaling pathway provides novel anti-cancer drug targets. *Oncotarget*, 2017, Vol. 8, (No. 9), pp: 16084-16098.
- [121] Mauricio Burotto, Victoria L. Chiou, Jung-Min Lee, and Elise C. Kohn. The MAPK pathway across different malignancies: A new perspective. *Cancer*. 2014 November 15; 120(22): 3446–3456.
- [122] Lova Segerström, Ninib Baryawno, Baldur Sveinbjörnsson, Malin Wickström, Lotta Elfman, Per Kogner and John Inge Johnsen. Effects of small molecule inhibitors of PI3K/Akt/mTOR signaling on neuroblastoma growth in vitro and in vivo. *Int. J. Cancer*, 129, 2958–2965 (2011).

- [123] Junjira Suebsoonthron, Thiranut Jaronwitschawan, Montarop Yamabhai and Parinya Noisa. Inhibition of WNT signaling reduces differentiation and induces sensitivity to doxorubicin in human malignant neuroblastoma SH-SY5Y cells. *Anti-Cancer Drugs* 2017, Vol 28 No 5.
- [124] Christopher D Richardson, Graham J Ray, Mark A DeWitt, Gemma L Curie & Jacob E Corn. Enhancing homology-directed genome editing by catalytically active and inactive CRISPR-Cas9 using asymmetric donor DNA. *Nature Biotechnology*, Volume 34, Number 3, March 2016.
- [125] Reto Eggenschwiler, Mohsen Moslem, Mariane Serra Fráguas, Melanie Galla, Oliver Papp, Maximilian Naujock, Ines Fonfara, Ingrid Gensch, Annabell Wähner, Abbas Beh-Pajooh, Claudio Mussolino, Marcel Tauscher, Doris Steinemann, Florian Wegner, Susanne Petri, Axel Schambach, Emmanuelle Charpentier, Toni Cathomen, & Tobias Cantz. Improved bi-allelic modification of a transcriptionally silent locus in patient-derived iPSC by Cas9 nickase. *Scientific Reports*, 6:38198, December 2016.
- [126] Hiroshi Nishimasu and Osamu Nureki. Structures and mechanisms of CRISPR RNA-guided effector nucleases. *Current Opinion in Structural Biology* 2017, 43:68–78.
- [127] Fuguo Jiang and Jennifer A. Doudna. CRISPR–Cas9 Structures and Mechanisms. *Annu. Rev. Biophys.* 2017. 46:505–29.
- [128] Mikihiro Shibata, Hiroshi Nishimasu, Noriyuki Kodera, Seiichi Hirano, Toshio Ando, Takayuki Uchihashi, & Osamu Nureki. Real-space and real-time dynamics of CRISPR-Cas9 visualized by high-speed atomic force microscopy. *Nature Communications*, volume 8, Article number: 1430 (2017).
- [129] Bernd Zetsche, Jonathan S. Gootenberg, Omar O. Abudayyeh, Aviv Regev, Eugene V. Koonin, Feng Zhang. Cpf1 Is a Single RNA-Guided Endonuclease of a Class 2 CRISPR-Cas System. *Zetsche et al.*, 2015, *Cell* 163, 759–771.
- [130] Anne Bothmer, Tanushree Phadke, Luis A. Barrera, Carrie M. Margulies, Christina S. Lee, Frank Buquicchio, Sean Moss, Hayat S. Abdulkerim, William Selleck, Hariharan Jayaram, Vic E. Myer & Cecilia Cotta-Ramusino. Characterization of the interplay between DNA repair and CRISPR/Cas9-induced DNA lesions at an endogenous locus. *Nature Communications*, volume 8, Article number: 13905 (2017).
- [131] Michael R. Lieber. The Mechanism of Double-Strand DNA Break Repair by the Nonhomologous DNA End Joining Pathway. *Annu Rev Biochem.* 2010 ; 79: 181–211.
- [132] Maria Jasin and Rodney Rothstein. Repair of Strand Breaks by Homologous Recombination. *Cold Spring Harb Perspect Biol*, 2013 Nov 1.

- [133] Lorraine S. Symington, Rodney Rothstein, and Michael Lisby. Mechanisms and Regulation of Mitotic Recombination in *Saccharomyces cerevisiae*. *Genetics*, Vol. 198, 795–835 November 2014.
- [134] Carlos Pulido-Quetglas, Estel Aparicio-Prat, Carme Arnan, Taisia Polidori, Toni Hermoso, Emilio Palumbo, Julia Ponomarenko, Roderic Guigo, Rory Johnson. Scalable Design of Paired CRISPR Guide RNAs for Genomic Deletion. *PLOS Computational Biology*, March 2, 2017.
- [135] Peter Cameron, Chris K Fuller, Paul D Donohoue, Brittnee N Jones, Matthew S Thompson, Matthew M Carter, Scott Gradia, Bastien Vidal, Elizabeth Garner, Euan M Slorach, Elaine Lau, Lynda M Banh, Alexandra M Lied, Leslie S Edwards, Alexander H Settle, Daniel Capurso, Victor Llaca, Stéphane Deschamps, Mark Cigan, Joshua K Young & Andrew P May. Mapping the genomic landscape of CRISPR–Cas9 cleavage. *Nature Methods*, 600, Vol. 14, N° 6, June 2017.
- [136] David W. Morgens<sup>1</sup>, Michael Wainberg, Evan A. Boyle, Oana Ursu, Carlos L. Araya, C. Kimberly Tsui, Michael S. Haney, Gaelen T. Hess, Kyuho Han, Edwin E. Jeng, Amy Li, Michael P. Snyder, William J. Greenleaf, Anshul Kundaje & Michael C. Bassik. Genome-scale measurement of off-target activity using Cas9 toxicity in high-throughput screens. *Nature Communications*, volume 8, Article number: 15178 (2017).
- [137] Janice S. Chen, Yavuz S. Dagdas, Benjamin P. Kleinstiver, Moira M. Welch, Alexander A. Sousa, Lucas B. Harrington, Samuel H. Sternberg<sup>6</sup>, J. Keith Joung, Ahmet Yildiz, & Jennifer A. Doudna. Enhanced proofreading governs CRISPR–Cas9 targeting accuracy. *Nature*, 19 October 2017, vol 550.
- [138] Lianne E.M. Vriend, Rohit Prakash, Chun-Chin Chen, Fabio Vanoli, Francesca Cavallo, Yu Zhang, Maria Jasin, and Przemek M. Krawczyk. Distinct genetic control of homologous recombination repair of Cas9-induced double-strand breaks, nicks and paired nicks. *Nucleic Acids Research*, 2016, Vol. 44, No. 11.
- [139] Takeshi Maruyama, Stephanie K Dougan, Matthias C Truttmann, Angelina M Bilate, Jessica R Ingram & Hidde L Ploegh. Increasing the efficiency of precise genome editing with CRISPR-Cas9 by inhibition of nonhomologous end joining. *Nature Biotechnology*, volume 33, number 5, May 2015.
- [140] Jun Song, Dongshan Yang, Jie Xu, Tianqing Zhu, Y. Eugene Chen, Jifeng Zhang. RS-1 enhances CRISPR/Cas9- and TALEN-mediated knock-in efficiency. *Nature Communications*, 2016 Jan 28.

- [141] Y. Bill Kim, Alexis C. Komor, Jonathan M. Levy, Michael S. Packer, Kevin T. Zhao, and David R. Liu. Increasing the genome-targeting scope and precision of base editing with engineered Cas9-cytidine deaminase fusions. *Nat Biotechnol.* 2017 April ; 35(4): 371–376.
- [142] Baohui Chen, Luke A. Gilbert, Beth A. Cimini, Joerg Schnitzbauer, Wei Zhang, Gene-Wei Li, Jason Park, Elizabeth H. Blackburn, Jonathan S. Weissman, Lei S. Qi, and Bo Huang. Dynamic Imaging of Genomic Loci in Living Human Cells by an Optimized CRISPR/Cas System. *Cell* 155, 1479–1491, December 19, 2013.
- [143] David A. Nelles, Mark Y. Fang, Mitchell R. O’Connell, Jia L. Xu, Sebastian J. Markmiller, Jennifer A. Doudna, Gene W. Yeo. Programmable RNA Tracking in Live Cells with CRISPR/Cas9. *Cell* 165, 488–496, 2016.
- [144] Silvana Konermann, Mark D. Brigham, Alexandro E. Trevino, Julia Joung, Omar O. Abudayyeh, Clea Barcena, Patrick D. Hsu, Naomi Habib, Jonathan S. Gootenberg, Hiroshi Nishimasu, Osamu Nureki, and Feng Zhang. Genome-scale transcriptional activation by an engineered CRISPR-Cas9 complex. *Nature.* 2015 January 29; 517(7536): 583–588.
- [145] Paul Enríquez. CRISPR-Mediated Epigenome Editing. *Yale Journal of Biology and Medicine*, 89 (2016), pp.471-486.
- [146] Miles W. Gander<sup>1</sup>, Justin D. Vrana<sup>2</sup>, William E. Voje<sup>3</sup>, James M. Carothers<sup>3,4</sup> & Eric Klavins. Digital logic circuits in yeast with CRISPR-dCas9 NOR gates. *Nature Communications*, volume 8, number 15459, (2017).
- [147] Neville E. Sanjana, Ophir Shalem, and Feng Zhang. Improved vectors and genome-wide libraries for CRISPR screening. *Nat Methods.* 2014 August ; 11(8): 783–784.
- [148] Wei Leong Chew, Mohammadsharif Tabebordbar, Jason K.W. Cheng, Prashant Mali, Elizabeth Y. Wu, Alex H.M. Ng, Kexian Zhu, Amy J. Wagers, and George M. Church. A multi-functional AAV-CRISPR-Cas9 and its host response. *Nat Methods.* 2016 October ; 13(10): 868–874.
- [149] Brett T Staahl, Madhurima Benekareddy, Claire Coulon-Bainier, Ashwin A Banfal, Stephen N Floor, Jennifer K Sabo, Cole Urnes, Gabriela Acevedo Munares, Anirvan Ghosh & Jennifer A Doudna. Efficient genome editing in the mouse brain by local delivery of engineered Cas9 ribonucleoprotein complexes. *Nature Biotechnology*, volume 35, number 5, May 2017.
- [150] Leonela Amoasii, John C.W. Hildyard, Hui Li, Efrain Sanchez-Ortiz, Alex Mireault, Daniel Caballero, Rachel Harron, Thaleia-Rengina Stathopoulou, Claire Massey, John M. Shelton, Rhonda Bassel-Duby, Richard J. Piercy, Eric N. Olson. Gene editing restores dystrophin expression in a canine model of Duchenne muscular dystrophy. *Science*, 30 Aug 2018.

- [151] Andrew Hammond, Roberto Galizi, Kyros Kyrou, Alekos Simoni, Carla Siniscalchi, Dimitris Katsanos, Matthew Gribble, Dean Baker, Eric Marois, Steven Russell, Austin Burt, Nikolai Windbichler, Andrea Crisanti & Tony Nolan. A CRISPR-Cas9 gene drive system targeting female reproduction in the malaria mosquito vector *Anopheles gambiae*. *Nature Biotechnology*, volume 34, number 1, January 2016.
- [152] Junghee Kanga, Piotr G. Rychahoua, Titilope A. Isholaa, Jingbo Qiaoa, B. Mark Eversa, and Dai H. Chunga. MYCN Silencing Induces Differentiation and Apoptosis in Human Neuroblastoma Cells. *Biochem Biophys Res Commun*. 2006 December 8; 351(1): 192–197.
- [153] Emma Haapaniemi, Sandeep Botla, Jenna Persson, Bernhard Schmierer and Jussi Taipale. CRISPR–Cas9 genome editing induces a p53-mediated DNA damage response. *Nature Medicine*, volume 24, July 2018.
- [154] Atsuka Matsui, Tatsuya Ihara, Hiraku Suda, Hirofumi Mikami and Kentaro Semba. Gene amplification: mechanisms and involvement in cancer. *BioMol Concepts* 2013; 4(6): 567–582.
- [155] Laura D. Gamble, Ursula R. Kees, Deborah A. Tweddle, John Lunec. MYCN sensitizes neuroblastoma to the MDM2-p53 antagonists Nutlin-3 and MI-63. *Oncogene*. 2012 February 9; 31(6): 752–763.
- [156] F Ann Ran, Patrick D Hsu, Jason Wright, Vineeta Agarwala, David A Scott & Feng Zhang. Genome engineering using the CRISPR-Cas9 system. *Nature Protocols*, vol.8 n° 11, 2013.
- [157] Han Li, Kyle A. Beckman, Veronica Pessino, Bo Huang, Jonathan S. Weissman and Manuel D. Leonetti. Design and specificity of long ssDNA donors for CRISPR-based knock-in. Pre-printed by bioRxiv, 2018.
- [158] Rémi Veneziano, Tyson R. Shepherd, Sakul Ratanalert, Leila Bellou, Chaoqun Tao & Mark Bathe. In vitro synthesis of gene-length single-stranded DNA. *Scientific Reports*, (2018) 8:6548.
- [159] Yu Zhang, Chengzu Long, Hui Li, John R. McAnally, Kedryn K. Baskin, John M. Shelton, Rhonda Bassel-Duby, Eric N. Olson. CRISPR-Cpf1 correction of muscular dystrophy mutations in human cardiomyocytes and mice. *Sci. Adv.* 2017;3: e1602814.
- [160] Tingting Wang, Lingling Liu, Xuyong Chen, Yuqing Shen, Gaojian Lian, Nilay Shah, Andrew M Davidoff, Jun Yang and Ruoning Wang MYCN drives glutaminolysis in neuroblastoma and confers sensitivity to an ROS augmenting agent. *Cell Death and Disease* (2018) 9:220.

- [161] Edmond Chipumuro, Eugenio Marco, Camilla L., Nicholas Kwiatkowski, Tinghu Zhang, Clark M. Hatheway, Brian J. Abraham, Bandana Sharma, Caleb Yeung, Abigail Altabef, Antonio Perez-Atayde, Kwok-Kin Wong, Guo-Cheng Yuan, Nathanael S. Gray, Richard A. Young, and Rani E. George. CDK7 Inhibition Suppresses Super-Enhancer-Linked Oncogenic Transcription in MYCN-Driven Cancer. *Cell*. 2014 November 20; 159(5): 1126–1139.
- [162] Ali Rihani, Jo Vandesompele, Frank Speleman and Tom Van Maerken. Inhibition of CDK4/6 as a novel therapeutic option for neuroblastoma. *Cancer Cell Int* (2015) 15:76.
- [163] Giselle L. Saulnier Sholler, William Ferguson, Genevieve Bergendahl, Jeffrey P. Bond, Kathleen Neville, Don Eslin, Valerie Brown, William Roberts, Randal K. Wada, Javier Oesterheld, Deanna Mitchell, Jessica Foley, Nehal S. Parikh, Francis Eshun, Peter Zage, Jawhar Rawwas, Susan Sencer, Debra Pankiewicz, Monique Quinn, Maria Rich, Joseph Junewick & Jacqueline M. Kravka. Maintenance DFMO Increases Survival in High Risk Neuroblastoma. *Scientific Reports*, (2018) 8:14445.
- [164] Vijaya L. Simhadri, Joseph McGill, Shane McMahon, Junxia Wang, Haiyan Jiang, and Zuben E. Sauna. Prevalence of Pre-existing Antibodies to CRISPR-Associated Nuclease Cas9 in the USA Population. *Molecular Therapy: Methods & Clinical Development*, Vol. 10, September 2018.
- [165] Shu Su, Bian Hu, Jie Shao, Bin Shen, Juan Du, Yinan Du, Jiankui Zhou, Lixia, Lianru Zhang, Fangjun Chen, Huizi Sha, Lei Cheng, Fanyan Meng, Zhengyun Zou, Xingxu Huang & Baorui Liu. CRISPR-Cas9 mediated efficient PD-1 disruption on human primary T cells from cancer patients. *Scientific Reports*, 6:20070, 2016.
- [166] Hong Ma, Nuria Marti-Gutierrez, Sang-Wook Park, Jun Wu, Yeonmi Lee, Keiichiro Suzuki, Amy Koski, Dongmei Ji, Tomonari Hayama, Riffat Ahmed, Hayley Darby, Crystal Van Dyken, Ying Li, Eunju Kang, A.-Reum Park, Daesik Kim, Sang-Tae Kim, Jianhui Gong, Ying Gu, Xun Xu, David Battaglia, Sacha A. Krieg, David M. Lee, Diana H. Wu, Don P. Wolf, Stephen B. Heitner, Juan Carlos Izpisua Belmonte, Paula Amato, Jin-Soo Kim, Sanjiv Kaul & Shoukhrat Mitalipov. Correction of a pathogenic gene mutation in human embryos. *Nature*, 2017, vol 548.
- [167] Christopher A. Lino, Jason C. Harper, James P. Carney & Jerilyn A. Timlin. Delivering CRISPR: a review of the challenges and Approaches. *Drug Delivery*, 25:1, 2018.
- [168] Hidemi Toyoda, Eckard Wimmer and Jeronimo Cello. Oncolytic Poliovirus Therapy in a Mouse Model of Neuroblastoma: Preclinical Data Analysis and Future Studies. *Neuroblastoma: Present and Future*, 2012.

- [169] Mohanraj Ramachandran, Di Yu, Matheus Dyczynski, Sathishkumar Baskaran, Lei Zhang, Aleksei Lulla, Valeria Lulla, Sirle Saul, Sven Nelander, Anna Dimberg, Andres Merits, Justyna Leja-Jarblad, and Magnus Essand. Safe and Effective Treatment of Experimental Neuroblastoma and Glioblastoma Using Systemically Delivered Triple MicroRNA Detargeted Oncolytic Semliki Forest Virus. *Clin Cancer Res*; 23(6) March 15, 2017.
- [170] Joseph Mazar1, Yujia Li, Amy Rosado, Peter Phelan, Kritika Kedarinath, Griffith D. Parks, Kenneth A. Alexander, Tamarah J. Westmoreland. Zika virus as an oncolytic treatment of human neuroblastoma cells requires CD24. *PLOS ONE*, 13(7), 2018.

## *Acknowledgments*

An acknowledgement to Professor Giovanni Perini's laboratory and the Department of Pharmacy and Biotechnology of University of Bologna for hosting this PhD project.

An acknowledgement to Professor Michelle Haber's laboratory, Children's Cancer Institute of Sydney, for providing survival and genotyping data of neuroblastoma patients.

An acknowledgement to Professor Ernesto Guccione's laboratory, Institute of Molecular and Cellular Biology of Singapore, for hosting a training partnership.

An acknowledgement to Annalisa Astolfi and Valentina Indio (PhD), University of Bologna, for performing RNAseq analysis.

An acknowledgement to Federico Giorgi (PhD), University of Bologna, for providing bioinformatics support.